VERTICAL HEAT TRANSPORT MECHANISMS IN LAKES AND RESERVOIRS

by

KATHLEEN ANN HURLEY
BA, Clark University
(1974)

Submitted in partial fulfillment

of the requirements for the degree of

Master of Science

at the

Massachusetts Institute of Technology

June 1977

Signature of Author . . . . . .
Department of Civil Engineering, June 13, 1977

Certified by . . . . . .
Thesis Supervisor

Accepted by . . . . . .
Chairman, Departmental Committee on Graduate Students of the
Department of Civil Engineering

ABSTRACT

VERTICAL HEAT TRANSPORT MECHANISMS IN LAKES AND RESERVOIRS

by

KATHLEEN ANN HURLEY

Submitted to the Department of Civil Engineering on 13 June 1977 in partial fulfillment of the requirements for the degree of Master of Science.

As the demands on the world's water supplies increase, the necessity of protecting and enhancing the quality of water resources, while utilizing them as efficiently as possible, becomes more apparent. This can only be accomplished if the physical, chemical and biological processes affecting a water body are understood. Since the temperature structure of a water body has an important influence on all three types of processes, it is of fundamental concern.

The physical processes affecting the temperature structure of lakes and reservoirs are described. If a lake or reservoir is horizontally stratified, it can often be treated as one dimensional. The sensitivity of the one-dimensional, variable area M.I.T. Reservoir Model (Ryan and Harleman (1971)) to through-flow, vertical diffusivity, extinction coefficient for short wave solar radiation and model time step is examined. A dimensionless parameter which is a measure of the relative importance of advection and diffusion as heat transport mechanisms is defined. The sensitivity studies indicate that when the influence of advection is small, the representation of vertical turbulent diffusivity is not adequate.

The wind is a major cause of turbulence. Laboratory studies on the rate of entrainment from a stagnant lower layer by a turbulent upper layer are reviewed. Ocean and lake models that include the influence of the wind are examined. The M.I.T. Reservoir Model is modified to include the influence of the wind via an iterative heating-wind mixing procedure. The wind mixing algorithm is based on the rule that the rate of change of potential energy of the water column by entrainment is equal to the rate of kinetic energy input by the wind. The iterative procedure minimizes the accumulation of errors in the computation of the heat input. The sensitivity of the modified model to element thickness, time step and onset of stratification is examined. Good agreement between predictions and observations is obtained when the modified model is applied to an actual lake.

Thesis Supervisor: Donald R.F. Harleman
Title: Professor of Civil Engineering

ACKNOWLEDGEMENTS

My deepest appreciation goes to my husband, Miguel, for providing the loving atmosphere and inspiration necessary to keep going when things were rough.

Particular thanks go to Professor Donald R.F. Harleman, my thesis supervisor, for his untiring concern and his constructive criticism of this thesis.

I also wish to thank Drs. Gerhard H. Jirka, Dominique N. Brocard and Masataka Watanabe for their helpful discussions about the structure of the model additions.

Thanks are due to Ms. Susan M. Johnson for her excellent tuping of this manuscript.

This research was supported by the Virginia Electric Power Company. Their support is gratefully acknowledged. All computations were done at the M.I.T. Information Processing Center.

TABLE OF CONTENTS

LIST OF FIGURES

CHAPTER I

INTRODUCTION

Population growth and industrial expansion are placing increasing demands on the world's water supplies. Wastes from these sources have traditionally been disposed of in water bodies, often the same water bodies that provide water supplies. With the recognition that water bodies have a finite assimilative capacity, and that there are a limited number of sources of water supply, there has been a growing awareness of the need to protect and enhance the quality of water resources while utilizing them as efficiently as possible.

A water quality parameter of wide-spread interest is water temperature. A series of examples illustrates the importance of this parameter. One of the better known effects of temperature on the chemistry of a water body is the dependence on temperature of the solubility of oxygen, sulfides, calcium and carbon dioxide. Fish and aquatic plants cannot survive in water the temperature of which is not within a specie-specific tolerance range. The tolerance range may vary with stage in the life-cycle. Thus the temperature determines the plant and animal life that might be found in a given water body. The efficiency of a thermal power plant is directly related to the temperature of the intake water used to cool the condensers. Hence, it is desireable to use water that is as cool as possible for this purpose. The temperature of the return flow from the condensers, with or without intermediate cooling, is a function of the intake water temperature. The primary cause of density gradients is temperature gradients. Density gradients play an important role in influencing the patterns of movement of water and pollutants in a water

body by limiting the extent of withdrawal layers and by inhibiting transport across density interfaces. When a water body is stratified, the deeper water is isolated from the atmosphere and replenishment of the oxygen in the lower layers cannot take place. Decomposition of organic matter may deplete the oxygen, creating anoxic conditions that foster the growth of anaerobic microorganisms thereby producing unpleasant tastes and odors.

1.1 Stratification Cycle

In temperate climates, lakes and some reservoirs experience seasonal changes in their degree of stratification. In early spring, a lake is isothermal at about $4^{o}C$, the temperature of maximum water density. During the spring, a lake begins to warm, with the water near the surface warming faster than the deeper water due to differential absorption of short wave solar radiation. Evaporation, conduction, and net long wave radiation from the water surface continually cool the surface. If the surface temperature drops below the temperature of the water just beneath, the water column is unstable and convective currents restore stability by establishing an isothermal mixed layer. Wind induced mixing also contributes to the formation and maintenance of a mixed upper layer. As the lake continues to heat, two distinct regions evolve. The warm, upper region, called the epilmnion, is generally turbulent and isothermal. The cooler lower region, called the hypolimnion, is generally quiescent with the temperature decreasing with depth. If the lake is deep enough, the hypolimnion temperature asymptotically approaches $4^{o}C$. The zone of transition from one region to the other is called the metalimnion and is characterized by a steep temperature gradient. The thermocline

is defined as the location at which the temperature gradient is a maximum. This nomenclature is illustrated in Figure 1.1. By late summer, the lake attains its maximum heat content and begins to cool. The thermocline descends as convective mixing penetrates to greater depths. As the thermocline descends, the temperature gradient in the metalimnion decreases, until the lake becomes isothermal.

1.2 Stratification Criterion for Reservoirs

Reservoirs differ from lakes in that reservoirs are man-made impoundments, and thus the timing, magnitude and elevation of outflows can be selected. In lakes, these choices are not available. Not all reservoirs exhibit the horizontal stratification cycle of lakes described above. Some reservoirs are isothermal or exhibit both longitudinal and horizontal stratification. Others become weakly stratified only during parts of the summer. Factors influencing reservoir stratification include the ratio of inflow rate to reservoir volume (the inverse of residence time), reservoir depth, outlet position and the magnitude of short wave solar radiation incident on the reservoir. Vertically mixed reservoirs with short residence times are frequently termed "run-of-the-river" reservoirs since their main use is for power generation and not water storage. "Run-of-the-river" reservoirs do not exhibit thermal stratification, while deep reservoirs whose primary function is to store large spring river flows for release during the summer and fall generally become stratified. The most important parameter characterizing a reservoir as "run-of-the-river", weakly stratified, or stratified has the form of a densimetric Froude number. This densimetric Frounde number, expressing the ratio of inertial gravitational force, is a measure of the ability of

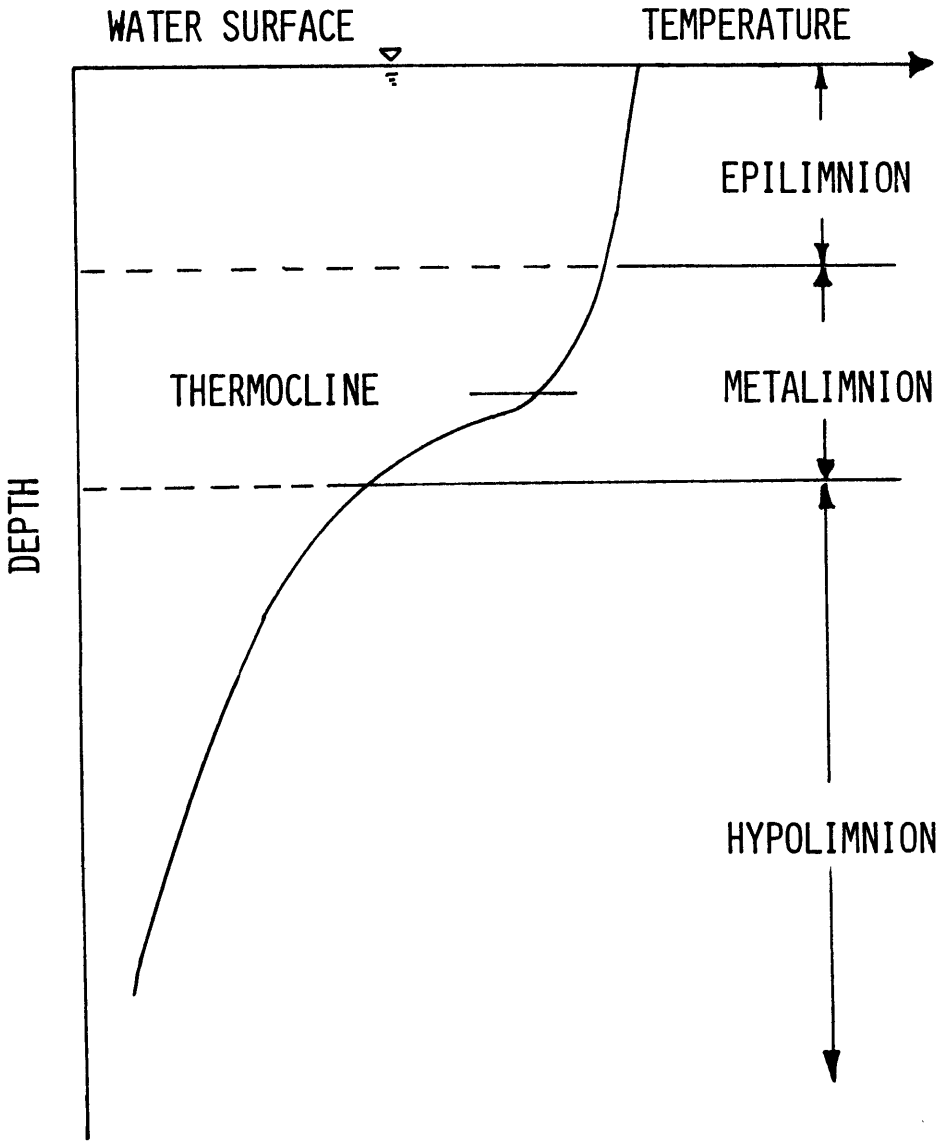

Figure 1-1 Typical Temperature Distribution in a Thermally Stratified Lake

through-flow to disturb the density structure of a reservoir from its gravitational equilibrium state. In reservoirs with horizontal isotherms, the through-flow is not sufficient to disturb the gravitational equilibrium state. Consequently, the densimetric Froude number is expected to be small. In "run-of-the-river" reservoirs, the through-flow has completely upset the gravitational structure and thus the densimetric Froude number is expected to be large. In weakly stratified reservoirs, neither force dominates and the densimetric Froude number is expected to have an intermediate magnitude.

Orlob (1969) has proposed the following criterion for the presence of horizontal isotherms in reservoirs

$$\mathbb{F}_D = \frac{LQ}{hV}\sqrt{\frac{\rho_o}{g\beta}} < \frac{1}{\pi} \qquad (1\text{-}1)$$

where L = reservoir length, Q = volumetric discharge through the reservoir, h = mean reservoir depth, V = reservoir volume, ρ_o = reference density (1000 kg m^{-3}), β = average density gradient in the reservoir (10^{-3} kg m^{-4}), and g = gravitational acceleration. For weakly stratified reservoirs, $\mathbb{F}_D \sim \frac{1}{\pi}$, while for "run-of-the-river" reservoirs, $\mathbb{F}_D > \frac{1}{\pi}$. The scope of this work will be confined to lakes and stratified reservoirs in which $\mathbb{F}_D < \frac{1}{\pi}$.

1.3 Wind Tilt Criterion for Lakes and Reservoirs

During periods of high winds, lakes and stratified reservoirs tend to have tilted isotherms. Sverdrup (1945) gives the inclination (i_s) of the water surface due to the wind as

$$i_s = 4x10^{-7} \frac{W^2}{h}$$

where h = mean water depth (m) and W = mean maximum wind speed (m/sec). The inclination of the thermocline is related to the inclination of the surface by

$$i_t = i_s \frac{\rho}{\Delta\rho}$$

where $\Delta\rho$ is the density difference between the hypolimnion and the epilimnion. Therefore the maximum vertical displacement of the thermocline by the wind is

$$d_t = i_t \frac{L_t}{2}$$

where L_t = average length of the lake or reservoir in the thermocline region in the direction of the wind (m).

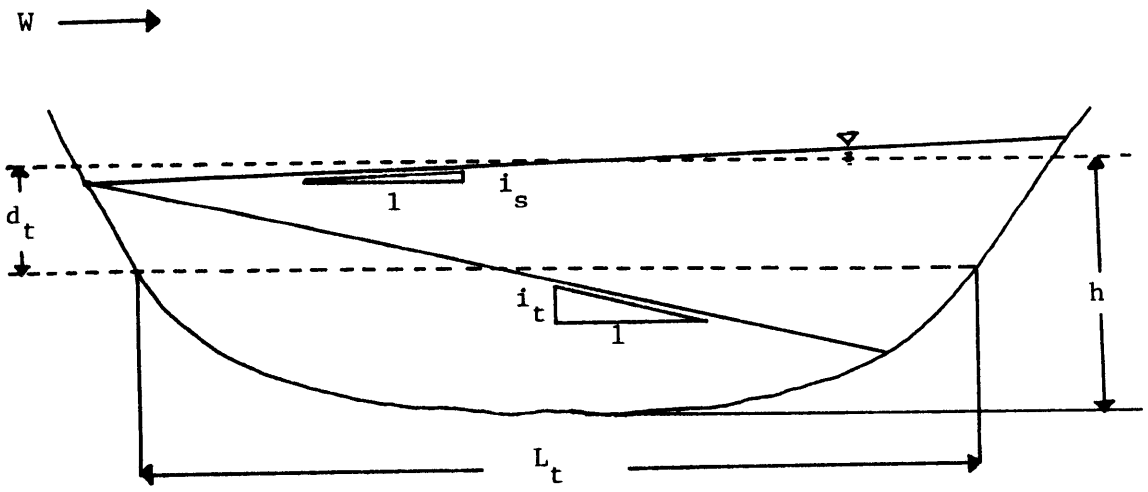

Figure 1-2 Effect of Wind on the Thermocline

If the calculated maximum displacement of the thermocline is larger than the depth of the epilimnion, the hypolimnion is uncovered at one end of the lake or reservoir and the assumption of horizontal isotherms, and thus the one-dimensionality of the system, is no longer valid. The criteria for wind effects not destroying the one-dimensional temperature structure of a lake or reservoir is

$$h_m > \frac{4\times10^{-7}W^2}{h} \quad \frac{\rho}{\Delta\rho} \quad \frac{L_t}{2} \tag{1-2}$$

where h_m is the epilimnion depth in mid-summer.

Equation (1-2) can be used to calculate the maximum wind speed that will not invalidate the assumption of one-dimensionality for a given water body. For an average-sized lake in the mid-Atlantic states ($L_t = 5\times10^3$ m, h = 11 m, h_m = 6 m and $\frac{\Delta\rho}{\rho} = 0.0028$) winds greater than 14 m/sec cause the hypolimnion to be uncovered. For a large lake, such as Lake Michigan ($L_t = 3\times10^5$ m, h = 1×10^2 m, h_m = 15 m and $\frac{\Delta\rho}{\rho} = 0.0032$) winds greater than 9 m/sec invalidate the assumption of one-dimensionality.

1.4 Objectives of this Study

The formulation of an effective management program that permits efficient utilization of a water body for a variety of purposes while maintaining the quality of the resource is not an easy task. Hydrodynamic, chemical and biological processes influencing the behavior of the water body must be understood. Since the temperature structure of a water body has an important influence on all three types of processes, effective water quality planning requires the capacity to predict the temporal and spatial variations

in temperature under alternative development plans.

The scope of this work will be limited to lakes and reservoirs that satisfy the criteria for horizontal stratification given above (Equations (1-1) and (1-2)). This allows the three dimensional problem to be reduced to a one-dimensional, variable area problem. The objectives of this study are two-fold:

1) to develop a one-dimensional, variable area mathematical model of the time-dependent vertical temperature structure of lakes and reservoirs,

2) to examine the relative influence of the vertical heat transport mechanisms, including advection, diffusion, the penetration and absorption of solar radiation, and wind mixing, on the temperature profile.

CHAPTER II

HEAT TRANSFER PROCESSES IN LAKES AND RESERVOIRS

A useful numerical model of a system must be based on a clear understanding of the major physical processes influencing the system. Processes affecting the temperature structure of a lake or reservoir can be conveniently divided into two categories - surface heat transfers and internal heat transfers. Heat transport mechanisms in these two categories are reviewed below.

2.1 Surface Heat Transfer

The ability to predict the transient temperature structure of lakes and reservoirs depends strongly on an accurate knowledge of the heat fluxes through the water surface. These fluxes are shown schematically in Figure 2-1.

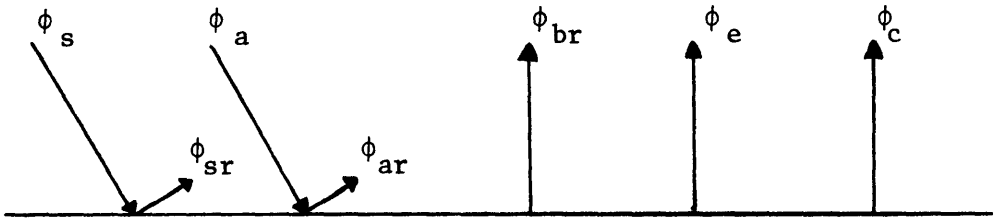

Figure 2-1 Heat Transfer Mechanisms at the Water Surface

where:

ϕ_s = incident solar radiation (short wave)

ϕ_{sr} = reflected solar radiation

ϕ_a = incident atmospheric radiation (long wave)

ϕ_{ar} = reflected atmospheric radiation

ϕ_{br} = long wave radiation from the water surface

ϕ_e = evaporative heat flux

ϕ_c = conduction (sensible heat flux)

Methods for estimating the above components of the total heat flux are well-established for a natural water surface and will be discussed below. The heat fluxes due to direct rainfall and the heat contained in the evaporated water can be neglected because they are generally much smaller than the other fluxes, and they tend to cancel each other in the long term averages. Heat fluxes will be given in joules/m^2-day.

2.1.1 Net Solar Radiation, ϕ_{sn}, (short wave)

Incident Solar Radiation

The radiation emitted by the sun reaches the earth's surface after passing through the atmosphere where it undergoes scattering, reflection and absorption by the air, dust and clouds. Consequently radiation reaching the earth is composed of both short and long wave components and is partly direct and partly diffuse. Short wave radiation can be evaluated by

a) direct measurement by pyrheliometer

or b) empirical formulae. Details of these formulae can be found in

Wunderlich (1972). The general form is

$$\phi_s = \phi_{sc}(1.0-0.65C^2) \qquad (2\text{-}1)$$

where ϕ_{sc} = clear sky solar radiation and C = fraction of the sky covered by clouds. ϕ_{sc} is a function of latitude and time of year. Plots of ϕ_{sc} can be found in Hamon, et. al. (1954). Direct measurement is essential when accuracy greater than approximately 15% is required.

Reflected Solar Radiation

Approximately 5-10% of the incoming solar radiation is reflected by the water surface. Since solar radiation can not be estimated with great accuracy, moderate errors in the reflected radiation are not important. The following table derived from the U.S.G.S. Lake Hefner study (1959) is sufficient in most cases.

Month	Jan.	Feb.	Mar.	Apr.	May	June	July	Aug.	Sept.	Oct.	Nov.	Dec.
ϕ_{sr}/ϕ_s%	9	7	7	6	6	6	6	6	7	7	9	10

The net incident solar radiation, ϕ_{sn}, can be approximated by

$$\phi_{sn} = \phi_s-\phi_{sr} \simeq 0.94\phi_{sc}(1.0-0.65C^2) \qquad (2\text{-}2)$$

2.1.2 Net Atmospheric Radiation, ϕ_{an}, (long wave)

Atmospheric radiation is primarily due to emission of absorbed solar radiation by water vapor, carbon dioxide and ozone in the atmosphere. The emission spectrum of the atmosphere is highly irregular, thus a precise analytic description is infeasible and empirical relations are used. Most formulae for atmospheric radiation have been derived for clear skies and the influence of clouds is included as a separate term. The basic equation for

incident atmospheric radiation, ϕ_a, from a clear sky is

$$\phi_a = \varepsilon\sigma T_a^4 \tag{2-3}$$

where ε = average emittance of the atmosphere (dimensionless)

σ = Stefan-Boltzmann constant = $4.9\text{x}10^{-3}$ joules/m^2-day-$^oK^4$

T_a = air temperature (absolute)

Various expressions and dependencies for ε have been proposed. Brunt (1932) proposed a dependency only on vapor pressure

$$\varepsilon = a+b\sqrt{e} \tag{2-4}$$

where e is vapor pressure and a and b are empirically determined constants. Swinbank (1963) and Idso and Jackson (1969) have proposed forms with a dependency only on absolute temperature. Swinbank's form is

$$\varepsilon = 0.398\text{x}10^{-5}T_{a_k}^{2.148}$$

where T_{a_k} = air temperature ^oK

which he rounds to

$$\varepsilon = 0.92\text{x}10^{-5}T_{a_k}^{2} \tag{2-5}$$

for convenience. Idso and Jackson's form is

$$\varepsilon = [1.0-0.26/\exp\{7.77\text{x}10^{-5}(T_{a_c}^2)\}] \tag{2-6}$$

where T_{a_c} = air temperature ^oC.

These two temperature dependent formulas are almost identical for air temperatures higher than 10°C. Below 4.5°C, Idso and Jackson's formula gives results in better agreement with measurements.

Brutsaert (1975) derived a dependence of the average emittance of the atmosphere, ε, on both vapor pressure and absolute temperature based on the assumptions of exponential profiles for temperature, vapor pressure, pressure and density. He approximated the emissivity of the atmosphere by fitting a power function through data points based on actual atmospheric measurements and calculations. His formula is

$$\varepsilon = 1.24\left(\frac{e}{T_{a_k}}\right)^{1/7} \tag{2-7}$$

where e is in millibars.

Mermier and Seguin (1976) report good agreement between measurements and Equation (2-7). Regression analysis of monthly mean data over a wide range of climatic conditions indicate that the vapor pressure, e, is proportional to $T_{a_k}^{17.8}$. Thus Brutsaert's formulation implies that the emissivity, ε, is proportional to $T_{a_k}^{2.4}$, which is not very different from Swinbank's equation. The two equations are compared for various values of relative humidity in Figure 2-2.

The presence of clouds can increase atmospheric radiation due to diffuse reflection from the clouds. The incident atmospheric radiation, ϕ_a, is given by

$$\phi_a = \phi_{ac}(1.0+kC^2) \tag{2-8}$$

where ϕ_{ac} = atmospheric radiation from a clear sky

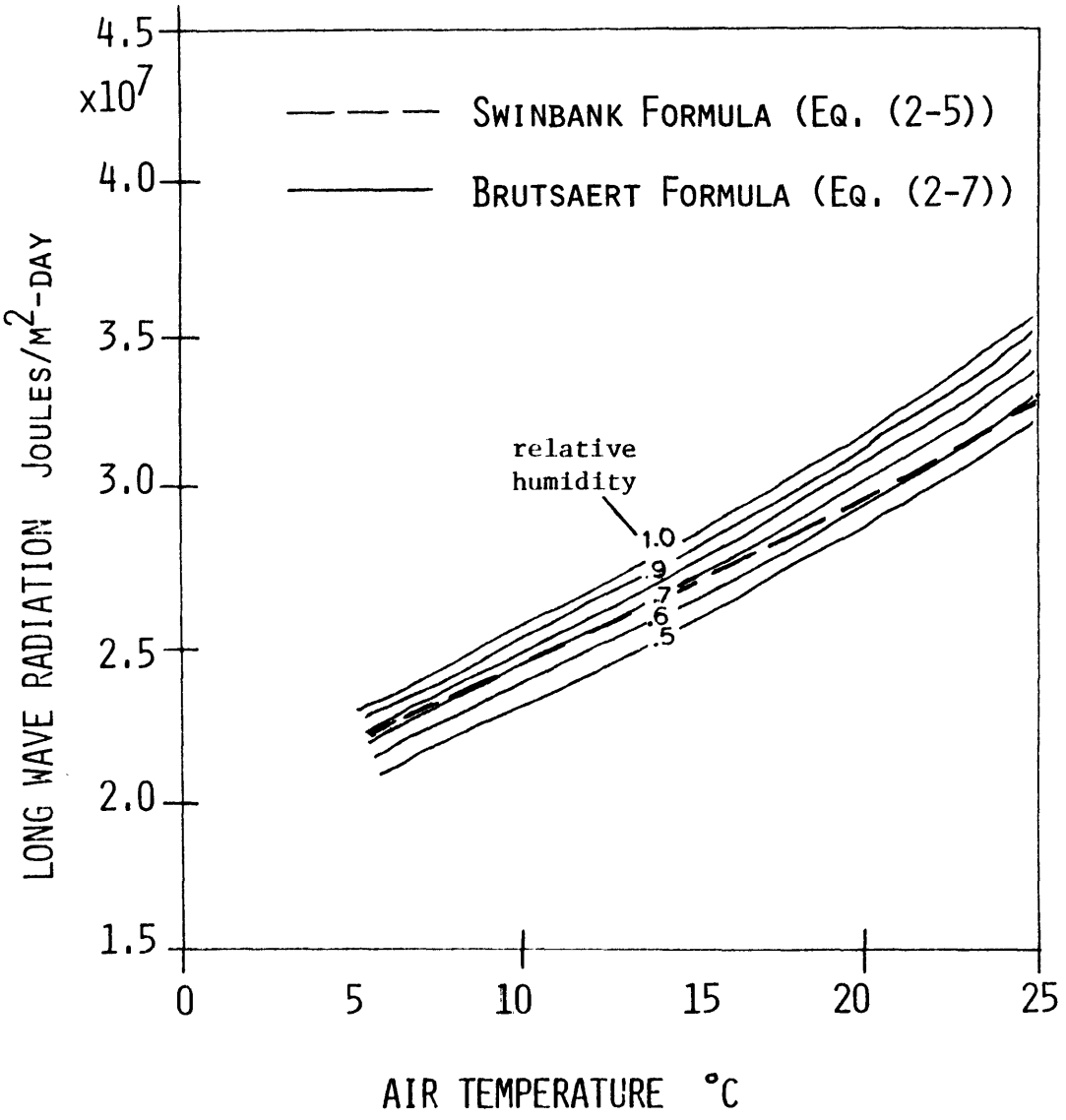

Figure 2-2 Comparison of Swinbank and Brutsaert Formulas for Clear Sky Long Wave Atmospheric Radiation for Various Values of Humidity

C = fraction of the sky covered by clouds (range 0 to 1)

k = dimensionless constant

The value of k depends on the type of clouds present. Wunderlich (1972) suggests an average value of k = 0.17.

A value of 3% is usually accepted as the reflectance of a water surface to long wave radiation. The formula for net atmospheric radiation is

$$\phi_{an} = 0.97\varepsilon\sigma T_a^4(1.0+0.17C^2)$$

where the value of ε depends on the formula used. Brutsaert's formula is recommended, making the complete formula

$$\phi_{an} = 5.9\times10^{-3}\left(\frac{e}{T_a}\right)^{1/7} T_a^4(1.0+0.17C^2) \qquad (2\text{-}9)$$

2.1.3 Back Radiation from the Water Surface, ϕ_{br}, (long wave)

Water radiates as a near black body. The deviation from ideal black body behavior is due to reflection at the air-water interface. The emissivity of a water surface is known relatively precisely, but due to the formation of a thin surface skin, the actual surface temperature is usually known to $\pm0.25^{o}C$. Back radiation is given by

$$\phi_{br} = 0.97\sigma(T_s+273.)^4$$
$$\phi_{br} = 5.9\times10^{-3}(T_s+273.)^4 \qquad (2\text{-}10)$$

where T_s = water surface temperature ^{o}C.

2.1.4 Evaporative Heat Flux

Evaporation from a water surface results from forced (wind driven) convection and free (buoyancy driven) convection. For water bodies with no artificial heat input, forced convection dominates. Most evaporation formula are based on Dalton's law of mass transfer, modified to allow for the effect of the wind. The general form is

$$E = \rho F(W_z)(e_s - e_z) \tag{2-11}$$

where

E = mass flux (mass/area-time)

ρ = density of water

W_z = windspeed at height z

$F(W_z)$ = wind speed function for mass flux including both free and forced convection effects (length/time-pressure)

e_s = saturated vapor pressure at the temperature of the water surface

e_z = vapor pressure at height z

In order to convert from a mass flux to a heat flux, it is necessary to multiply Equation (2-11) by the latent heat of vaporization, L_v.

$$L_v = (2493.-2.26T_s)\times 10^3 \text{ joules/Kg} \tag{2-12}$$

where T_s = water surface temperature, ^oC.

The evaporative heat flux, ϕ_e, is given by

$$\phi_e = L_v E \tag{2-13}$$

A wind speed function of the form

$$F(W_z) = a+bW_z \tag{2-14}$$

where a,b = constants

has been found to give acceptable results. Rohwer's (1931) formula of this type is

$$F(W_z) = 0.000308+0.000185W_z \text{ m/s-mmHg} \tag{2-15}$$

where z, the measurement height for the wind speed, is 6 inches above the water surface, and the units of wind speed are meters per second. The formula for evaporative heat loss is

$$\phi_e = (0.000308+0.000185W)\rho(e_s-e_z)(2493.-2.26T_s)x10^3 \tag{2-16}$$

2.1.5 Conductive Heat Flux

Bowen (1926) related the conduction heat flux to the evaporative mass flux by equating the eddy diffusivity of heat and mass. The conduction heat flux, ϕ_c, can be related to the evaporative mass flux by the Bowen ratio, R

$$\phi_c = RE = 269.1 \frac{(T_s-T_z)}{(e_s-e_z)} E \tag{2-17}$$

where

T_s = water surface temperature ^oC

T_z = air temperature at height z ^oC

e_s = saturation vapor pressure of water at T_s (mm Hg)

e_z = vapor pressure of the air at height z (mm Hg)

2.1.6 Equilibrium Temperature

The net heat flux into a water body is given by

$$\phi_n = \phi_{sn}+\phi_{an}-\phi_{br}-\phi_e-\phi_c \qquad (2\text{-}18)$$

The water temperature at which there is no net heat transfer across the surface is called the equilibrium temperature, T_E. At this temperature, the short and long wave radiation heat inputs are exactly balanced by the heat losses from evaporation, conduction and back radiation. T_E, which is solely dependent upon the meteorological conditions at a given site, can be used as an indicator of whether a water body is heating or cooling on a given day. A water body with a surface temperature T_s greater than T_E will have a net heat loss and thus will tend to decrease in temperature, while a water body with a surface temperature T_s less than T_E will have a net heat gain and thus will tend to increase in temperature. The equilibrium temperature incorporates all the external influences upon ambient temperatures. It can be calculated by setting $\phi_n = 0$ and $T_E = T_s$ in Equation (2-18) and solving iteratively for T_E.

Figure 2-3a shows that the daily equilibrium temperature varies greatly from day to day at a given site. The seasonal trend in T_E can be seen clearly in Figure 2-3b, which shows monthly averaged equilibrium temperatures. Monthly averages can be computed in two ways. First, the daily equilibrium temperatures can be averaged over a month. Alternatively, the meteorological conditions can be averaged over a month and the equilibrium temperature associated with the average weather conditions

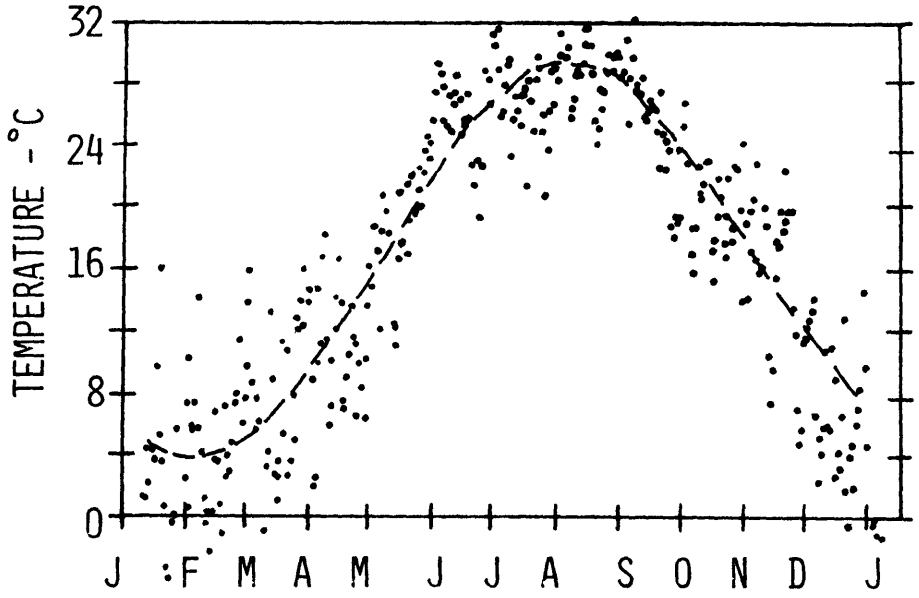

a) Daily equilibrium temperature

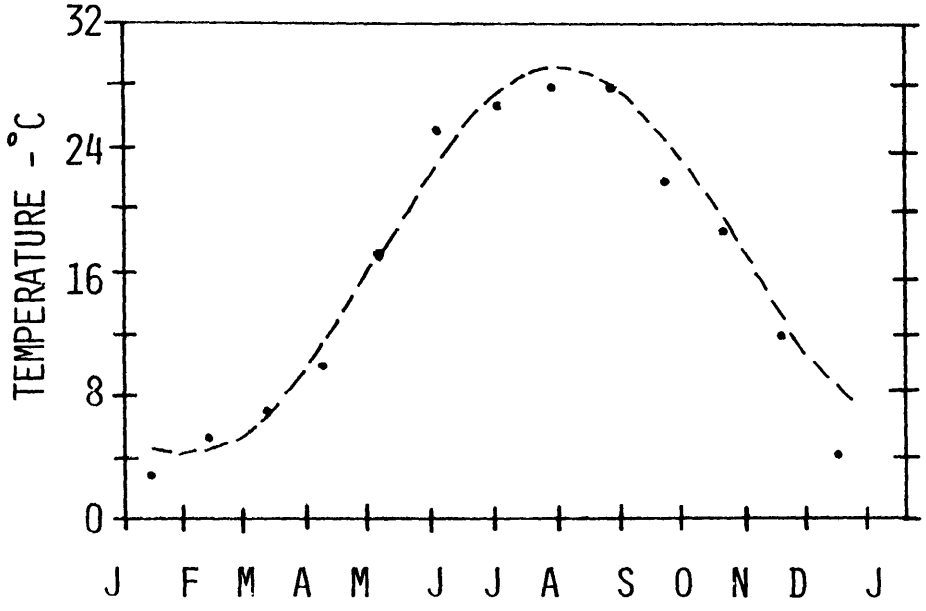

b) Monthly averaged equilibrium temperature

Figure 2-3 Daily and Monthly Averaged Equilibrium Temperature in Mid-Atlantic States

computed. Both methods give essentially the same results. The trend in equilibrium temperature is often represented by a sine function (shown in Figure 2-3) of the form

$$\phi_n = a+b\sin\frac{2\pi}{365}t \qquad (2\text{-}19)$$

where t is the day of the year.

It should be emphasized that the use of this approximation implicitly averages the meteorological conditions over a period of approximately one month and does not give the equilibrium temperature for any given day.

2.1.7 The Linearized Heat Flux Equation

It is a common practice to simplify the expression for the net heat flux (Equation 2-18) using the concepts of equilibrium temperature and surface heat exchange coefficient, K. The linearized heat flux equation developed by Edinger and Geyer (1965) is

$$\phi_n = -K(T_s-T_E) \qquad (2\text{-}20)$$

The surface heat exchange coefficient is defined as the incremental change in net heat exchange induced by an incremental change in surface temperature

$$K = -\frac{\partial\phi_n}{\partial T_s} \qquad (2\text{-}21)$$

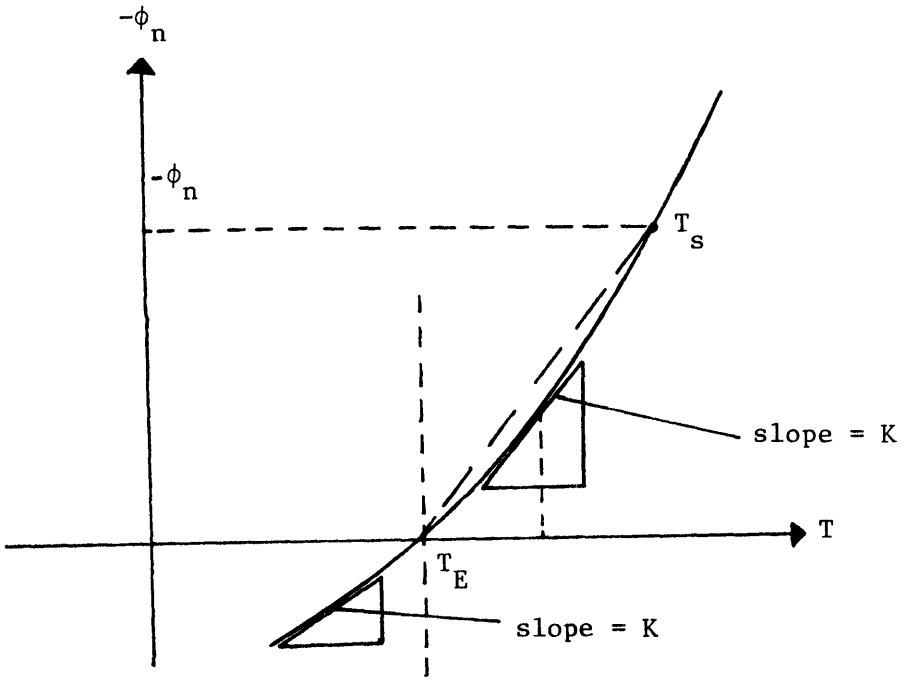

Figure 2-4 Variation of Heat Transfer Coefficient K with Water Surface Temperature T_s

Note that the slope may be defined at any value of T_s, above or below the equilibrium temperature. Charts for evaluating K, which depends both on the meteorological conditions and on T_s, can be found in Ryan and Harleman (1973).

Since the computation of T_E requires the iterative evaluation of the components of the net heat flux, the linearization has not simplified the task of evaluating the net heat flux. However, the linearized heat flux equation is generally used in conjunction with Equation (2-19) to provide an analytical expression for the seasonal trend in the net heat flux.

2.2 Internal Heat Transfer

2.2.1 Internal Absorption of Solar Radiation

The absorption of solar radiation is not solely a surface phenomenon. Short wave radiation can be transmitted to depths of the order of 3 to 30 meters, depending on the clarity of the water, while longer wave radiation is absorbed very near the surface. Dake and Harleman (1969) have shown that it is convenient to separate incoming solar radiation (insolation) into the longer wave portion, β, which is absorbed near the surface, and the remaining portion, $1-\beta$, which is absorbed internally. The insolation at any depth z is described by the equation

$$\phi_z = (1-\beta)\phi_{sn}e^{-\eta z} \qquad (2\text{-}22)$$

where η is the extinction coefficient of solar radiation in water. Values of η and β can be obtained from field measurements. β is typically in the range 0.4 to 0.5. η can be related to the Seechi disk depth, d_D by the simple formula

$$\eta = 1.7/d_D \ (\text{meters}^{-1}) \qquad (2\text{-}23)$$

Equation (2-19) is not accurate near the surface (depth $<\eta/3$).
If a detailed description of the radiation flux near the surface is required, Snider and Viskant (1974) have shown that the summation of at least three exponential terms is needed. This is important for laboratory experiments with shallow depths (<0.5 meter), but for field applications (resolution on the order of 1 meter) Equation (2-19) is adequate. On the basis of Snider and Viskant's experiments in the laboratory a value of

$\beta \approx 0.55$ is appropriate.

2.2.2 Advection Due to Through-Flows

The change in a physical quantity at a point due to the movement of water is called advection. The energy budget of a lake or reservoir is increased by heat entering with incoming water and is decreased by heat leaving with outgoing water. Within a water body the flow patterns due to inflows and outflows redistribute heat as the water moves. Elder and Wunderlich (1968) have shown by dye tests in Fontana Reservoir that the horizontal velocity profile of an inflow may be approximated by a Gaussian curve, although the dependence of the standard deviation is not known. The outflow horizontal velocity profile may also be treated as Gaussian. Koh (1964) and Kao (1965) have suggested expressions for the outflow standard deviation. Horizontal water movements due to inflows and outflows may cause vertical displacements of water as the continuity condition is satisfied.

2.2.3 Seiching and Wind Mixing

Wind stress acting on a water surface induces currents that drive water downwind. As a consequence of the currents and the return flows the isotherms are tilted. When the wind stress stops, the isotherms return to a horizontal position, overshoot and set up an oscillatory motion called seiching. In some cases seiching may be severe and the system can not be treated as one dimensional.

Mixing is associated with the wind induced currents. When a lake is unstratified, the wind may cause the water to circulate through the entire depth of the lake, but when a lake is stratified, the induced currents are confined by the thermocline, leaving the hypolimnion relatively unaffected.

Thus in a stratified lake, wind stress at the surface may not directly create turbulence in the hypolimnion. Turbulence in the hypolimnion is only created indirectly by such mechanisms as degradation of internal waves and internal seiches and by water withdrawal.

2.2.4 Convective Mixing

Another type of large scale water movement occurs when a density instability develops. The denser upper water sinks, resulting in turbulence and mixing and the elimination of the instability. This type of turbulence is called convective mixing.

2.2.5 Diffusivity

Molecular diffusion transports heat whenever temperature gradients are present. Although molecular diffusion is generally small, it is often included in numerical models for computational convenience.

Turbulent diffusion transports heat whenever temperature gradients and turbulence are present. The causes of turbulence are varied and sometimes ill-defined. Sources include convection, wind mixing, entrance mixing of tributaries, fish and people swimming, boats and precipitation.

CHAPTER III

SENSITIVITY OF THE M.I.T. RESERVOIR MODEL TO VARIOUS PARAMETERS

The major distinction between lakes and reservoirs is that lakes have negligible inflows and outflows while the flow through reservoirs is significant. Thus, the relative importance of heat transport mechanisms may be different in reservoirs and lakes.

To ascertain which heat transport mechanisms must be understood and modeled in detail, so as to predict the vertical temperature structure of a lake or reservoir, it is necessary to investigate the sensitivity of the vertical temperature profiles to the magnitude of the various transport mechanisms in a given mathematical model.

In this chapter, the M.I.T. Reservoir Model, described below, is used as the basic mathematical model for the investigation of the sensitivity of predicted temperature profiles to various transport mechanisms. Parameters which are examined include through-flow, vertical eddy diffusivity, the time step corresponding to the time scale of the transient meteorology, and the extinction coefficient of solar radiation in water. The emphasis of this chapter is not on verification or prediction, but rather on the relative influence of the parameters.

3.1 The M.I.T. Reservoir Model

The M.I.T. Reservoir Model is a one-dimensional, time dependent, variable area model based on the absorption and transmission of radiation, diffusion, convection, and advection due to inflows and outflows. A detailed description and a user's manual are given by Ryan and Harleman (1971).

The basic heat transport equation in the vertical direction is obtained by considering heat and mass flow through an internal control volume taken as a horizontal slice of the water body. The model schematization is shown in Figure 3.1. The slice has a thickness Δz and a horizontal area A(z). River inflow enters the element at the upstream end and outflow leaves through the downstream end. The basic heat transport equation for an internal element is

$$\frac{\partial T}{\partial t} + \frac{1}{A}\frac{\partial}{\partial z}(Q_v T) = \frac{E}{A}\frac{\partial}{\partial z}\left[A\frac{\partial T}{\partial z}\right] + \frac{Bu_i T_i}{A} - \frac{Bu_o T}{A} - \frac{1}{\rho c}\frac{\partial \phi_z}{\partial z} \qquad (3\text{-}1)$$

where T is the temperature at depth z, A = area of the element, B = width of the element, u_i = horizontal inflow velocity, T_i = temperature of the inflow, u_o = horizontal outflow velocity, Q_v = vertical flow rate, ϕ_z = internal short wave solar radiation flux per unit horizontal area (see Equation (2-19)), E = vertical turbulent diffusion coefficient, assumed constant with depth, c = heat capacity of water and ρ = density of water. The quantity ρcT represents the heat per unit volume and it is assumed that ρc is constant. The equation is solved using an explicit finite difference scheme.

To satisfy the surface boundary condition, the governing equation for the surface element includes in addition to the terms for the intermediate layers, the heat fluxes due to surface phenomena, i.e. back radiation, evaporation, conduction, atmospheric radiation, and the portion of the solar radiation which is absorbed at or near the surface,

$$\frac{1}{\rho c \Delta z_s}\left[\beta\phi_{sn} + \phi_{an} - \phi_{br} - \phi_e - \phi_c\right] \qquad (3\text{-}2)$$

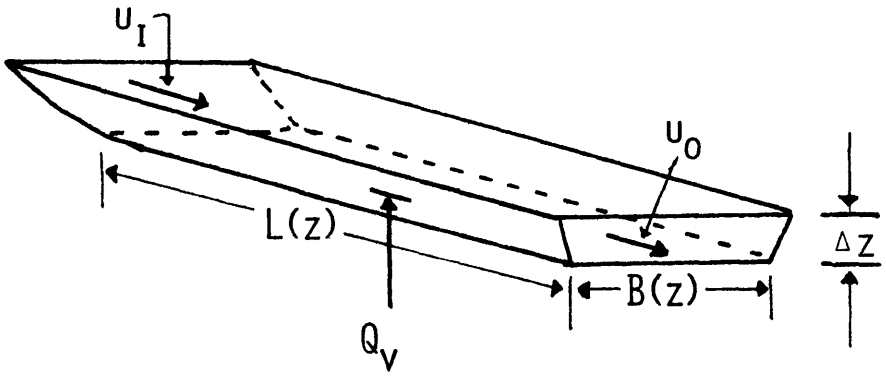

(a) CONTROL VOLUME SLICE

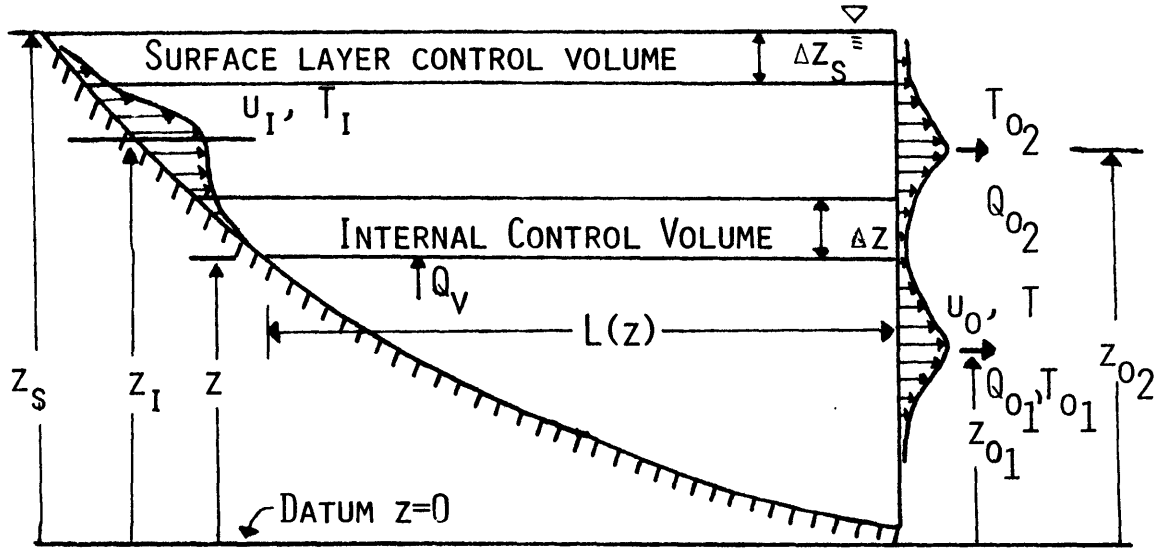

(b) SIDE ELEVATION

Figure 3-1 Schematization and Control Volume for Mathematical Model

Equations (2-9), (2-10), (2-16) and (2-17) are used to compute the fluxes. It is assumed that there is no heat flux to or from the earth through the bottom or sides of the lake.

Horizontal velocities are computed from inflow and outflow rates, assuming Gaussian velocity distributions about the entry and exit elevation. The width of the Gaussian outflow profile is a function of the vertical stratification and is computed with a modified Kao equation (1965). There is a built-in cut-off value of the gradient which restricts the withdrawal layer to the hypolimnion. When there are multiple outlets at different elevations, the velocity profiles are superposed. Entrainment of lake water by inflowing river water is included as an option. The river water is mixed with water from the surface elements in a user specified ratio, changing both the temperature and volume of the inflow. Inflows are assumed to enter the main water column centered at the elevation at which the density is equal to the inflow density. The width of the Gaussian inflow velocity profile is fixed. When entrance mixing is considered, the outflow velocity from the surface layer due to the entrainment into the inflowing river water is computed also.

Vertical velocities are computed from the continuity equation for each element. Thus

$$u_o \Delta z B - u_i \Delta z B = Q_v - [Q_v + \frac{\partial Q_v}{\partial z} \Delta z] \qquad (3\text{-}3)$$

where

$$\frac{\partial Q_v}{\partial z} = B(u_i - u_o)$$

or

$$Q_v(z,t) = B\int_o^z u_i(z,t)dz - B\int_o^z u_o(z,t)dz \qquad (3-4)$$

The approach taken in the M.I.T. Model in selecting a constant vertical diffusion coefficient is to subordinate the importance of turbulent diffusion and to take all other known forms of heat transport into account as accurately as possible, including the turbulent mixing induced by inflows as they enter the main water body. Molecular diffusion is included as a minimum, depth-independent value for the diffusion coefficient for computational convenience in the numerical scheme and for use in connection with laboratory experiments, where turbulence is generally absent. If marked discrepancies occur between the predicted profiles and measured profiles, an allowance for turbulent diffusion is made by uniformly increasing the value of the diffusion coefficient. It has been found that in general a value for the diffusion coefficient of fifty (50) times molecular diffusivity gives acceptable results in reservoirs. At times when there is a net cooling at the surface, convection due to density instability plays an important role in determining the temperature profile. Whenever a density instability exists, elements adjacent to the instability are mixed to eliminate it in such a way that thermal energy is conserved. This is a modification of the model described by Ryan and Harleman (1971), which checks for instabilities using the temperature profile. The technique used for locating density instabilities with the temperature profile is incorrect for temperatures below 4^oC, while the technique involving the density profile is correct to 0^oC. When convection eliminates near surface temperature

gradients, the choice of a vertical diffusion coefficient has little effect on the temperature distribution in the surface mixed layer. Under these conditions the diffusion coefficient has its primary effect in the hypolimnion.

The choice of element thickness and time step is subject to the numerical stability constraint

$$E \frac{\Delta t}{(\Delta z)^2} < \frac{1}{2}$$

An additional numerical constraint is the requirement that the through-flow through an element during a time increment must be less than the volume of the element. This constraint need not influence the choice of element size or time step, however, because the model has an internal provision for sub-dividing any time step in which this numerical stability constraint is violated. The model provides a sufficient number of sub-time steps to satisfy the constraint. The predicted profiles are not sensitive to the element thickness for element sizes in the range 0.6 meters to 2 meters.

3.2 Through-Flow

Internal flow patterns in a stratified reservoir may play an important role in transporting heat. The velocity distribution is influenced by inflow and outflow conditions and by the temperature (density) distribution. The vertical flow rate at a given elevation, $Q_v(z,t)$, is a function both of the magnitude and location of the inflows and outflows and is given by Equation (3-4).

Figure 3-2, taken from experiments done by Ryan and Harleman (1973) in the M.I.T. Reservoir Flume, illustrates the influence of flow rate and

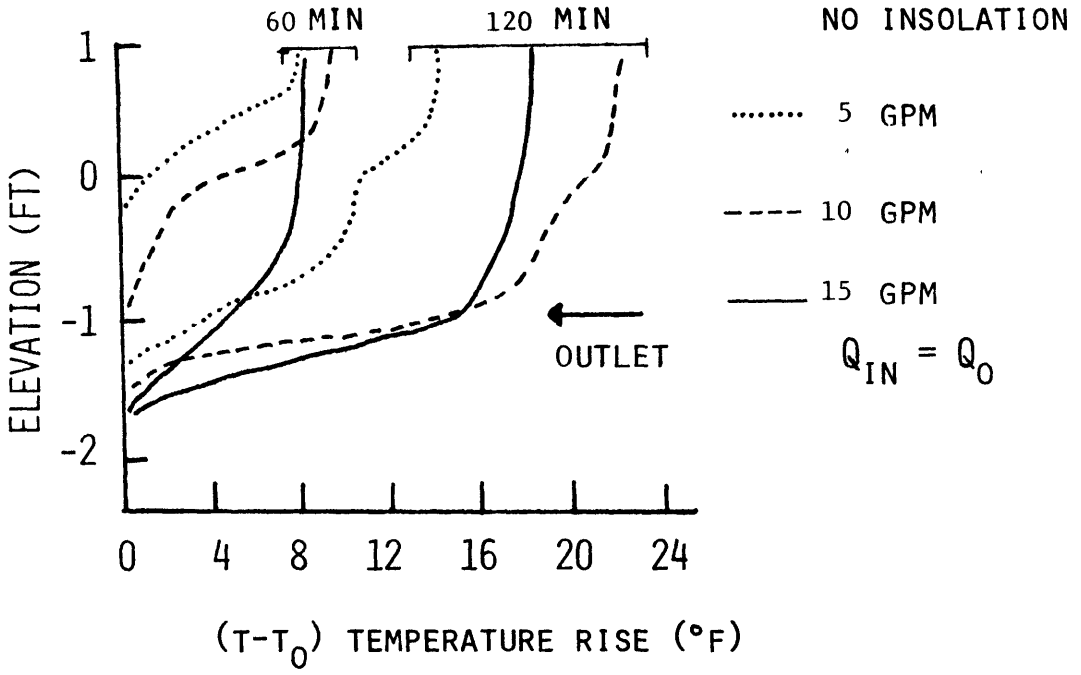

a) Effect of flow rate on temperature distribution

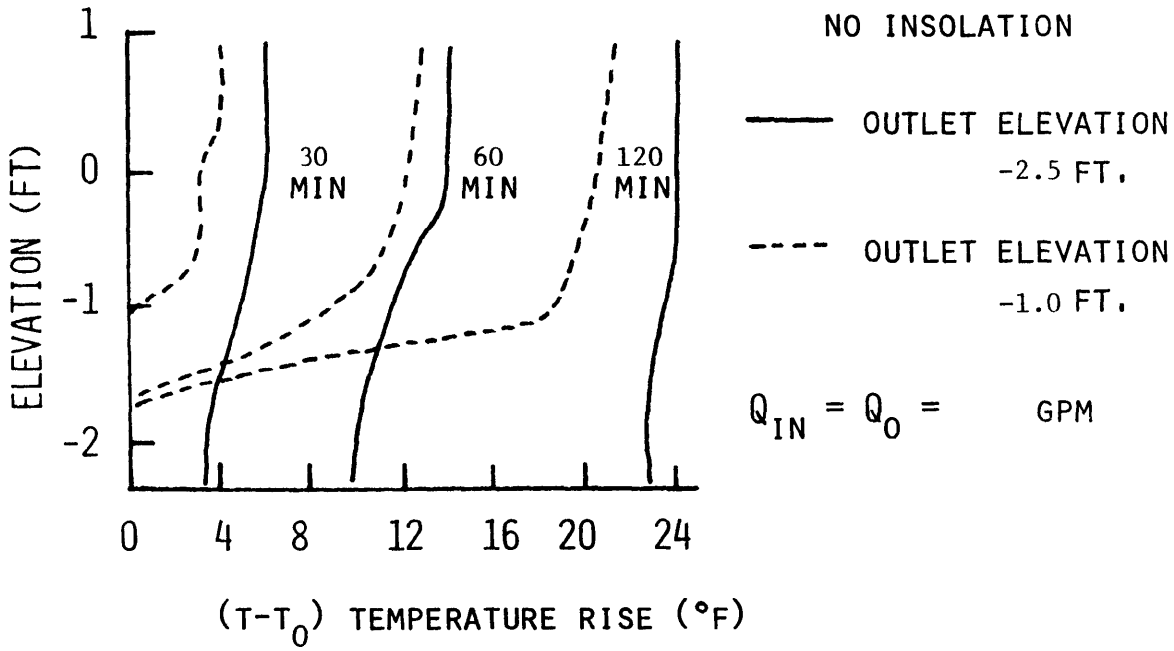

b) Effect of outlet elevation on temperature distribution

Figure 3-2 Effect of Flowrate and Outlet Elevation on the Temperature Distribution in the M.I.T. Reservoir Flume

outlet elevation on the temperature distribution. A submerged outlet draws the warmer surface water down at a velocity proportional to the flow rate. When the thermocline is at the elevation of the outlet, the strong temperature gradient results in a very narrow withdrawal layer which prevents further downward development of the interface.

The vertical transport of heat by advection is often large enough to dominate the transport of heat by diffusion, especially when the reservoir has a deep outlet. By non-dimensionalizing the governing equation, Equation (3-1), the relative influence of heat transport by advection compared to heat transport by diffusion in a given lake or reservoir may be determined. If the scaling parameters selected are Q, the discharge rate, D, the depth at which the outlet is located, A, the horizontal cross-sectional area at the depth of the outlet, E, the vertical diffusivity and $\phi_o/\rho c$ the non-dimensional governing equation is

$$\frac{\partial T_*}{\partial t_*} + \frac{1}{A}\frac{\partial}{\partial z_*} Q_{v_*} T_* = \left[\frac{AE}{DQ}\right] \frac{1}{A_*}\frac{\partial}{\partial z_*} A_* E_* \frac{\partial T_*}{\partial z_*} + \left[\frac{D}{A^{1/2}}\right] \frac{u_{i_*} T_{i_*}}{L_*} - \left[\frac{D}{A^{1/2}}\right] \frac{u_{o_*} T_*}{L_*}$$

$$+ \frac{\partial \phi_{z_*}}{\partial z_*}$$

Non-dimensional variables are indicated by an asterisk. Two dimensionless quantities are obtained. The quantity $\frac{D}{A^{1/2}}$ is a geometric shape factor. The quantity $\frac{AE}{QD}$ is the ratio of the rate of heat transport by diffusion to the rate of heat transport by advection. When $\frac{AE}{QD} << 1$, advection dominates diffusion, while when $\frac{AE}{QD} >> 1$, diffusion dominates advection. When $\frac{AE}{QD}$ is of the order of one, the transport mechanisms are competitive.

A comparison of model predictions for two reservoirs with different outlet conditions illustrates the use of this parameter.

The outlet of Fontana Reservoir, located on the Little Tennessee River in North Carolina, is approximately 60 meters beneath the surface. The reservoir has a volume of 2×10^9 m^3 and an average outflow rate of 8×10^6 m^3/day. Applying Orlob's criteria for stratification, Equation (1-1), to the reservoir gives $\mathbb{F}_D = 0.01$, therefore a one dimensional model is applicable. Predicted and measured profiles in Fontana Reservoir, Figures 3-3 and 3-4 (from Huber and Harleman (1968)), show that the role of advection in transporting heat vertically downward dominates over diffusion. An increase in the diffusion coefficient by a factor of 100 results in very little change in the predicted temperature profiles. With E equal to molecular diffusion (.0125 m^2/day), $\frac{AE}{QD} = 7 \times 10^{-4}$, while with E equal to 100 times molecular diffusion, $\frac{AE}{QD} = 7 \times 10^{-2}$, indicating that in both cases advection dominates diffusion.

A second, hypothetical reservoir located in the mid-Atlantic states has a volume of 2×10^8 m^3, a surface outlet ($D \simeq .5$ m) and an average release of 5×10^5 m^3/day. Predicted temperature profiles accounting for inflows and outflows are essentially the same as predicted profiles neglecting inflows and outflows. Figures 3-5 through 3-8 show that, when there is no through flow, increasing the diffusion coefficient by a factor of 50 results in large differences in the predicted temperature profiles. The figures should be read by relating pairs of curves, A and C or B and D, having equal values of the extinction coefficient. With E equal to molecular diffusion, $\frac{AE}{QD} = .15$, while with E equal to 50 times molecular

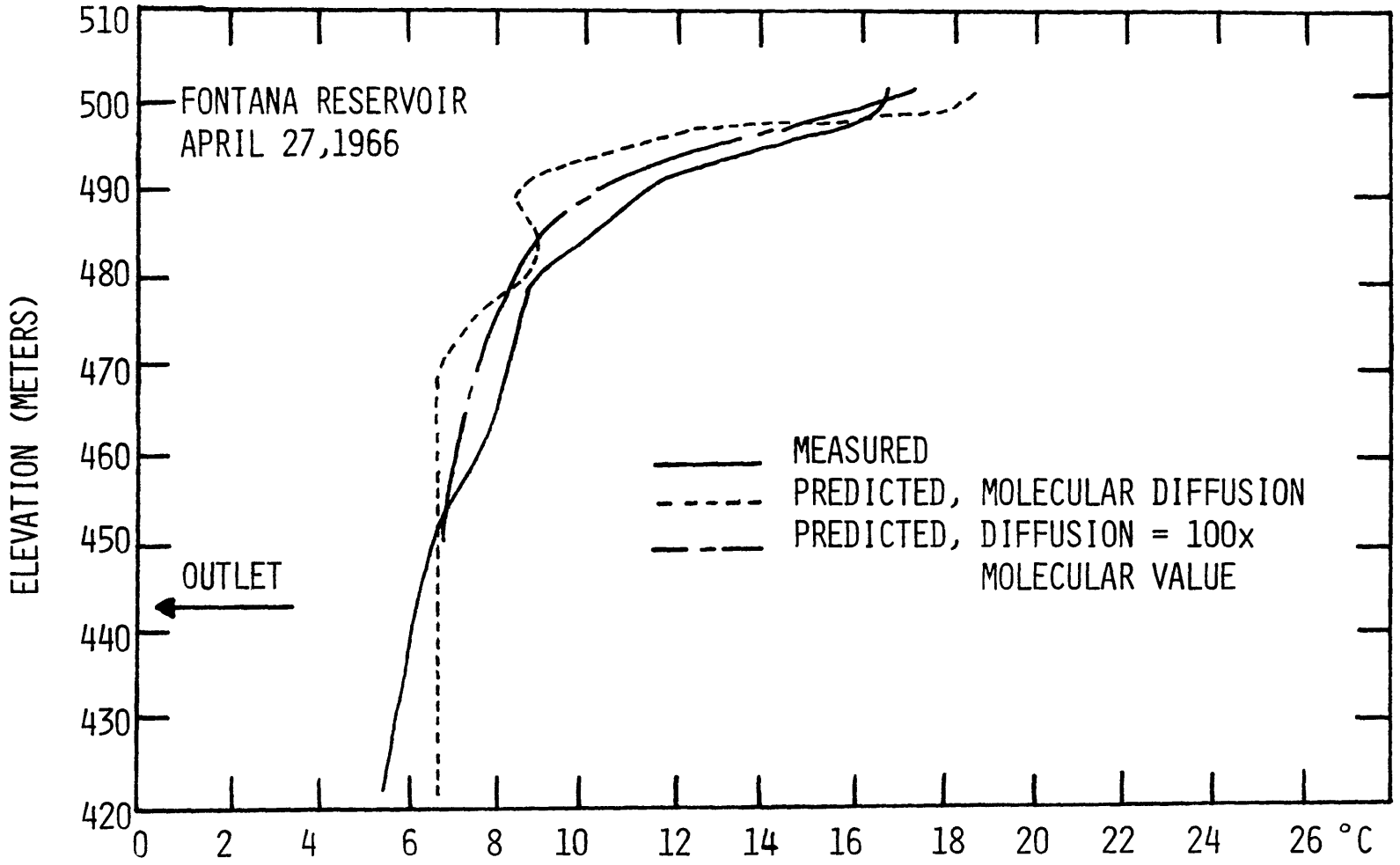

Figure 3-3 Comparison of Predicted Temperature Profiles in Fontana Reservoir Using Different Diffusion Coefficients

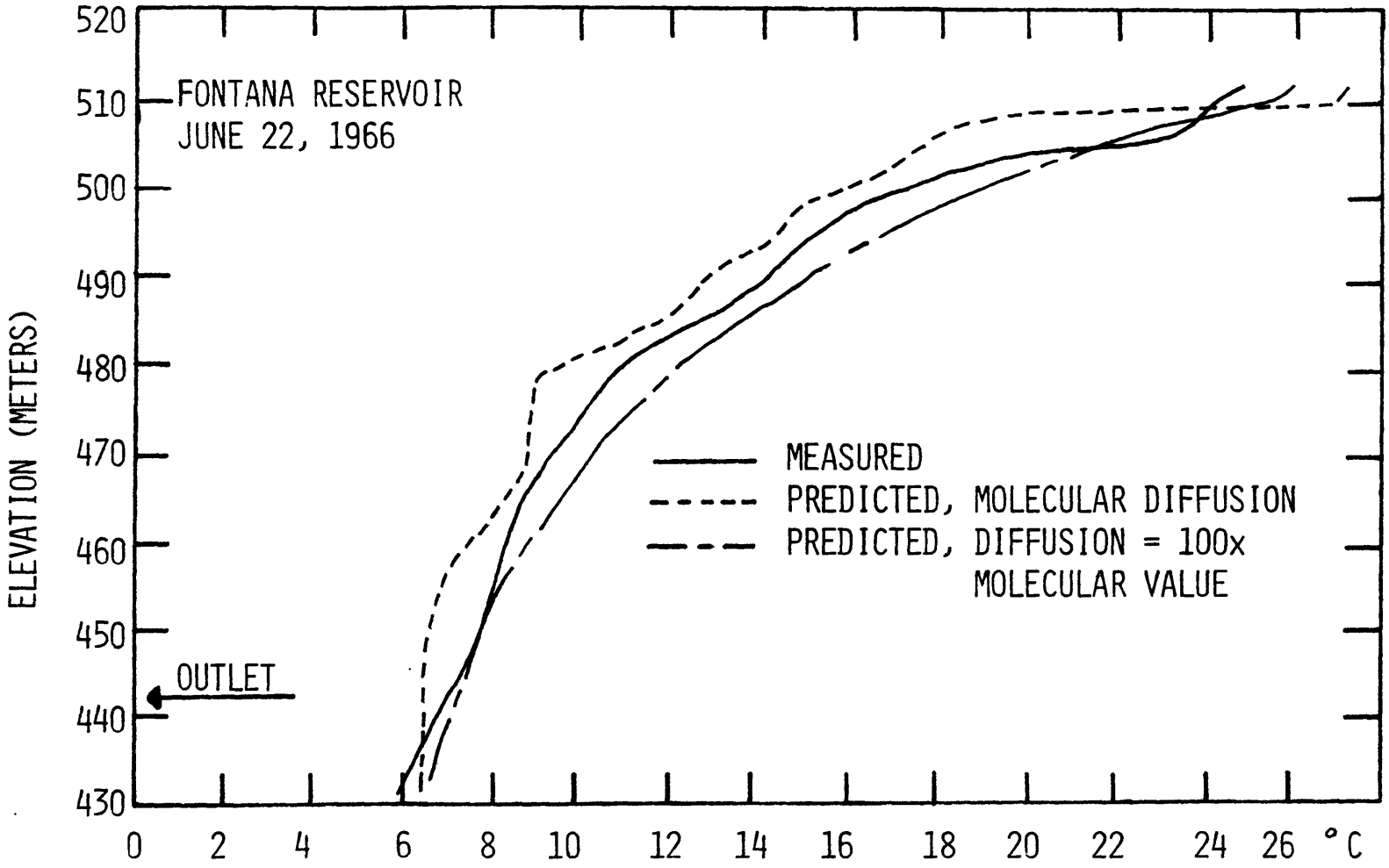

Figure 3-4 Comparison of Predicted Temperature Profiles in Fontana Reservoir Using Different Diffusion Coefficients

diffusion, $\frac{AE}{QD} = 7.5$, indicating that in both cases diffusion is important.

It is important when predicting the temperature structure of a deep reservoir or lake to know the magnitude and elevation of the inflows and outflows. In water bodies with surface outlets there may be little downward transport of heat by advection, especially if the flows are small, and thus accurate knowledge about the other heat transport mechanisms is important.

3.3 Vertical Diffusivity

The M.I.T. Reservoir Model has the option of including a depth independent vertical turbulent diffusivity, which may be any arbitrary multiple of molecular diffusivity. As shown in Figures 3-3 and 3-4, when the model is applied to a reservoir with through flows, the predicted profiles are relatively insensitive to the value of the turbulent diffusivity within the range of one to one hundred times the molecular value. However, when the model is applied to a lake, with no through flow as in Figures 3-5 through 3-8, the predicted profiles are so sensitive to the value of the vertical diffusivity that choosing a value of vertical diffusivity greater than molecular amounts to tuning the profiles to the data in some average sense. Therefore, in lakes it is important to represent the effects of turbulence on the temperature profile. This can be done with a time-varying depth-dependent turbulent diffusion coefficient or with an explicit time-dependent wind mixing scheme. These approaches will be discussed further in Chapter V.

The heat content of a water body can be computed from the temperature

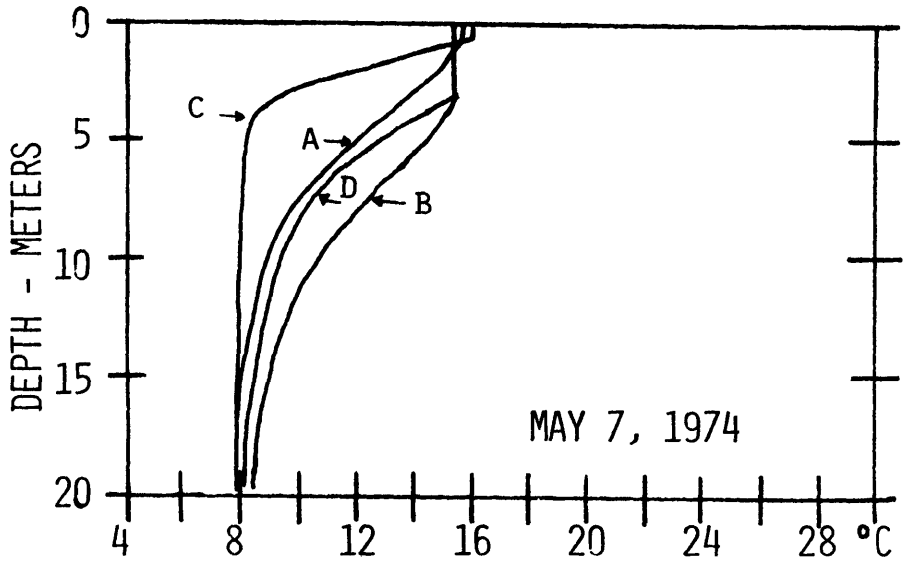

Figure 3.5 Comparison of Predicted Temperature Profiles Using Different Diffusion and Extinction Coefficients

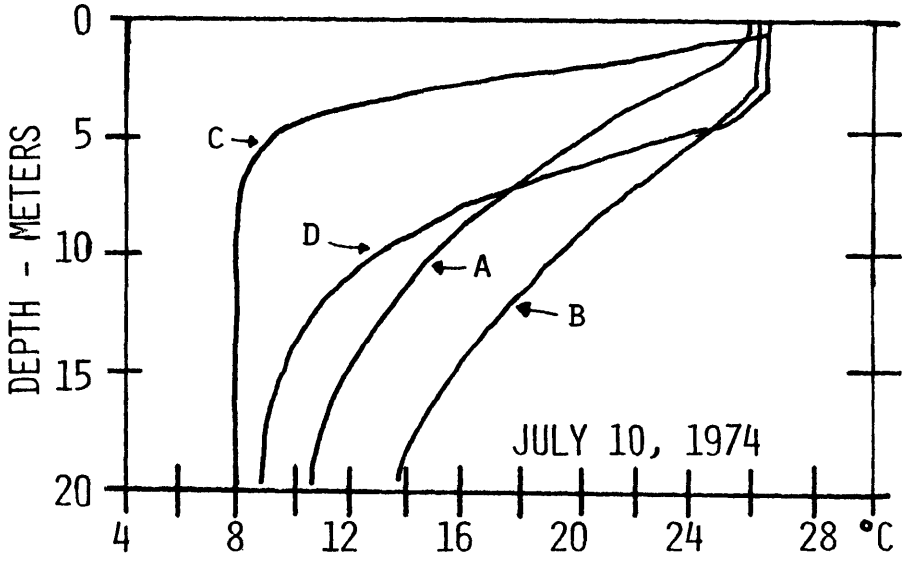

Figure 3.6 Comparison of Predicted Temperature Profiles Using Different Diffusion and Extinction Coefficients

A 50x molecular diffusivity
$\eta = 1.0\ m^{-1}$

B 50x molecular diffusivity
$\eta = 0.125\ m^{-1}$

C molecular diffusivity
$\eta = 1.0\ m^{-1}$

D molecular diffusivity
$\eta = 0.125\ m^{-1}$

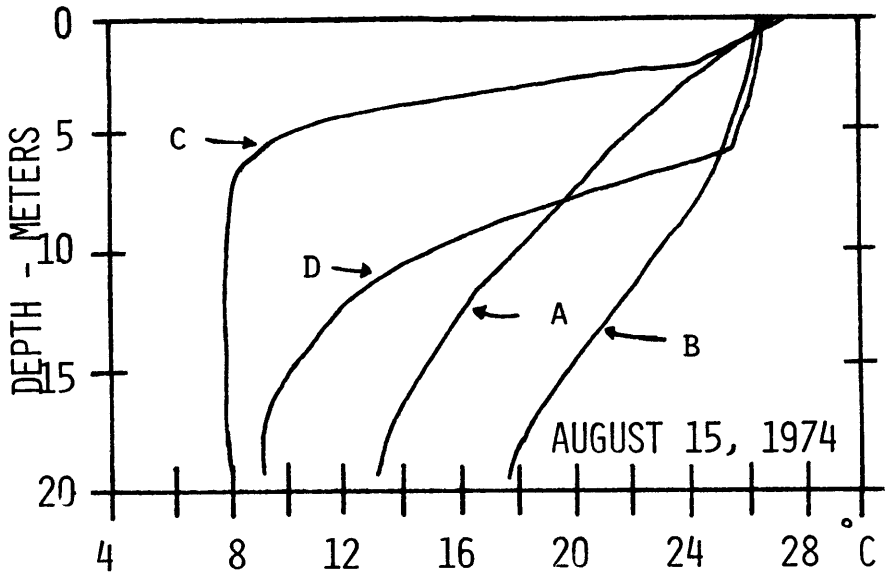

Figure 3.7 Comparison of Predicted Temperature Profiles Using Different Diffusion and Extinction Coefficients

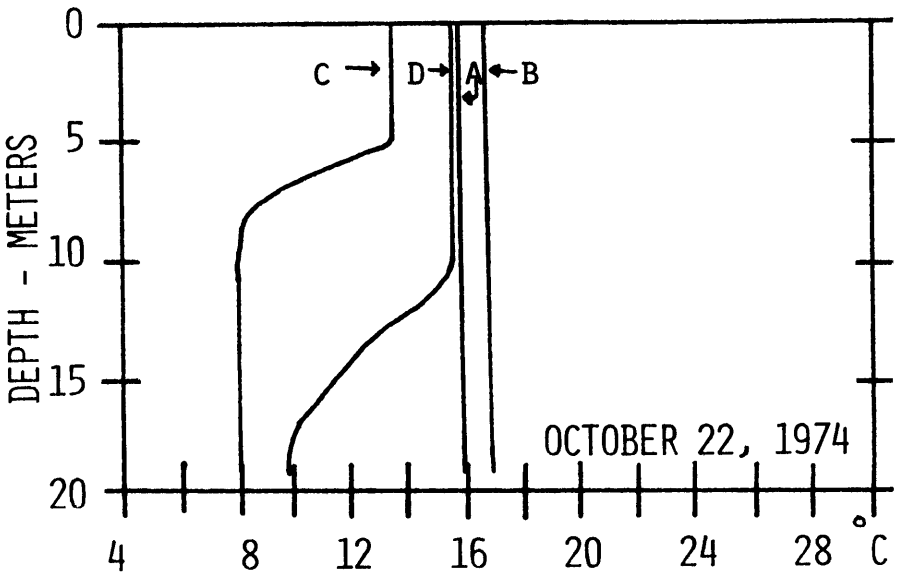

Figure 3-8 Comparison of Predicted Temperature Profiles Using Different Diffusion and Extinction Coefficients

A 50x molecular diffusivity
$\eta = 1.0\ m^{-1}$

B 50x molecular diffusivity
$\eta = 0.125\ m^{-1}$

C molecular diffusivity
$\eta = 1.0\ m^{-1}$

D molecular diffusivity
$\eta = 0.125\ m^{-1}$

profile and the area-depth relationship. Figures 3-5 through 3-8 indicate that by changing the vertical diffusivity (or the extinction coefficient) large differences in the predicted heat content can be caused without influencing the surface temperature very much. Figure 3-9 shows the time history of the heat content of the lake in case A and case C. The difference in heat content is due to different values for the surface heat fluxes that are functions of surface temperature, e.g. evaporation, conduction and back radiation. In order to determine the relative importance of each of these fluxes in causing a difference in heat content, consider the difference in heat content between case A and case C. The upper solid line in Figure 3-10 shows the time history of the difference in the heat content for the two cases. The difference between the combined evaporative and conductive heat losses and the difference between the back radiation heat losses for case A and case C have been computed. As expected from conservation of energy considerations, the sum of the cummulative difference in evaporation, conduction and back radiation losses is equal to the difference in heat content. Figure 3-10 indicates that the difference in heat content is principally due to the difference in the evaporative-conductive heat losses. The small difference between the predicted surface temperatures is due to the fact that the surface temperature is primarily determined by the meteorological conditions. Persistent small differences in surface temperature can account for large variations in the heat content.

3.4 Extinction Coefficient

The reciprocal of the extinction coefficient is a measure of the depth of penetration of solar heating. In clear water short wave radiation is

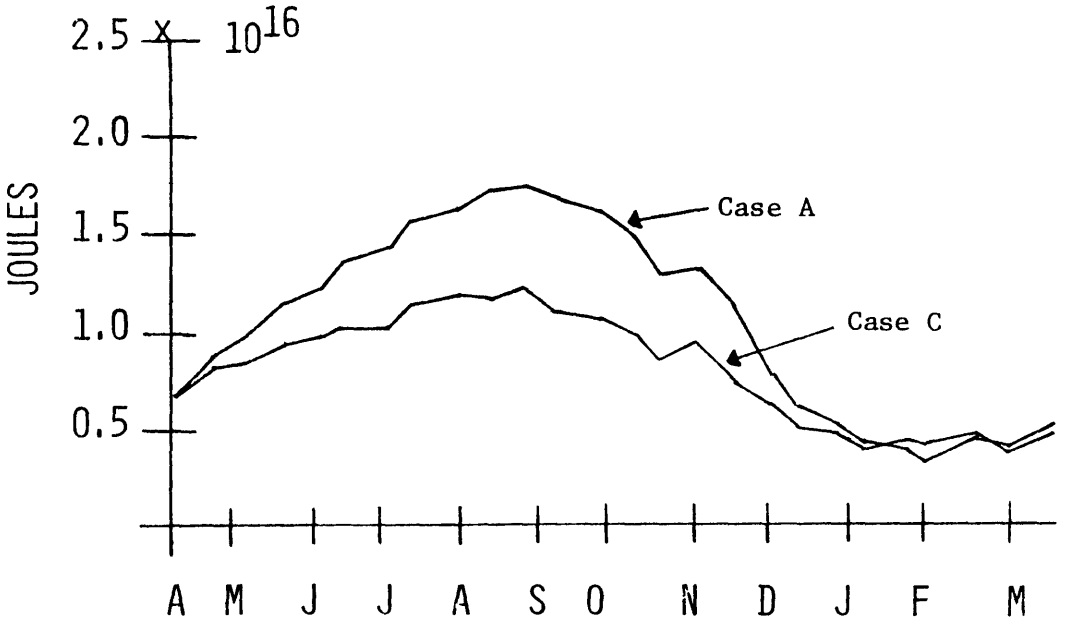

Figure 3-9 Comparison of the Heat Content in Case A and Case C

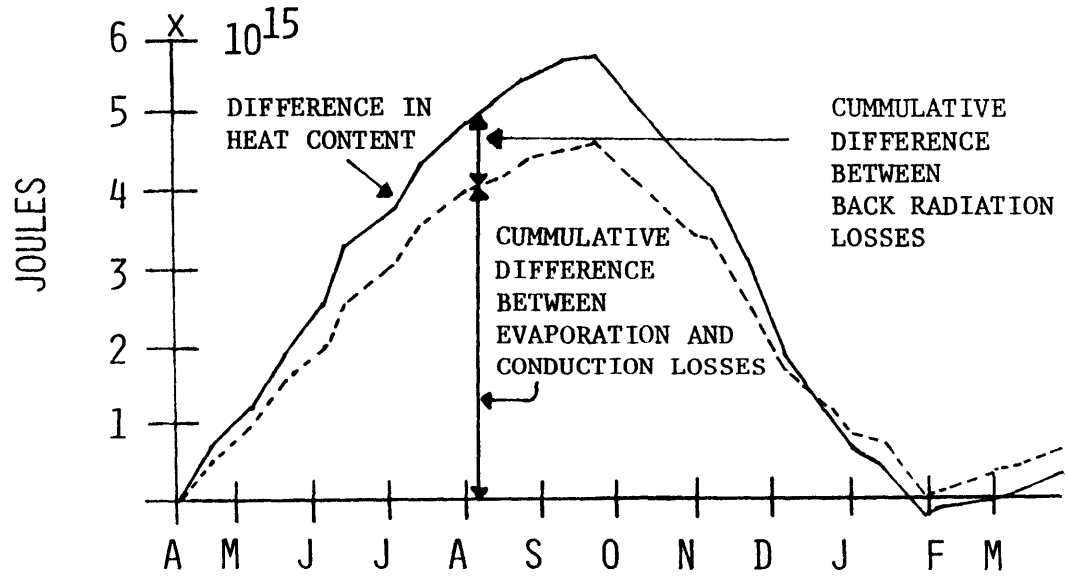

Figure 3-10 Comparison of the Difference in Cumulative Surface Heat Losses Between Case A and Case C and the Difference in Heat Content

transmitted to large depths, causing deep heating and small gradients while in turbid water, the depth of penetration is small and steep gradients develop. The extinction coefficient for distilled water is .03/m and for Lake Tahoe, noted for its exceptional clarity, it is .08-.1/m. Turbid lakes may have extinction coefficients of the order of 1-2/m.

Pairs of temperature profiles computed with no advection, A and B or C and D, having equal diffusivities and extinction coefficients of 0.25/m and 1/m are shown in Figures 3-5 through 3-8. These values are characteristic of the range of values observed in nature. As is the case for diffusivity, the value of the extinction coefficient influences the heat content of a lake, without causing significant differences in the surface temperature for the reasons mentioned previously. It is important, therefore, to use a value of the extinction coefficient determined by field measurements using the Sechi disk.

3.5 Time Step

Meteorological data is usually available as daily averages or as three hour averages. Since the cost of running a model is directly related to the number of time steps in the calculations, the sensitivity of the predicted profiles to the time scale of the transient meteorology is of interest. Figure 3-11 compares a temperature profile predicted using daily averaged meteorology and a corresponding model time step of one (1.0) day with the profiles predicted for that day using three hour averaged meteorology and a model time step of three hours (0.125 day). It shows that the model feels the influence of diurnal meteorological fluctuations only near the surface. This is in accord with observations. Long-term simulations of

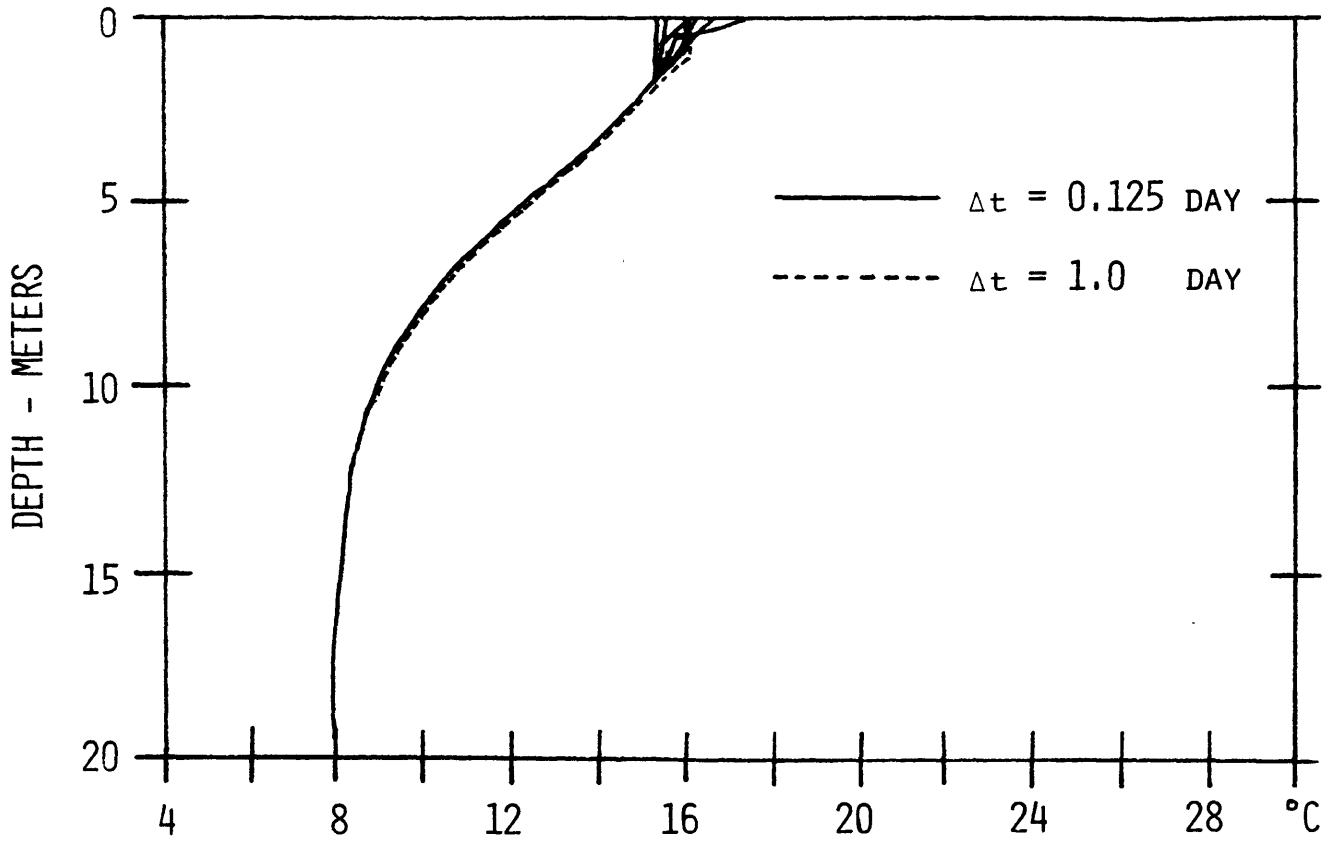

Figure 3-11 Comparison of Predicted Temperature Profiles Using Different Time Steps (50x molecular diffusion, $\eta = 1.0\ m^{-1}$)

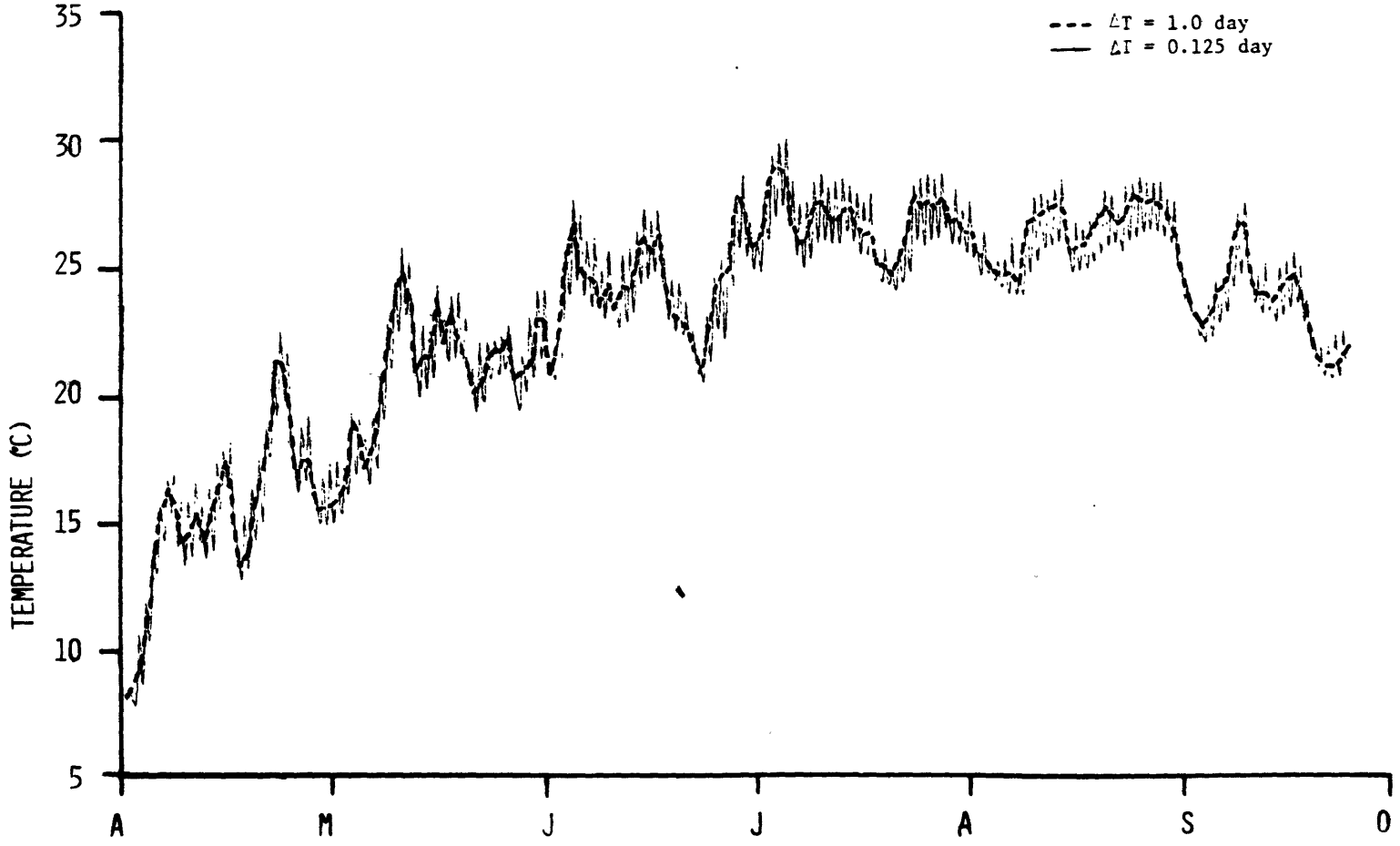

Figure 3-12 Comparison of the Effect of Time Step on the Surface Element Temperature. Surface Element Thickness = .6 m, 50x molecular diffusivity, $\eta = 1.0\ m^{-1}$

the surface temperature using different time steps corresponding to different averaging periods for the meteorology are shown in Figure 3-12. The computed variation in surface temperature over a day is between 2-3^{o}C. Thus, unless diurnal temperature fluctuations in the upper 2-4 meters of a water body are of specific interest, the use of daily averaged meteorological inputs with a corresponding time step is adequate.

3.6 Summary

A dimensionless parameter, $\frac{AE}{QD}$, which is a measure of the relative importance of advection and diffusion as heat transport mechanisms has been defined. When deep outlets release substantial flows from a reservoir, the temperature structure is dominated by advection; thus in this case it is more important to model advection than it is to represent the vertical diffusivity accurately. When there is little through-flow, as in a lake, or the only releases from a reservoir are from surface outlets, vertical diffusivity becomes significant and the representation of the vertical diffusivity governs the predicted temperature profile. Thus, when vertical diffusivity is a significant heat transport mechanism, it is important to model sources of turbulence other than convection, especially during the early part of the heating season when convective mixing is generally absent. The major source of turbulence which has been omitted thus far from the M.I.T. Reservoir Model is wind mixing. The remainder of this investigation will focus on the development of a mathematical representation of the influence of wind mixing.

CHAPTER IV

REVIEW OF LAKE AND RESERVOIR MODELS

Mathematical models for the time-dependent thermal structure of lakes and reservoirs range from phenomenological descriptions of the general seasonal behavior (Hutchinson (1957)) to numerical models that calculate the temperature distribution and flow pattern in a water body at intervals of a minute or less. Numerical models of water bodies can be divided into three groups depending on the length of the time step used. Models having a time step of a month (Beard and Willey (1970), Goodling and Arnold (1972), Burt (1974)), use time averaged data and are useful for predicting seasonal trends over the course of a simulation lasting several decades. However, they can not provide information about daily transient variations in the temperature structure. Models requiring a time step of the order of seconds or minutes provide a wealth of information about short term fluctuations in the flow pattern and surface configuration. They solve the Navier-Stokes equations (in two dimensions (Robert and Street (1975) or three dimensions (Spraggs and Street (1975))), the continuity equation and a heat flux equation simultaneously. These models are primarily concerned with the flow pattern and the surface configuration since it is the flow equations and not the heat flux equation that necessitates the short time step. These models are too expensive to use for long term simulations of the temperature structure of a water body. Models having a time step of a day strike a balance between the two extremes just mentioned. They can be

used to predict transient temperature variations but not internal flow patterns. They are, in general, inexpensive enough to use for simulations lasting a decade.

In this chapter, numerical models with a time step of the order of one day will be reviewed. The review will be limited to models applicable to lakes and to reservoirs which satisfy the stratification criteria

$$IF = \frac{LQ}{HV}\sqrt{\frac{\rho_o}{g\frac{\partial\rho}{\partial z}}} < \frac{1}{\pi}$$

and

$$h_m > \frac{4x10^{-7}W^2}{h}\quad\frac{\rho}{\Delta\rho}\quad\frac{L_t}{2}$$

where h_m is the epilimnion depth in mid-summer. (see Chapter I). Although no lake or reservoir has completely horizontal isotherms at all times during the year, for practical purposes, a time dependent, one-dimensional vertical temperature distribution is sufficient to define the thermal structure of water bodies that satisfy these criteria. Current one-dimensional models can be categorized into two classes, those that do not account for through-flow and thus are only applicable to lakes, and those that do account for through-flow and thus can be applied to reservoirs. Several models in each category will be presented in this section, starting with lake models.

4.1 Lake Models

4.1.1 Rahman and Marcotte Model

Rahman and Marcotte (1974) schematize lakes as having two distinct regions, an isothermal surface layer and a stratified diffusion layer beneath it (see Figure 4-1). Since the upper layer is isothermal, the heat exchange at the surface causes a uniform temperature change over the depth of the mixed layer. The governing equation for the surface layer is

$$\frac{\partial T_s}{\partial t} = \frac{Q_n}{\rho_s c z_s} \qquad (4\text{-}1)$$

where T_s is the surface temperature, ρ_s is the density of the water in the surface layer, c is the heat capacity of water and z_s is the depth of the surface layer. Q_n, the net heat flux into the surface layer, is the difference between the net surface heat flux, ϕ_n, and the heat flux into the diffusion layer, described below. It is assumed that all short wave radiation is absorbed in the surface layer.

The depth of the isothermal layer is assumed to vary linearly with time from a depth of 0 meters in January at ice melt to a depth of 100 meters in October. This restricts the model as formulated to lakes deeper than 100 meters, or the model must be stopped before October. The isothermal layer depth assumption is not representative of field data, since isothermal conditions are observed through March. The approach implies that the thermocline forms in all lakes at the same

time and descends at the same rate, regardless of the latitude and climate.

In the subsurface layer, heat transport occurs only by molecular diffusion. The penetration of short wave radiation is neglected, a reasonable assumption when the surface layer is deep, but not realistic at the start of the year when the surface layer is only a few meters deep. The governing equation for the diffusion layer is

$$\frac{\partial T}{\partial t} = \frac{\partial}{\partial z} \left[E(z,t) \frac{\partial T}{\partial z} \right] \qquad (4\text{-}2)$$

where E(z,t) is molecular diffusivity. Its weak dependence on T(z,t) is considered. As a boundary condition, the temperature at the top of the diffusion layer is set equal to the surface layer temperature. The temperature at the bottom of the diffusion layer is held constant, a reasonable assumption only if the lake is very deep. The rate of heat transfer from the surface layer to the diffusion layer varies with time and is related to the variation of the surface temperature with time.

The non-linear partial differential equations are solved using a similarity technique. The heat transport mechanisms eliminated by the initial assumptions of this model cannot be added to it easily because of the solution technique, so the primary criticism of this model is its inability to accommodate other heat transport mechanisms.

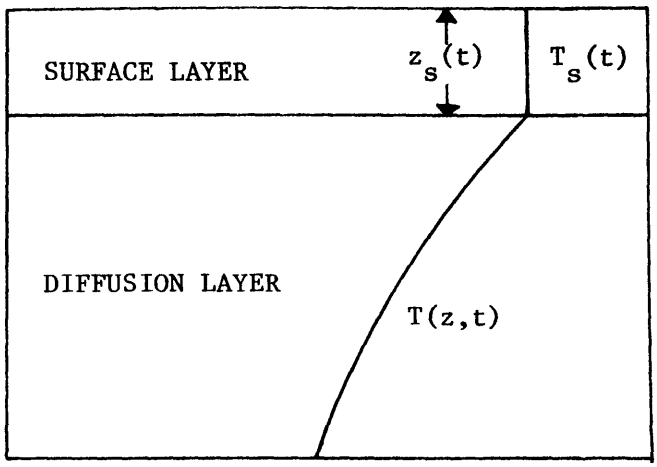

Figure 4-1 Schematic of Temperature Profile Computed by Rahman and Marcotte Model

4.1.2 Sundaram and Rehm (Cornell) Model

Sundaram and Rehm (1973) constructed a model of the temperature structure of deep lakes based on the interaction between wind-generated turbulence and the stratification of the water body. The interaction appears in the expression for E(z,t), the eddy diffusivity. The eddy diffusivity is taken as the product of the eddy diffusivity in the absence of stratification, E', given by

$$E' = cu_* \tag{4-3}$$

where c is a coefficient that depends on the lake (for Lake Cayuga $c = 2.82 \times 10^{-2}$ m) and $u_* = \sqrt{\tau_o/\rho}$ = friction velocity due to the stress exerted by the wind, and some function of the stratification. Sundaram

and Rehm suggest

$$E(z,t) = E'(1+\sigma Ri)^{-n} \qquad (4-4)$$

where Ri, the local Richardson number is

$$Ri = \frac{gz^2 \frac{\partial \rho}{\partial z}}{u_*^2}$$

and σ is an empirical constant equal to 0.1 and n is an empirical constant equal to 1. In the model, eddy diffusion is entirely responsible for the vertical transport of heat. Advection and the penetration of short wave radiation are neglected. The governing equation in the model is

$$\frac{\partial T}{\partial t} = \frac{\partial}{\partial z} \left[E(z,t) \frac{\partial T}{\partial z}\right]$$

Some restrictions on the applicability of Equation (4-4) are made. First, after the formation of a thermocline, the water below the thermocline is sheltered from the effects of the wind by the steep density gradient. Thus, Equation (4-4) is valid only above the thermocline, defined as the depth at which E attains its minimum value. In the hypolimnion, the value of E is set equal to the minimum value predicted by Equation (4-4). This value is constant with depth but not with time.

When convective mixing occurs because of density instabilities, convection is the dominant turbulent mechanism. It is not related to

the wind speed. In order to account for convective mixing, a large constant value of E, say E_m, is introduced into the eddy diffusivity-depth relation in those regions where there is a density instability. Equation (4-4) is matched to the value of E_m at the depth separating the stable and unstable parts of the profile so that E remains a continuous function of depth.

The neglect of the change in area with depth in the governing equation introduces a distortion in the vertical scale of the predicted temperature profile, which makes direct comparison of predicted and measured profiles difficult. Bedford and Babajimopoulis (1977) present a method to empirically relate the eddy diffusivity for a model with a constant area-depth relation to the eddy diffusivity for a model with variable area-depth relation, so that the same profile is obatined in both cases.

In the literature, there is not agreement on the form of the eddy diffusivity. Henderson-Sellers (1976) examined five proposed expressions for the neutral eddy diffusivity and suggests a dependence of E' on the wind shear and the current structure. Newbold and Liggett (1974) have suggested that the values $\sigma = 1.76 \times 10^{-3}$ and $n = 0.5$ be used in Equation (4-4). At present, it is concluded that there is no generally satisfactory specification of the turbulent diffusivity as a function of depth and time.

4.2 Reservoir Models

4.2.1 Orlob and Selna (WRE) Model

Although there are a number of important differences, the Orlob and Selna Model (1970) and the M.I.T. Reservoir Model (Ryan and Harleman (1971)) are conceptually very similar since both include the effects of the absorption and transmission of radiation, advection due to inflows and outflows, convection and diffusion. The governing equation is derived by considering an internal control volume as shown in Figure 3-1a. In the notation of this report, the governing equation of the Orlob and Selna model for an internal element is:

$$\frac{\partial T}{\partial t} + \frac{1}{A}\frac{\partial}{\partial z} Q_v T = \frac{1}{A}\frac{\partial}{\partial z} AE(z,t) \frac{\partial T}{\partial z} + \frac{Bu_i T_{in}}{A} - \frac{Bu_o T}{A} - \frac{1}{\rho c} \frac{\partial \phi_z}{\partial z} \qquad (4\text{-}5)$$

where E(z,t) is the eddy diffusivity. The other parameters are as previously defined. The equation is solved using an implicit finite difference scheme.

Inflows are assumed to enter the water column at the elevation at which the density is equal to the inflow density. Horizontal velocities are computed from inflow and outflow rates, assuming a uniform velocity throughout the inflow or withdrawal layers. The width of the inflow or withdrawal layer, w, is computed based on Debler's (1959) critical densimetric Froude number criteria

$$\frac{Q}{Bw^2}\left(\frac{\rho_o}{-g\frac{\partial\rho}{\partial z}}\right)^{1/2} = 0.24$$

Q is the flow and B is the element width at the outlet or inflow level. The value of w obtained is subject to the restriction that the layer can not extend through physical boundaries or the thermocline.

Vertical velocities are computed from the continuity equation for each element.

Orlob and Selna include convective mixing as a mechanism separate from "effective" diffusivity. Mixing is induced whenever there is a density instability. The elements adjacent to the instability are mixed, conserving the thermal energy of the system, until the instability is eliminated.

The "effective" diffusion coefficient can have a significant influence on the predicted profiles when the through flow is small. In general it is a function of space and time and cannot be determined independently of the environment. For an existing lake or reservoir, it can be determined using measured temperature profiles and solving Equation (4-5) for E. This approach has been applied to a number of water bodies and a characteristic shape, but not scale, can be discerned for the summer stratification period. The approximation to the general shape suggested by Orlob and Selna is

$$E(z,t) = E_o(t)e^{-\delta z} \qquad z \leq z_T \qquad (4\text{-}6a)$$

$$E(z,t) = E(z_T,t) \qquad z > z_T \tag{4-6b}$$

where $E_o(t)$ is the diffusion coefficient at the surface, z_T is the depth at which the thermocline is located and δ is a decay coefficient. The values of $E_o(t)$ and $E(z_T,t)$ depend on the particular reservoir. z_T is computed from the temperature profile and is defined as the depth at which the second derivative of T with respect to z is zero. δ is uniquely determined by the ratio $E(z_T,t)/E_o(t)$ and the depth z_T. Reported values of E_o are of the order of one hundred (100) to one thousand (1000) times the value of molecular diffusivity (0.012 m^2/day).

In an earlier version of the model, Orlob (1969) suggested another form for the "effective" diffusion coefficient based on the stability of the profile.

$$E(z,t) = E_o(t)e^{-\delta z} \qquad z < z_E \tag{4-7a}$$

$$E(z,t) = 1.5\text{x}10^{-8}\ m^{1.3}/\text{sec}\ S^{-.7} \qquad z_E < z < z_H \tag{4-7b}$$

$$E(z,t) = 2.5\text{x}10^{-4}\ m^2/\text{sec} \qquad z > z_H \tag{4-7c}$$

where S = stability of the water column = $-\frac{1}{\rho}\frac{\Delta\rho}{\Delta z}$. z_E is the depth at which $S = 10^{-6}\ m^{-1}$ while z_H is the depth at which $S = \left(\frac{1.5\text{x}10^{-8}\ m^{1.3}/\text{sec}}{2.5\text{x}10^{-4}\ m^2/\text{sec}}\right)^{1/.7}$. The value of δ is such that

$e^{\delta z_E} = \frac{1.5\times10^{-8}\ m^{1.3}/sec}{E_o} (10^{-6})^{-.7}$. In the absence of better data from field observations in the lake or reservoir being considered, Orlob suggests setting $E_o = 2.5\times10^{-4}\ m^2/sec$ and $\delta = 0$. Both forms of the "effective" eddy diffusivity are shown in Figure 4-2.

Orlob noted that the use of Equation (4-7) may not give an accurate representation of the temperature profile in the hypolimnion for the following reasons. If the value of E at the thermocline is used for the value of $E(z_T,t)$, E is too small in the hypolimnion. Heat is trapped in the surface layers and not enough heat is transported downward by turbulence. If the value of $E(z_T,t)$ is selected such that the surface temperature is represented accurately, the temperature at the thermocline is too high while the temperature in the hypolimnion is still too low. He concludes that Equation (4-7) is applicable only to reservoirs in which advective flows are the dominant vertical heat transport mechanism in the deep regions and thus an accurate representation of the eddy diffusivity is not critical.

It should be mentioned that improperly treated advection may appear in the diffusion coefficient. It is suggested therefore that before an empirical diffusion coefficient is resorted to, advection as well as known sources of turbulence such as convection and wind mixing be treated as quantitatively as possible. The necessity of using values of E determined from measured profiles weakens the predictive value of a model when there is no field data for a specific lake or reservoir available. Values of E_o derived for other lakes should be used with caution since

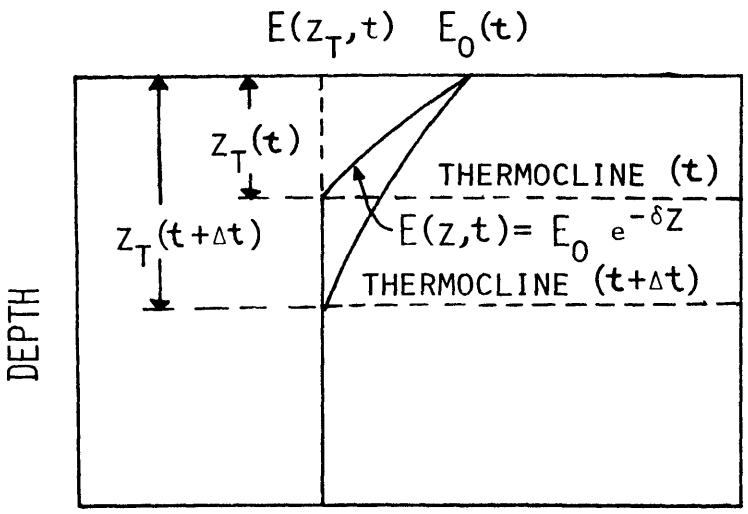

a) Definition sketch for Equation (4-6)

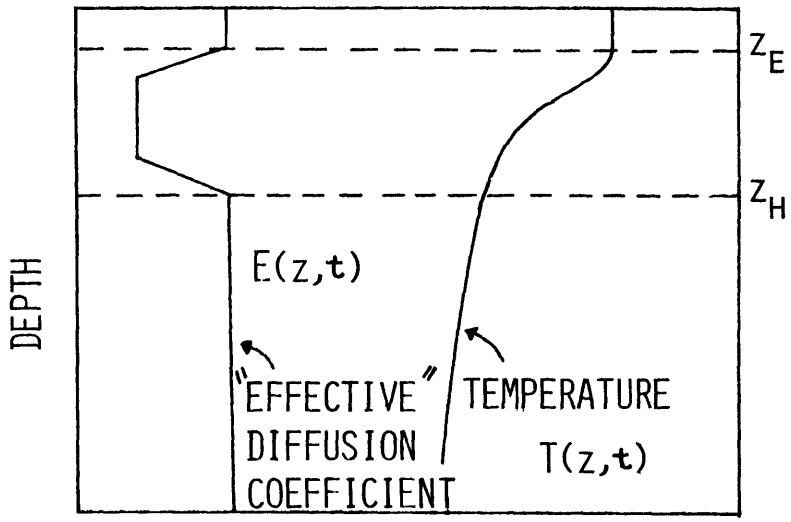

b) Definition sketch for Equation (4-7)

Figure 4-2 Definition Sketches for "Effective" Diffusion Coefficient vs. Depth, a) after Orlob and Selna (1970), b) after Orlob (1969)

each lake has a different internal circulation pattern influencing E. When there is field data on the temperature structure available for computing E(z,t), the extrapolation of the derived "effective" diffusion coefficient to periods other than the calibration periods removes the causal relationship between sources of turbulence and turbulent diffusion.

Parker, Benedict and Tsai (1975) report that this model is sensitive to the choice of the layer thickness for layer thicknesses in the range 0.6 meters to 2.0 meters. In general they found that the thicker the layers, the higher the temperature over the entire profile. Thus the choice of the element thickness must be made with care, based on a knowledge of observed profiles and on a consideration of the numerical stability criterion that the through-flow through an element during a time increment must be less than the volume of the element.

4.2.2 Imberger Model

The Imberger, Patterson, Hebbert and Loh (1977) model is based on surface heating and cooling, the absorption and transmission of radiation, inflows and outflows, diffusion and wind mixing. Lakes and reservoirs are schematized as a series of horizontal elements with different cross-sectional areas and thicknesses. A Lagrangian formulation is employed to keep track of the elements, eliminating the numerical dispersion intrinsic to Eulerian models. Because of the Lagrangian scheme, inflow corresponds to an insertion of volume and outflow to a reduction. Those elements experiencing a change in volume shift the

elevation of the elements above them. The volume of each element is kept within specified bounds by splitting or combining elements on the basis of volume as necessary. Vertical velocities are not computed since vertical advection of the fluid is associated with the motion of an element, not with the motion of fluid across the horizontal element boundaries.

Outflow is apportioned to the elements surrounding the outlet elevation assuming a cosine bell velocity distribution

$$u = u_{max}(\cos \frac{\pi(H-z)}{w} + 1) \tag{4-8}$$

where H is the total depth of the water body and z is the depth of the element. u_{max} is determined from conservation of mass. w is a measure of the withdrawal layer thickness and depends on the parameter $R = FGr^{1/3}$. F, the densimetric Froude number, is $Q/(NL^2)$, while Gr, the Grashoff number, is N^2L^4/ν^2. Q is the discharge, L the width of the outlet opening, N the Brunt-Vaisala frequency $(\frac{g}{\rho} \frac{\partial \rho}{\partial z})^{1/2}$ and ν the kinematic viscosity. Two regimes are distinguished

$$\begin{aligned} R \leq 1 \qquad & w = 2LF^{1/2} \\ R > 1 \qquad & w = 2LGr^{-1/6} \end{aligned} \tag{4-9}$$

Inflow is assumed to enter the water column at a depth such that the local Froude number is one. The inflow is distributed over the elements surrounding the inflow level using the cosine bell velocity

distribution given by Equation (4-8) with the layer thickness parameter for inflows given by

$$w = \frac{Q}{e}\left(1 - \frac{e}{L}\right) \tag{4-10}$$

Here Q is the inflow. e is a function of the parameter R and has the values

$$\begin{aligned} R &< 1 \qquad & e &= 0.57\ LR^{2/3}(t') \\ R &\geq 1 \qquad & e &= 0.44\ LR^{1/2}(t') \end{aligned} \tag{4-11}$$

where the dimensionless time $t' = tN/Gr^{1/6}$. The development of Equations (4-9), (4-10) and (4-11) can be found in Imberger, Thompson and Fandry (1976).

The representation of turbulence and mixing is composed of two parts. The influence of the wind is patterned on the Kraus and Turner (1965) mixed layer model for the ocean. The Kraus and Turner model is discussed in detail in Chapter V. In order to account for the long term effects of sporadic mixing events in the hypolimnion, a time varying, depth-independent eddy diffusivity is applied to the hypolimnion. The magnitude of the eddy diffusivity depends on the reservoir geometry, the stratification, the magnitude of the inflow and the wind speed. During periods with little inflow, the eddy diffusivity may be of the order of molecular diffusivity of heat, while during periods of high flow, it may be as large as one thousand (1000) times the molecular diffusivity.

During normal flow conditions, the value of the eddy diffusivity is of the order of the numerical dispersion of an Eulerian solution technique, thus the gain in using a Lagrangian scheme to compute the temperature profile is negligible. However, when the concentration of a tracer, such as salinity, is being computed, the Lagrangian scheme is superior since the molecular diffusivity of mass is two orders of magnitude smaller than the molecular diffusivity of heat.

Of the models discussed above, the author has easy access to and is most familiar with the M.I.T. Reservoir Model reviewed in Chapter III. Although treatment of wind induced mixing is missing in the present version of the model, it treats other heat transport phenomena in a correct causal manner. It will be used as the basis for the rest of the work in this report in which the objective is a model equally applicable to lakes and reservoirs.

CHAPTER V

REVIEW OF WIND MIXING

The influence of the wind in mixing the upper portion of a water body is an example of the general problem of the development and deepening of interfaces between fluids of different densities and the related problem of mass or heat flux across the interface. In the literature, this problem has been approached empirically, analytically and experimentally. In this chapter, results from all three approaches will be reviewed. Laboratory experiments investigating the mechanisms of mixing across density interfaces, in conjunction with observations in nature, have led to the development of models of the influence of the wind in the establishment and deepening of the thermocline in water bodies, usually in the ocean. Ocean models of this sort which do not consider Coriolis effects, and thus can be applied conceptually to smaller water bodies, will also be reviewed. In addition, an alternative approach to the representation of wind mixing, the use of a depth and time dependent turbulent eddy diffusivity will be examined.

5.1 Laboratory Studies

Numerous experiments have been performed to study directly the formation of mixed layers by turbulence and the rate of entrainment across the resulting density interface. These experiments provide evidence that the entrainment velocity, u_e, is related to the density stratification. In the lab, turbulence can be generated by mechanical

stirring or by the application of a shear stress that induces a mean turbulent flow. Experimental results for entrainment rate do not seem to be dependent on the manner in which turbulence is generated. The experimental results are applicable to the formation and deepening of an isothermal surface layer in lakes by the action of the wind.

Turner (1968) generated turbulence with a grid located a fixed distance from an interface between two layers of water with different densities. It should be noted that although the use of a grid is a convenient way to generate turbulence, it fixes the scale of the eddies. In order to study the influence of the molecular diffusivity on the rate of entrainment, Turner conducted experiments in which the density difference was due to the inclusion of salt in the bottom layer and experiments in which the density difference was due to a temperature difference. The molecular diffusivity of heat is approximately two orders of magnitude greater than the molecular diffusivity of mass (salt). Using an overall Richardson number based on the stirring frequency, n, and the length scale of the grid (and hence the eddies), ℓ, he found for both sets of experiments, for $Ri_n = \frac{g\Delta\rho\ell}{\rho\ell n^2} < 1$,

$$\frac{ue}{n\ell} \propto Ri_n^{-1} \tag{5-1}$$

where $n\ell$ is a scaling velocity, u_e, the entrainment velocity, is $\frac{dH}{dt}$, H is the depth of the mixed layer and $\Delta\rho$ is the density difference between the upper and lower layers. For $Ri_n > 1$, a different relation

is obtained when the density difference is produced by salt.

$$\frac{u_e}{n} \propto Ri_n^{-3/2} \tag{5-2}$$

His results are shown in Figure 5-1.

Kato and Phillips (1969) generated turbulence by applying a stress with a rotating plastic cover on the surface of saline water with a linear density stratification in an annular tank. The results were consistent with Equation (5-1). Kato and Phillips defined an overall Richardson number $Ri_* = \frac{g\Delta\rho H}{\rho u_*^2}$, where u_* is the friction velocity due to the surface stress $\sqrt{\tau_o/\rho}$, H is the depth of the mixed layer, and $\Delta\rho$ is the density jump at the interface, and found

$$\frac{u_e}{u_*} = 2.5Ri_*^{-1} = 2.5\ \frac{\rho u_*^2}{g\Delta\rho H} \tag{5-3}$$

The constant 2.5 has an uncertainty of about 30%. Although Kato and Phillips define the overall Richardson number differently than Turner and use a different scaling velocity, this only affects the proportionality constant, the functional dependence was not altered. If the initial stratification is linear, $\rho(z) = \rho_o - \beta z$, Equation (5-3) implies that depth of the mixed increases as

$$H(t) = u_* \left(\frac{15t\rho_o}{g\beta}\right)^{1/3} \tag{5-4}$$

Moore and Long (1971) applied a shear stress by injecting and withdrawing fluid from an annular flume. They examined entrainment in

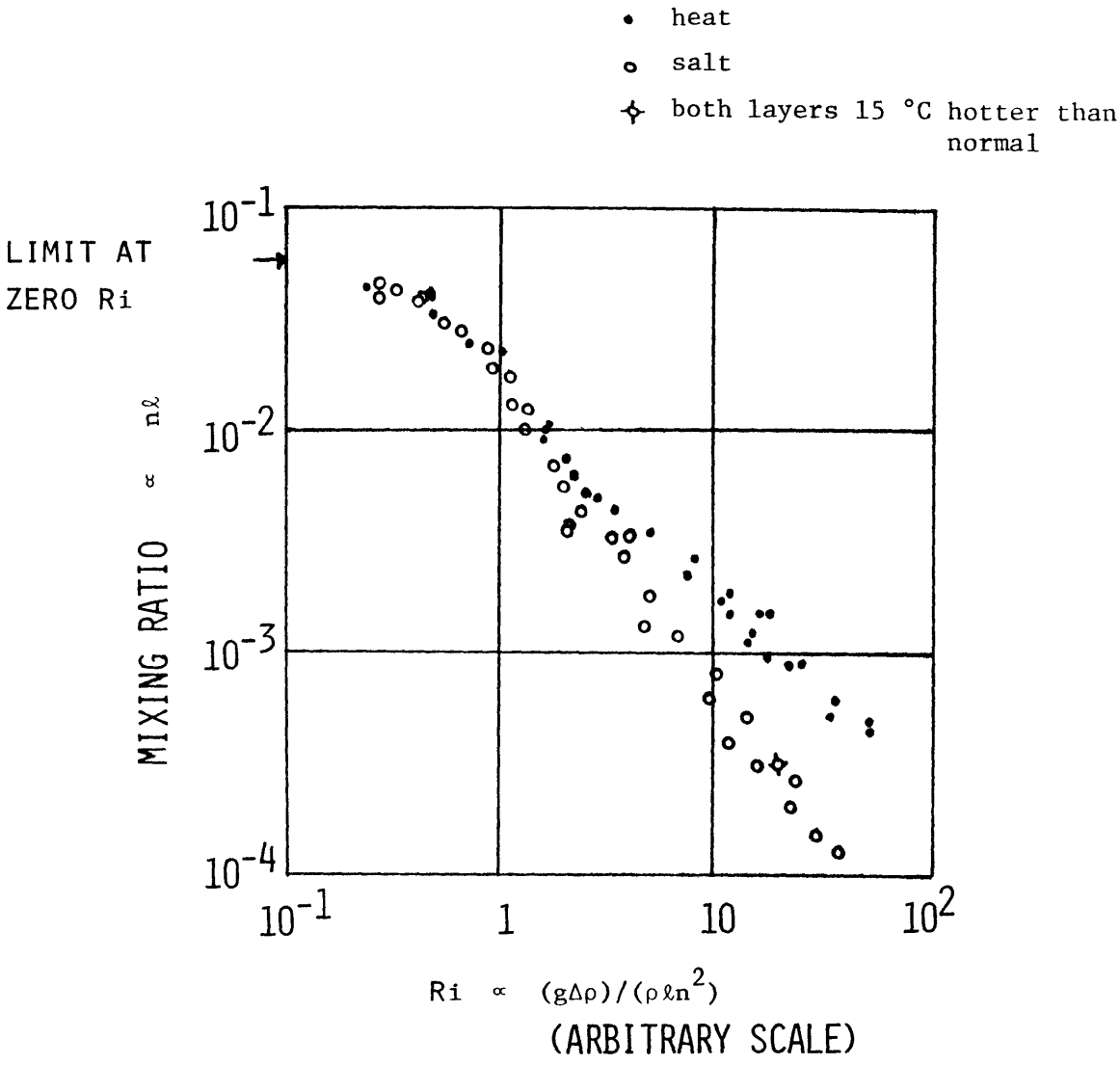

Figure 5-1 Turner's (1968) Measured Entrainment Velocities with Stirring on One Side of the Interface vs. Richardson Number

systems with either salt or temperature induced linear stratification. Their results agree with Equation (5-1).

Wu (1973) provided a shear stress by passing wind over a flume containing two layers of water of different density. He obtained the relation

$$\frac{u_e}{u_*} = 0.23 Ri_*^{-1} \tag{5-5}$$

The constant of proportionality is much smaller than that found by Kato and Philips because in Wu's experiment, the flow induced by the wind was confined to a thin surface boundary layer in the upper layer due to scale effects.

For small Richardson numbers all the investigators found the same functional dependence of the entrainment rate on the Richardson number, regardless of the molecular diffusivity of the substance responsible for the density stratification, namely

$$\frac{u_e}{u_{**}} \propto Ri_{**}^{-1} \tag{5-6}$$

where u_{**} is a scaling velocity and Ri_{**} is an overall Richardson number based on the scaling velocity u_{**}.

Turner originally explained the difference in the functional dependence he observed at large Ri_n for heat and mass in terms of an energy balance.

To explain the difference between the results with mass and with heat Turner (1968) states:

> "an element of heavy fluid in the form of a sheet ... is lifted out of the interface by a large eddy of the stirring motion, an action which involves a certain amount of mechanical work. If the velocity of ejection and the molecular diffusivity are high enough, this element becomes indistinguishable from its surroundings before it can fall back, and all the work done in lifting it appears as potential energy. This is the case for heat, so an energy argument is applicable. For the same velocity of ejection and a much lower diffusivity, on the other hand, a heavy sheet of fluid can fall back to the interface before it has diffused into its surroundings. For salt, therefore, only part of the work done remains permanently as potential energy, and the rest is dissipated in wave-like motions near the interface".

In the salt case, it is clear that an additional parameter, K_m the molecular diffusivity of the substance responsible for the density stratification, must be included in the analysis. An additional dimensionless group can be formed from the parameters. The grouping

$$Ri_{**}P_e = \frac{g\Delta\rho\ell_1^2}{\rho K_m u_1} \tag{5-7}$$

where Pe = Péclet number = $u_1\ell_1/K_m$, and u_1 and ℓ_1 are the velocity scale and the length scale of the energy containing eddies near the interface, is the appropriate choice. A function of the form

$$\frac{u_e}{u_1} = Ri_{**}^{-1} f(Ri_{**}Pe) \tag{5-8}$$

has the necessary features to describe Turner's experimental results and is consistent with the phenomenological description given above. $Ri_{**}Pe$ expresses the balance between buoyancy, which is tending to return an element of fluid to the interface, and diffusion, which causes it to merge with the turbulent layer. $Ri_{**}Pe$ is small when Ri_{**} is small or K_m is large. Pe effectively had two different values in Turner's experiments, most of the difference being due to the difference in the value of K_m for heat and mass.

The experimental work can be summed up as follows:

(1) An energy argument based on the conversion of kinetic to potential energy can be applied to entrainment across temperature induced density interfaces because a Ri_*^{-1} dependence holds,

(2) For large Pe, the basic rate of entrainment in the buoyancy controlled turbulent regime is proportional to $Ri_*^{-3/2}$.

Turner showed that Equation (5-3) is equivalent to making a statement about the rate at which the potential energy per unit horizontal area of the density field is increased by entrainment. In time Δt, a layer of thickness $\Delta H = u_e \Delta t$ and density $\rho+\Delta\rho$ is entrained and replaced by fluid with density ρ; the density difference is distributed throughout the upper mixed layer. The center of mass of the entrained fluid is therefore raised by H/2. The change in potential energy per unit area is

$$\frac{\Delta(P.E.)}{A} = \frac{\Delta\rho\Delta HgH}{2} = \frac{\Delta\rho u_e \Delta t g H}{2} \qquad (5\text{-}9)$$

Manipulating Equation (5-3) gives

$$\frac{\Delta(P.E.)}{\Delta t} = \frac{\Delta\rho A u_e g H}{2} = \frac{2.5}{2}\rho u_*^3 A \qquad (5\text{-}10)$$

The rate of work per unit area done by shear on the fluid below is $\tau_o u$ where u is the fluid velocity. A representative value for velocity in the tank experiments is the friction velocity $u_* = \sqrt{\tau_o/\rho}$. Thus the rate of work done by the shear stress is approximately

$$\tau_o u_* A = \rho u_*^3 A \qquad (5\text{-}11)$$

Equation (5-10) states that the rate of change of potential energy is equal to the rate of work done by the shear stress. This can also be rewritten in a form which expresses the ratio of the rate of change of potential and kinetic energies.

$$\frac{2.5\rho u_*^3 A}{2\Delta\rho g H A u_e (1/2)} = 1 \qquad (5\text{-}12)$$

In Equation (5-11), there is no depth dependence of the rate of work done by the surface shear stress. In experiments in which turbulence is generated by other means, Crapper and Linden (1974), Linden (1975) and Long (1975) have shown that the kinetic energy of the turbulence decays with depth. In those cases, the rate of change of potential energy due to entrainment is equal to the rate of work done at the interface.

5.2 Emperical and Analytical Studies

Blanton (1973) has shown a correlation between the stability, i.e. the square of the Brunt-Vaisala frequency., $N^2 = \frac{g}{\rho} \frac{\partial \rho}{\partial z}$, where g = gravitational acceleration and ρ = density, and the entrainment velocity, (the rate at which the thermocline moves downward) in various lakes. Although the results exhibit wide scatter because the correlation was developed without reference to the wind conditions, the correlation confirms that the rate of entrainment is a function of the Richardson number.

Phillips (1966) formulated the momentum equation for the development of flow in a stratified water body exposed to a wind stress at the surface. In order to solve the momentum equation it is necessary to assume similarity of velocity profiles in the water. Hansen (1975) asserts that in principle, the velocity in the surface layer can be related to the shear stress. He treats the case of flow in a deep two layered lake. Since the wind action tilts the isotherms, the lake is viewed in two dimensions. Making the assumptions:

i. uniform density in the upper layer,

ii. sufficient lake length for fully developed flow,

iii. Coriolis forces can be neglected,

iv. horizontal pressure gradients are small,

v. the Boussinesq approximation holds.

Hansen solves the momentum and continuity equations and shows that

$$\frac{u_e}{u_*} = 2.2Ri_*^{-1} \qquad (5\text{-}13)$$

where Ri_*, the overall Richardson number is defined as $Ri_* = \frac{g\Delta\rho H}{\rho u_*^2}$ H is the depth of the upper layer and $\Delta\rho$ is the density difference between the layers. Equation (5-13) agrees with Equation (5-3) deduced from laboratory experiments.

5.3 Bulk Ocean Models

Kraus and Turner (1967) developed a time dependent, one-dimensional model of the development of the seasonal thermocline in the ocean that includes wind mixing, surface heating and cooling, and the transmission and absorption of short wave solar radiation in the wind mixed layer. Advection is not considered. Their model is based on an energy argument which relates the change in potential energy of the water column to the input of kinetic energy by the wind. The potential energy changes both by changes in density due to heating and cooling and by entrainment of cooler water into the wind mixed upper layer. The model assumes (as discussed in Section 5.1) that the rate of kinetic energy input per unit area available for changing the potential energy per unit area is given by

$$\tau_o u_* = \rho u_*^3 \qquad (5\text{-}14)$$

where u_* is the friction velocity and τ_o is the surface shear stress due to the wind. Convective mixing of density instabilities is an

intrinsic part of the computation of the mixed layer depth. The lower region of the water remains at the initial temperature or the temperature of the mixed layer when it last reached the given depth. No vertical diffusion of heat was considered.

Denman (1973) expanded the Kraus and Turner model to include upwelling and considered the absorption and transmission of short wave solar radiation in the lower layer. Niiler (1975) considered the rate of production of turbulent kinetic energy: i) by shear at the mixed layer interface, ii) by the breaking of surface waves, and iii) by atmospheric pressure perturbations over the waves. He finds that the dominant rate of energy input at the mixed layer interface is $\tau_o u_*$, confirming Kraus and Turner's (1967) depth independent relationship given in Equation (5-14). Haney and Davies (1976) made simplifying assumptions in the solution for the mixed layer depth and computed the temperature profile in the lower region using an arbitrary vertical diffusion coefficient. Kim (1976) kept convective mixing of unstable density profiles distinct from the deepening effect of the wind in order to distinguish between modes of deepening and shallowing of the mixed layer.

5.4 Lake Models

Rather than solving the governing equations derived in a model such as the Kraus and Turner (1967) model numerically, Stefan and Ford (1975) use an alternating heating-mixing algorithm to represent the influence of the wind in the formation of the thermocline. The model is

intended primarily for application to lakes rather than reservoirs since advection is not considered. Because of the simplicity of the mixing algorithm, it will be described in detail.

The water body is schematized as a number of variable area, horizontally homogeneous elements. Surface heat transfer is considered, as well as the absorption and transmission of short wave solar radiation. The input of heat and wind energy are treated separately, even though they occur simultaneously. During each time step, the change in water temperature in each element due to heat input through the water surface is computed. The mixing algorithm is then applied to the updated temperature profile. During mixing, all changes in the density profile are associated with entrainment.

The mixing rule is based on the ratio of the turbulent kinetic energy input by the wind to the potential energy of the isothermal wind mixed layer relative to the element immediately below it. As shown in Figure 5-2, the summed potential energy of the i^{th} elements above the j^{th} element is defined as

$$P.E. = g \sum_{i} A(i)\Delta z(\rho(j,t)-\rho(i,t))D(i,t) \qquad (5\text{-}15)$$

where i runs through the elements above the j^{th} layer

$A(i)$ = area of the i^{th} element,

$\rho(i,t)$ = density of the i^{th} element at time t,

$\rho(j,t)$ = density of the element immediately below the mixed layer at time t,

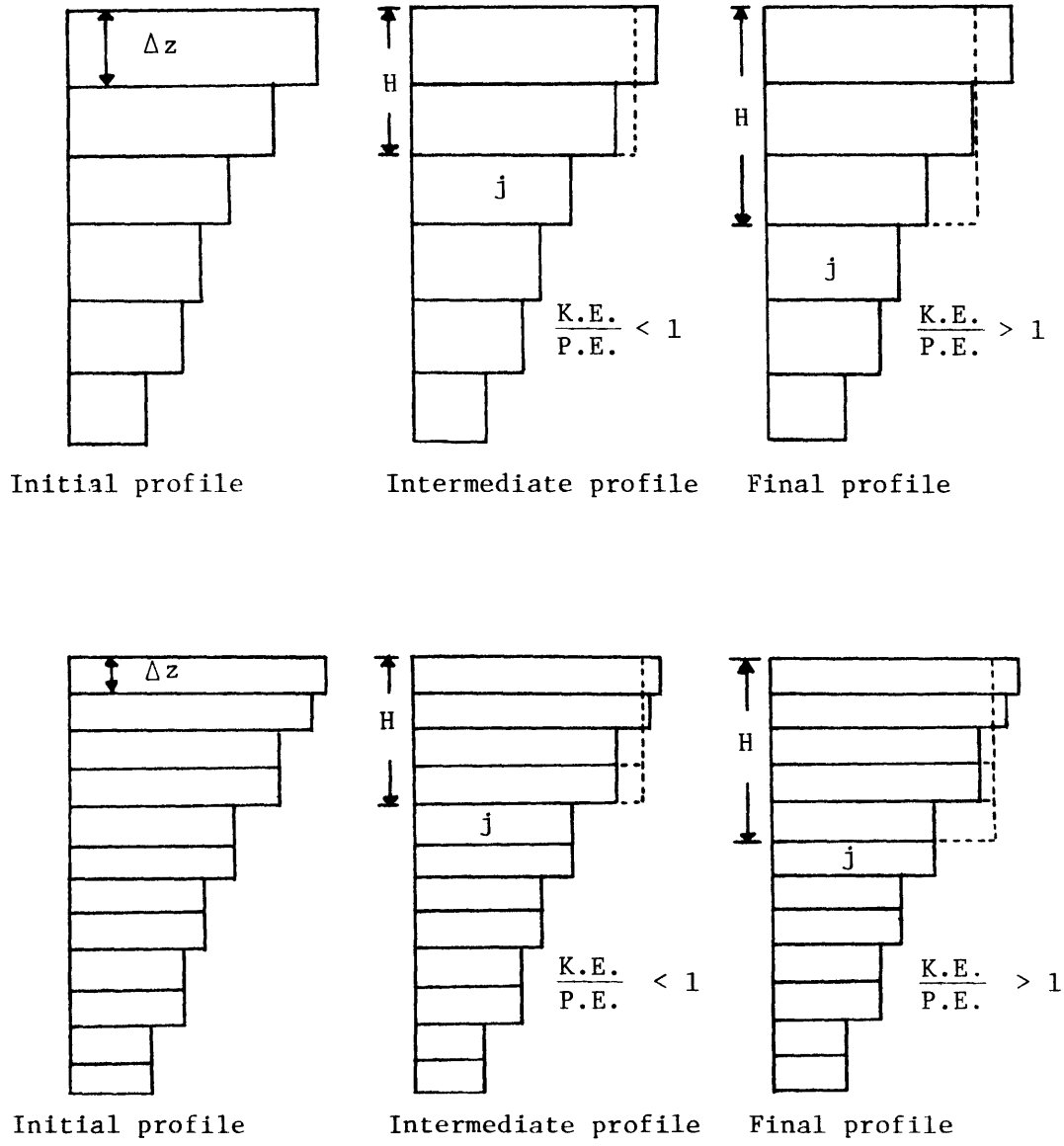

Figure 5-2 Illustration of the Sensitivity of the Stefan and Ford (1975) Wind Mixing Algorithm to Element Thickness

Δz = thickness of an element

$D(i,t)$ = distance between the i^{th} element and the j^{th} element at time t

Since the mixed layer is assumed to be isothermal, it can be shown that

$$P.E. = g\Delta\rho V_m \Delta z \frac{m}{2} = g\Delta\rho \bar{A} H \Delta z \frac{m}{2} \quad (5\text{-}16)$$

where m = the number of i^{th} elements in the mixed layer, $m\Delta z$ = depth of the mixed layer = H, V_m = volume of the mixed layer = $\bar{A}H$, where $\bar{A}$ is the average cross-sectional area of the mixed layer, and $\Delta\rho$ = density difference between the mixed layer and the j^{th} element immediately below. A measure of the energy input by the wind is;

$$K.E. = \tau_o u_* A_{surface} \Delta t = \rho u_*^3 A_{surface} \Delta t \quad (5\text{-}17)$$

Stefan and Ford state that when the energy ratio K.E./P.E. has a critical value, it is equivalent to the overall Richardson number relationship developed by Kato and Phillips (1969). Citing the work of Linden (1973), the critical ratio is taken as

$$\frac{K.E.}{P.E.} = 1 \quad (5\text{-}18)$$

Substituting Equations (5-16) and (5-17) into Equation (5-18) gives

$$\frac{K.E.}{P.E.} = \frac{\rho u_*^3 A_{surface} \Delta t}{\Delta\rho g \bar{A} H (1/2)} = 1 \quad (5\text{-}19)$$

Comparing Equation (5-19) and Equation (5-12), the analogous form of the Kato and Phillips relationship, it can be seen that the two equations are equivalent, within the accuracy of Kato and Phillips empirical constant, under the conditions that: i) there is no variation of area with depth; $\bar{A} = A_{surface}$, and ii) in each time step, after heating is applied to the profile, the depth of the mixed layer is zero. Then $H = 0+\Delta H = \Delta H = u_e \Delta t$.

The mixing algorithm states that if K.E./P.E. $<$ 1, there will be no mixing, while if K.E./P.E. $>$ 1, layers will be mixed one by one, and the ratio rechecked after mixing each layer, until the ratio becomes $<$ 1 (see Figure 5-2).

Because of the mixing algorithm employed, the mixed depth must be sensitive to the choice of element thickness. Consider the example illustrated in Figure 5-2. If the ratio K.E./P.E. is slightly greater than 1, the next element is mixed. Suppose that the element size is halved and the case run again. It is probable that mixing only the first of the two elements corresponding to the original thicker element would be sufficient to make the energy ratio less than 1. This locates the bottom of the mixed layer at a different depth than in the other case, and results in a different value for the temperature of the mixed layer. Stefan and Ford use a rather small distance increment, 0.25 meters, so the difference in the mixed depth and surface temperature is small. When typical field size elements of 1 to 2 meters are used, the problem may become more apparent.

An additional question raised by the mixing algorithm involves the approximation of the simultaneous input of wind and heat energy. Should heating or mixing be treated first? Predicted profiles are sensitive to order chosen, so some sort of iterative procedure would be indicated.

5.5 Variable Eddy Diffusivity Models

Attempts have been made to incorporate the influence of the wind in the temporal and vertical variations of eddy diffusivity. In general, measured temperature profiles have been used to tune predicted profiles by varying the eddy diffusivity with depth and time. Using this technique, Jassby and Powell (1975) show that beneath the thermocline the value of the eddy diffusivity is generally only 10 to 40 times the value of molecular diffusivity. Sweers (1970) finds a range for eddy diffusivity in the hypolimnion of various lakes of from 1 to 100 times the value of molecular diffusivity. In the epilimnion, the values are typically several orders of magnitude larger. In retrospect, this approach is not predictive.

Weigel (1964) reports that the eddy diffusivity in the surface region of the ocean has been considered to be a function of the wind strength. Computed values have shown considerable scatter and he proposes that one reason for the scatter is that eddy diffusivity is related more closely to the wave spectrum generated by the wind than to the wind itself. Thus not only are the wind strength and variability important, but the fetch and duration are also important. This technique

requires considerably more input data than do existing lake and reservoir models.

Henderson-Sellers (1976) has analyzed several empirical-analytic expressions for the eddy diffusivity in a lake. He follows the approach of Sundaram and Rehm (1971) and expresses the eddy diffusivity as the neutral eddy diffusivity, E', multiplied by a function of a stability parameter having the form of a Richardson number. He recommends a form of the neutral eddy diffusivity which is a function of the wind shear and the current structure. This requires a current model to be coupled with the temperature model of a lake, expanding greatly the scope of the problem.

Spalding and Svenson (1976) compute turbulent exchange coefficients from a turbulence closure model which solves the momentum equations and equations for the turbulent kinetic energy, K, and the dissipation of turbulent kinetic energy, ε. The model is not verified for buoyancy affected flows.

At present it is concluded that there is no generally satisfactory specification of the turbulent diffusivity as a function of depth and time.

CHAPTER VI

MODIFICATION OF THE MIT RESERVOIR MODEL TO INCLUDE WIND MIXING

In reservoirs, the dominant vertical heat transport mechanism is advection. By accounting for this mechanism, the M.I.T. Reservoir Model is able to predict temperature profiles in reservoirs in good agreement with measurements. In lakes, a dominant vertical heat transport mechanism is diffusion. At present, there is no generally satisfactory representation of the vertical eddy diffusivity as a function of depth and time. The M.I.T. Reservoir Model assigns an arbitrary constant value of the order of 50 to 100 times molecular diffusivity to the vertical eddy diffusivity. Sensitivity studies in Chapter III have shown that the predicted temperature profiles for a lake are very sensitive to the value of the vertical eddy diffusivity. The agreement between measured and predicted temperature profiles in lakes is not satisfactoy.

In this chapter, wind mixing concepts discussed in Chapter V will be incorporated into the M.I.T. Reservoir Model in place of the arbitary vertical eddy diffusivity. Molecular diffusivity is retained for computational convenience and for application of the model to laboratory measurements where turbulence is absent. Bulk ocean models cannot be used directly as lake models because lakes exhibit a variation of horizontal cross sectional area with depth which the bulk ocean models do not consider. The goal is a single model applicable to both lakes and reservoirs.

6.1 Proposed Numerical Formulation

In order to incorporate the influence of wind mixing directly into the governing equation for T(z,t), Equation (3-1), it would be necessary to express the wind mixing in terms of an eddy diffusivity. However, the demonstration by Kraus and Turner (1967) of the formation of an isothermal upper layer due to wind mixing is inconsistent with the Fickian diffusion term in Equation (3-1). For example, if $\overline{w'T'}$ represents the turbulent transport of heat, the Fickian analogy requires

$$E = \frac{\overline{w'T'}}{\frac{\partial T}{\partial z}}$$

and E becomes indeterminant as $\frac{\partial T}{\partial z} \to 0$ in the isothermal upper layer. An alternative, following the integral equation approach of Kraus and Turner's ocean thermocline model, was considered. The resulting equations for a lake or reservoir are much more cumbersome due to the presence of the through-flow terms and the variation of cross sectional area with depth. An iterative numerical approach in which heating and mixing in a given time step are carried out sequentially is adopted. The algorithms for the heating and mixing steps are described in detail below.

Conceptually, the sequential heating-mixing procedure is as follows. In each time step, the temperature profile from the previous time step is incremented by the various heat inputs. The wind mixing rule is then applied and the depth and temperature of the wind mixed layer are computed. The surface heat flux is recomputed using the temperature of the wind mixed layer. This quantity is averaged with the surface heat flux computed

using the surface temperature from the previous time step to obtain a new value for the surface heat flux. The temperature profile from the previous time step is reincremented by the various heat inputs using the new value of the surface heat flux. These steps are repeated until there is no change in the surface heat flux from one iteration to the next. This procedure is illustrated in Figure 6-1. Because of the necessity of dealing with heating and mixing separately and alternately, an implicit or iterative scheme for the computation of the heat input is required to avoid the accumulation of errors. This also avoids the problem of obtaining different results when the system is heated and then mixed or mixed and then heated.

6.1.1 Heating Algorithm

The equation governing the input of heat remains unchanged from the present model. Setting the eddy diffusivity, E, equal to the molecular diffusivity of heat, α, Equation (3-1) becomes

$$\frac{\partial T}{\partial t} + \frac{1}{A}\frac{\partial}{\partial z}(Q_v T) = \frac{\alpha}{A}\frac{\partial}{\partial z}\left(A\frac{\partial T}{\partial z}\right) + \frac{Bu_i T_i}{A} - \frac{Bu_o T}{A} - \frac{1}{\rho c}\frac{\partial \phi_z}{\partial z} \qquad (6\text{-}1)$$

The surface layer has an additional term due to surface heat exchange,

$$\frac{\beta\phi_{sn} + \phi_{an} - \phi_{br} - \phi_e - \phi_c}{\rho c \Delta z_s} \qquad (6\text{-}2)$$

In each time step Δt, Equations (6-1) and (6-2) are solved with an explicit, forward difference technique. All terms involving temperature are evaluated using the temperature from the previous time step, that is

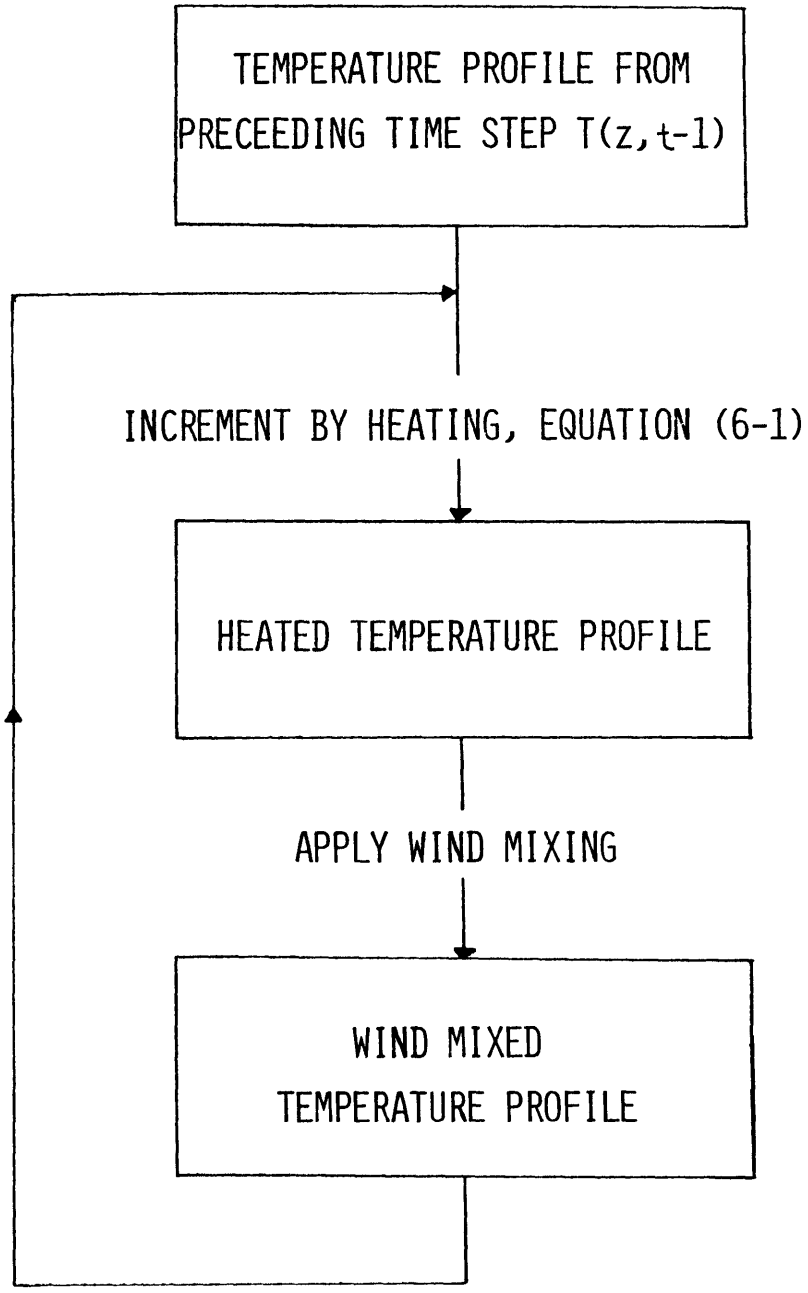

Figure 6-1 Schematic of Iterative Heating-Wind-Mixing Procedure

$$T(z,t) = T(z,t-1)+\Delta T(z,t-1) \qquad (6\text{-}3)$$

where $\Delta T(z,t-1) = \frac{\partial T(z,t-1)}{\partial t}\Delta t$. In particular, the surface heat fluxes at time t are computed by inserting $T_s(t-1)$ into the appropriate equations in Chapter II. A detailed description of the explicit finite difference formulation of Equation (6-1) can be found in Ryan and Harleman (1971).

6.1.2 Wind Mixing Algorithm

During a given time interval, the potential energy of the water column is altered by changes in density due to heating or cooling and by the re-arrangement of the density profile as fluid is entrained into the wind mixed layer. This can be expressed as

$$PE(t) = PE(t-1) + \frac{d(PE)^h}{dt}\Delta t + \frac{d(PE)^e}{dt}\Delta t \qquad (6\text{-}4)$$

where the superscript h refers to heating and the superscript e refers to entrainment. The use of Equation (6-1) in the heating algorithm accounts for the change $\frac{d(PE)^h}{dt}\Delta t$. Experiments discussed in Chapter V on the rate of entrainment from a stagnant lower layer by a turbulent upper layer, in the absence of heating and cooling, have shown that the rate of change of potential energy is equal to the rate of working of the shear stress due to the wind, or

$$\frac{d(PE)^e}{dt}\Delta t = \rho u_*^3 A\Delta t \qquad (6\text{-}5)$$

The wind mixing rule is based on Equation (6-5). It is assumed that in each time step, a steady state is reached in which Equation (6-5) is exactly satisfied. It is applied to the temperature profile after it has been incremented by Equation (6-1).

Since the shear stress is assumed constant over the time interval, the right hand side of Equation (6-5) is known. The problem is to compute the mixed layer depth that is associated with the given change in potential energy. In the context of the M.I.T. Reservoir Model, which schematizes a water body as a number of horizontal elements of thickness Δz, the depth of the mixed layer, H, must be expressed as

$$H = N\Delta z \tag{6-6}$$

where N is the number of elements of thickness Δz included in the mixed layer. Although N need not be an integer, the suggested technique will first take N to be an integer and later its fractional part will be determined. Because of the model structure, N cannot be less than 1.

For an arbitrary initial temperature distribution in a constant area system, N is found as follows (see Figure 6-2). First, the top element, element 1, is mixed with the element below it, element 2. The change in potential energy of this profile relative to the original profile is

$$d(PE)^{e}_{N=2} = Ag\Delta z(\rho_{(2)}-\rho_{(1)})\Delta z \tag{6-7}$$

The index refers to the element number, with 1 being the surface element. $d(PE)^{e}_{N=2}$ is compared to $A\rho u_{*}^{3}\Delta t$ and if

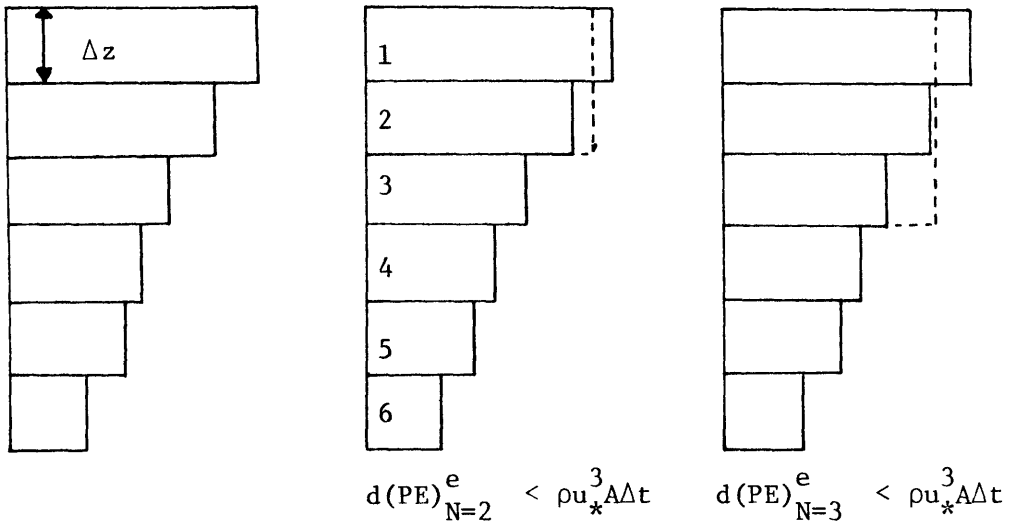

Figure 6-2 Schematic of Wind-Mixing Algorithm

$$d(PE)^{e}_{N=2} < A\rho u_{*}^{3}\Delta t \tag{6-8}$$

the next element is included in the wind mixed layer. In general, for N elements in the wind mixed layer, the difference in potential energy between the wind mixed temperature profile and the initial temperature profile is

$$d(PE)^{e}_{N} = \sum_{i=2}^{N} Ag\Delta z(\rho_{(i)} - \bar{\rho}_{(i-1)}) \frac{i}{2} \Delta z \tag{6-9}$$

where $\bar{\rho}_{(i)}$ is the average density of the wind mixed layer when it incompasses i elements. N is incremented until

$$d(PE)^{e}_{N} > A\rho u_{*}^{3}\Delta t \tag{6-10}$$

In the example this occurs when N = 4. To this point the mixing part of the algorithm corresponds to the one proposed by Stefan and Ford (1975).

Since equality of $d(PE)^{e}_{N}$ and $A\rho u_{*}^{3}\Delta t$ is required by the mixing rule, N in general will not be an integer. The above technique identifies the smallest integer greater or equal to N, call it M. The non-integer fraction of N can be found as follows. The energy available for mixing a portion of element M is known since the increase in potential energy due to mixing down through element M-1 is known and the total energy available for use by mixing is known. The difference is the energy available for mixing a fraction of element M. Call this amount of energy Δ_{M}. There is a depth increment ΔH such that

$$\Delta_M = \Delta\rho\Delta H g \frac{(M-1)\Delta z}{2} \tag{6-11}$$

where $\Delta\rho$ is the density difference between the mixed layer of M-1 elements and element M (element 4 in the example). Solving for ΔH

$$\Delta H = \frac{\Delta_M}{g \frac{(M-1)\Delta z}{2} \Delta\rho} \tag{6-12}$$

The fraction of element M that can be mixed is $\Delta H/\Delta z$. The depth of the wind mixed layer is now determined.

The temperature of the isothermal mixed layer is

$$\hat{T} = \frac{(M-1)\bar{T}_{(M-1)}\Delta z + T_{(M)}\Delta H}{(M-1)\Delta z + \Delta H} \tag{6-13}$$

where $\bar{T}_{(i)}$ is the average temperature of the wind mixed layer when it encompasses i elements. $\hat{T}$ is the temperature of elements 1 through (M-1) and a fraction of element M. In the context of the discretized model, however, an element cannot have more than one temperature associated with it. The average temperature of element M is

$$\bar{T}_M = \hat{T} \frac{\Delta H}{\Delta z} + T_{(M)}\left(1 - \frac{\Delta H}{\Delta z}\right) \tag{6-14}$$

where $\bar{T}_M$ is the average temperature and $T_{(M)}$ is the temperature of element M before the initiation of wind mixing.

Implicit in the above derivation is the assumption that the horizontal cross-sectional area of the water body does not change with depth. In lakes and reservoirs, the area is generally a function of the

depth, so the following argument for the appropriate area to use in Equation (6-5) is made. Entrainment can only occur in those parts of the water body where the water depth is greater than the thickness of the wind mixed layer. In the shallow regions, the bottom stress dissipates the turbulent energy without increasing the potential energy of the system. It is assumed therefore that the area over which the wind induced shear stress generates turbulent energy used for entrainment is equal to the area of the next increment of depth to be entrained (see Figure 6-3). Otherwise, the procedure is unchanged.

When horizontal cross-sectional area variations are considered, the average temperature of layers 1 through M-1 is

$$\bar{T} = \frac{1}{\sum_{i=1}^{M-1} A_{(i)}\Delta z} \sum_{i=1}^{M-1} T_{(i)} A_{(i)} \Delta z \qquad (6\text{-}15)$$

where $T_{(i)}$ is the average temperature of the i^{th} element from the surface and $A_{(i)}$ is the area of the element. The temperature of the isothermal wind mixed layer of depth H is

$$\hat{T} = \frac{\sum_{i=1}^{M-1} \bar{T} A_{(i)} \Delta z + T_{(M)} A_{(M)} \Delta H}{\sum_{i=1}^{M-1} A_{(i)} \Delta z + A_{(M)} \Delta H} \qquad (6\text{-}16)$$

The depth of the wind mixed layer is

$$H = (M-1)\Delta z + \Delta H \qquad (6\text{-}17)$$

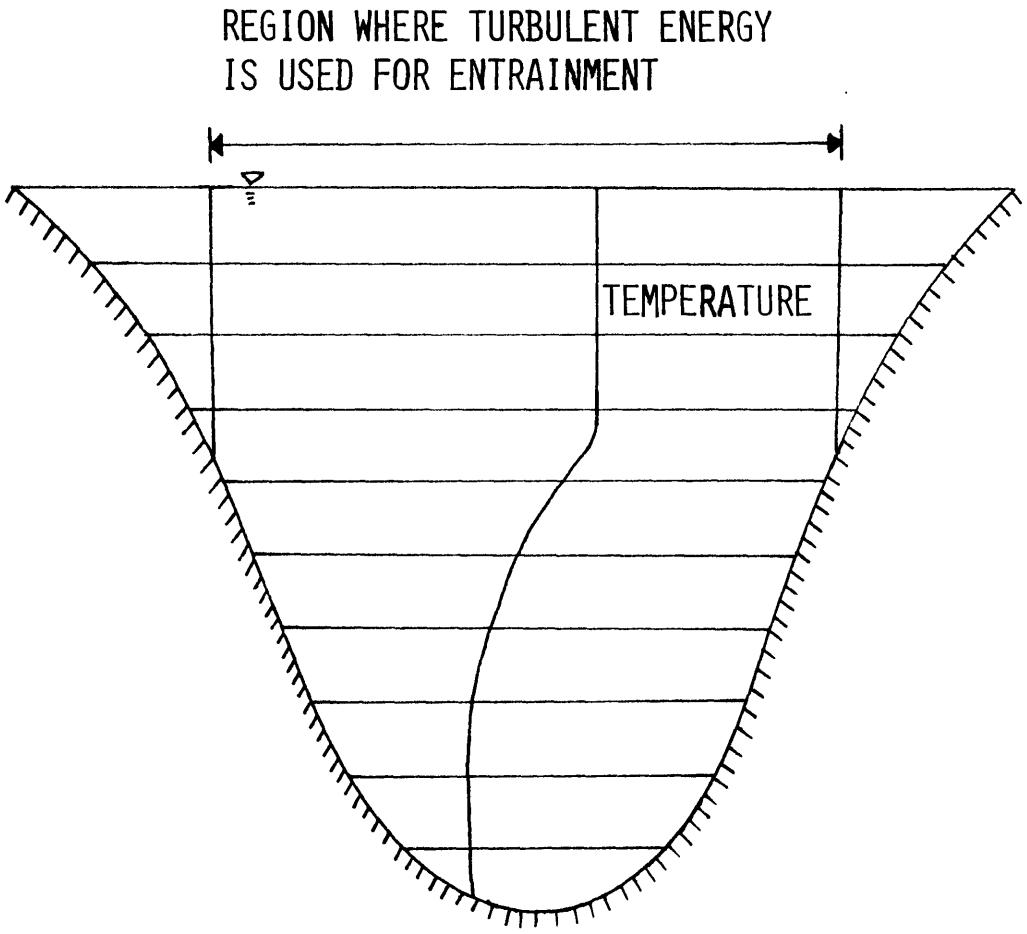

Figure 6-3 Surface Area over Which Kinetic Energy from the Wind is Used for Entrainment

6.1.3 Behavior of the Wind Mixing Algorithm in the Absence of Wind

It is instructive to investigate the behavior of the wind mixing algorithm during periods when there is no wind. Two situations can be distinguished according to whether the water body is heating or cooling on a given day. First suppose that the system is heating and that there is a stable density profile. Since the wind speed is assumed to be zero, τ_o is zero and u_* is zero. Thus the energy input by the wind, the right-hand side of Equation (6-5), is zero. The mixing algorithm begins by mixing elements 1 and 2. The change in potential energy due to mixing elements 1 and 2, $d(PE)^e_{N=2}$, will be positive. Since $d(PE)^e_{N=2} > 0$, the algorithm will proceed to search for the fractional part of element 2 that will satisfy the equality. The only value that will satisfy the equality is $\Delta H = 0$. Thus, in this case, when there is no wind, the profile is not altered from that obtained by heating alone.

The second possibility is that there is no wind, the water body is cooling, which results in an unstable density profile. Again, the energy input by the wind, the right hand side of Equation (6-5), is zero. The mixing algorithm begins by mixing elements 1 and 2. The change in potential energy due to mixing elements 1 and 2, $d(PE)^e_{N=2}$ will be negative. Since $d(PE)^e_{N=2} < 0$, the algorithm will continue and will add element 3 to the mixed layer. Eventually the increments to the change in potential energy will become positive and the magnitude of $d(PE)^e_N$ will decrease as N increases. For some value of N, $d(PE)^e_{N=M}$ will be greater than 0 and the algorithm will search for the fractional part of element M that makes the equality hold. The center of mass of the mixed layer

will be at the same elevation as the center of mass of the corresponding elements before mixing. The density instability has been eliminated without changing the potential energy of the water column.

6.2 Choice of the Surface Shear Stress Coefficient

The expression for the turbulent kinetic energy input contains the surface shear stress due to the wind. A specific relationship between the shear stress and the wind speed has not been discussed previously. In this section, the shear stress coefficient, C_z, which relates the wind speed, W_z, at elevation z, and the shear stress, τ_o, by

$$\tau_o = C_z \rho_{air} W_z^2$$

will be defined.

The majority of the work that has been done on the determination of the shear stress from the wind speed has been done at sea where the fetch is very long or in the laboratory, where the fetch is very short. Wu (1971) has shown that the observed deviation between the two types of data can be attributed to the difference in fetch. Since the fetch over inland water bodies is between the two extremes, expressions derived for either extreme may not be appropriate for use in conjunction with a lake model. Wu suggested an equation for determining the wind stress coefficient, C_z, that is independent of the fetch length based on Froude scaling

$$\frac{1}{C_z^{1/2}} = \frac{1}{K} \ln\left(\frac{1}{0.011 C_z F^2}\right) \qquad (6\text{-}18)$$

where $F = W_z/\sqrt{gz}$, z is the wind measurement height, W_z is the wind speed at z, and K is the Karman constant = 0.41. The factor 0.011 is obtained from a relation between the shear velocity and the dynamic roughness of the water surface at equilibrium with the wind.

Other investigators have developed different equations for the shear stress coefficient for use in lakes. Based on measurements in lakes, Van Dorn (1953) has suggested the following expression for the shear stress coefficient.

$$C_{10} = 1.0 \times 10^{-3} \qquad W_{10} < 5.6 \text{ m/s}$$

$$C_{10} = \left[1.0 + 1.9\left(1 - \frac{5.6}{W_{10}}\right)^2\right] \times 10^{-3} \qquad W_{10} > 5.6 \text{ m/s} \qquad (6\text{-}19)$$

Bengtsson (1973) suggests

$$C_{10} = 1.1 \times 10^{-3} \qquad W_{10} < 18 \text{ m/s} \qquad (6\text{-}20)$$

Shear stress coefficients derived from ocean data are occasionally used for lakes, also. Wu's (1969) expression for the ocean shear stress coefficient is

$$C_{10} = 1.25\, W_{10}^{-1/2} \times 10^{-3} \qquad W_{10} < 1 \text{ m/s}$$

$$C_{10} = 0.5\, W_{10}^{1/2} \times 10^{-3} \qquad 1 < W_{10} < 15 \text{ m/s} \qquad (6\text{-}21)$$

$$C_{10} = 2.6 \times 10^{-3} \qquad W_{10} > 15 \text{ m/s}$$

There is significant scatter of the data and hence of the curves used to fit the data (see Figure 6-4). Wu's equation for the shear stress coefficient over inland water bodies, Equation (6-18) is recommended.

Wu (1975) has shown that the shear stress coefficient for pulsating winds are smaller than those for steady winds. If this were not so, the use of wind data averaged over different time intervals would result in different values for the total kinetic energy input by the wind in a given day. The kinetic energy input is proportional to the third power of the wind speed. The wind speed fluctuates over the course of a day. Since averaging the cube of the fluctuations is not equivalent to cubing the average wind speed, a greater kinetic energy input is obtained when meteorological data is averaged over shorter time periods. A reduction coefficient that makes the kinetic energy input in a day computed using wind speeds averaged over three hour time intervals comparable to the kinetic energy input computed using the daily averaged wind speed for a given location can be calculated by taking the ratio of the mean of the daily averaged wind speed cubed and the mean of the three hour averaged wind speed cubed.

6.3 Sensitivity Studies

In this section the sensitivity of the M.I.T. Reservoir Model with wind mixing is examined. The effect of the inclusion of wind mixing on the stratification period is investigated, as well as the influence of the element size and the time step on the predicted temperature profiles. All figures are from simulations of the hypothet-

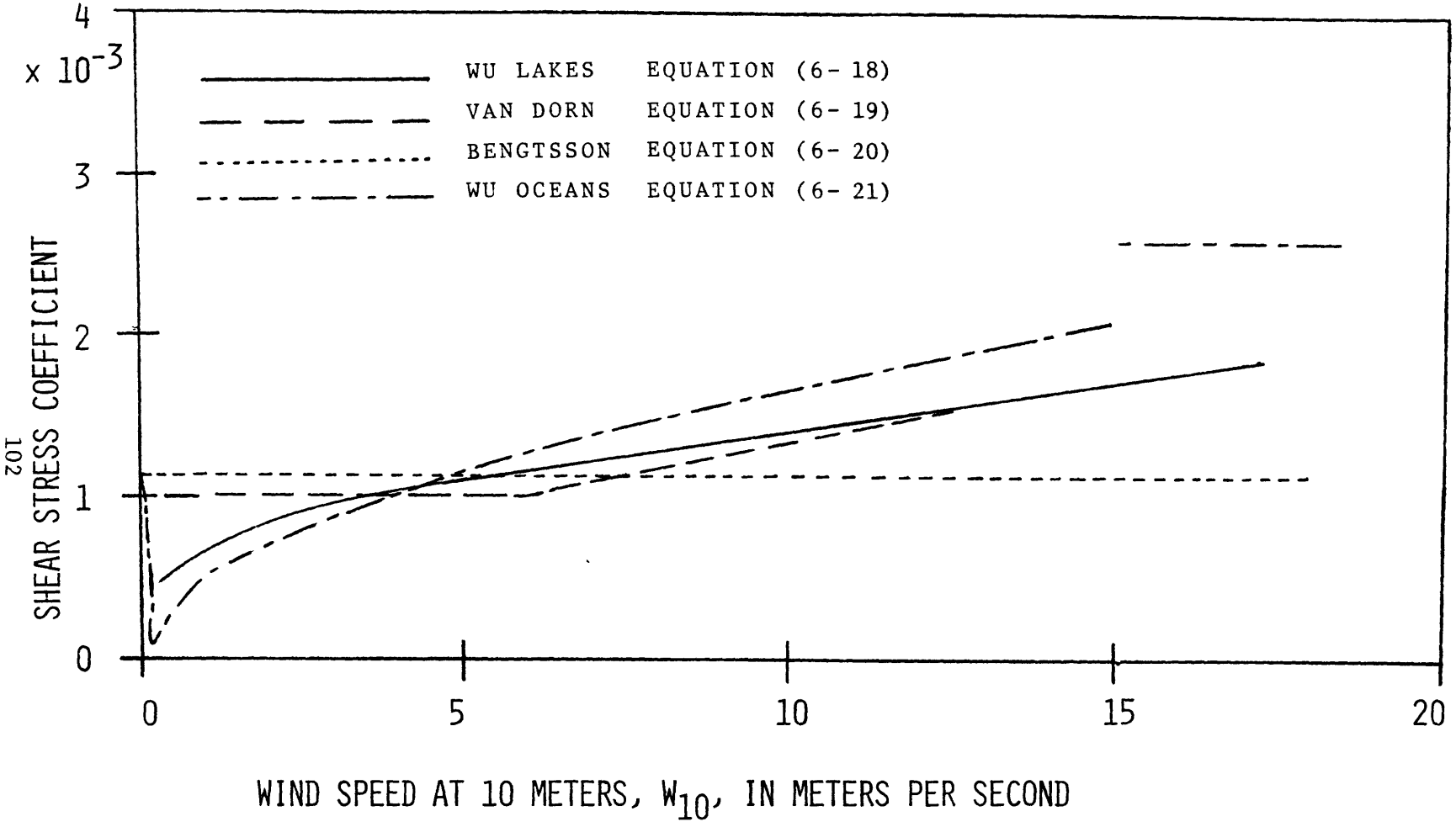

Figure 6-4 Shear Stress Coefficient, C_{10}, vs. Wind Speed W_{10}

ical lake described in Chapter III beginning with isothermal ($8^{o}C$) conditions in early April.

As can be seen in Figure 6-5, the inclusion of wind mixing has a significant influence on the predicted temperature profiles. For example, the predicted depth of the thermocline on May 7 with wind mixing is 7 meters, while without wind mixing it is only 1 meter. Later in the year, the influence of the wind in mixing the water body in the spring is still evident in the increased heat content of the lake. Wind mixing has only a small effect on the surface temperature since the surface temperature is primarily determined by the meteorological conditions.

6.3.1 Element Thickness

Figure 6-6 shows temperature profiles calculated using several values for the thickness of the elements. The dependence of the predictions on element size is of interest because the computation time required is related to the number of elements. There is a trade-off between resolution and expense. The profiles predicted using 0.61 meters and 1.22 meters as the element thickness are almost identical, except when, as is the case for the profile predicted for May 7, the thinner element size locates a step in the profile in the middle of one of the thicker elements. When a large element thickness of 2.44 meters is used, the temperature predicted in the region of the thermocline is consistently higher than the predicted temperature using thinner elements.

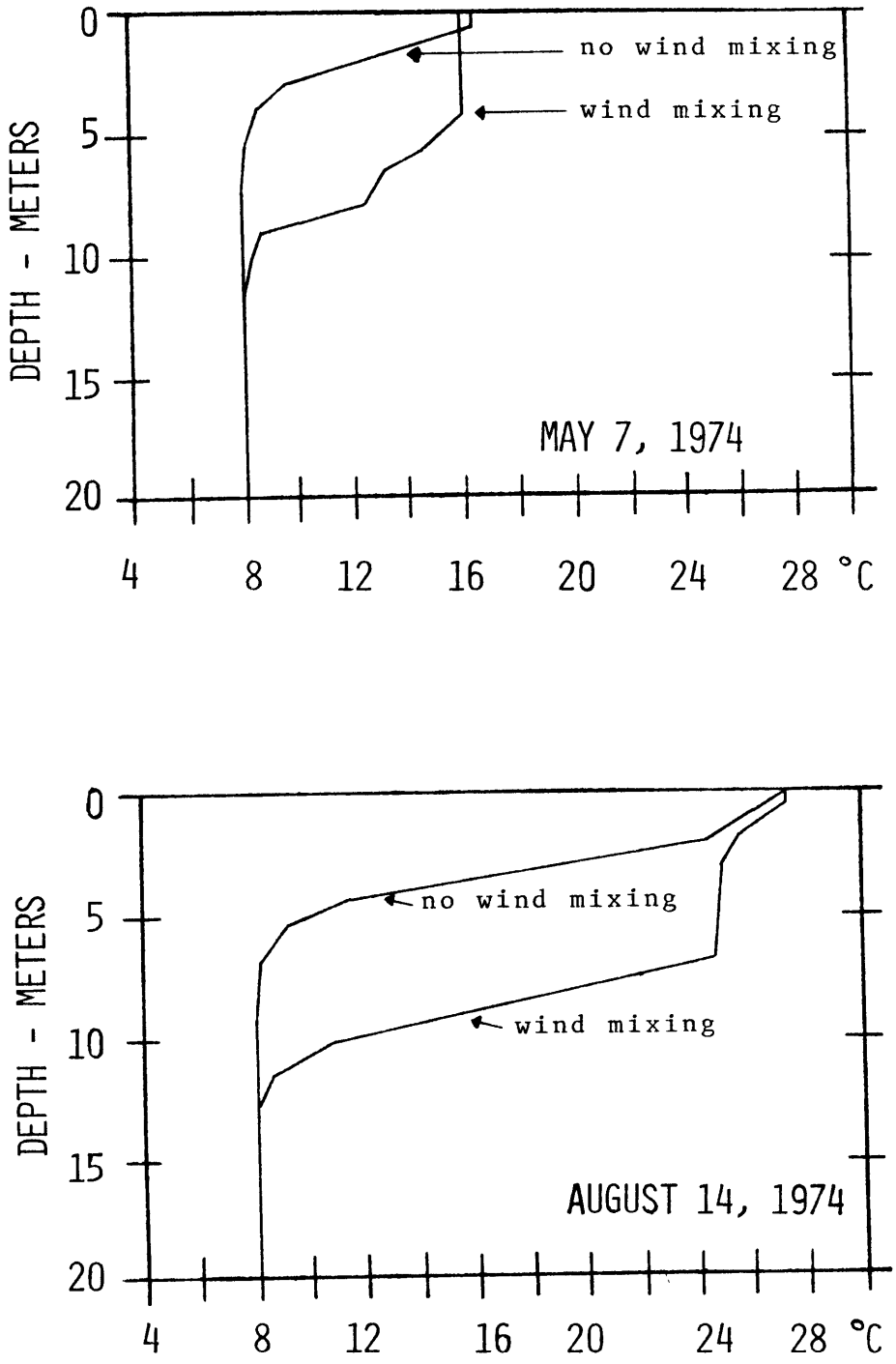

Figure 6-5 Comparison of Predicted Temperature Profiles With and Without the Inclusion of Wind Mixing (molecular diffusion, $\eta = 1.0\ m^{-1}$)

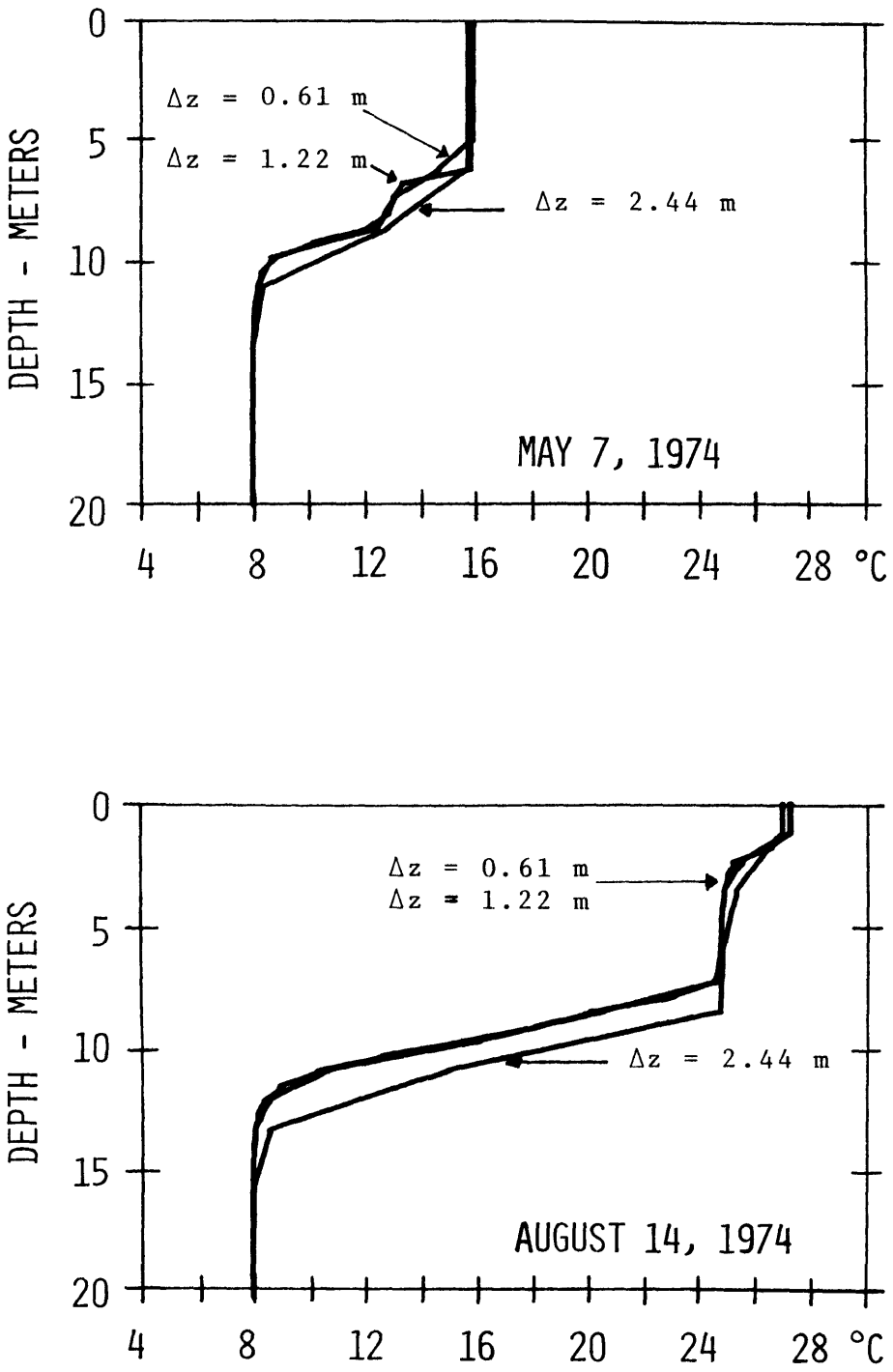

Figure 6-6 Comparison of Predicted Temperature Profiles with Wind Mixing with Different Values of the Element Thickness (molecular diffusion, $\eta = 1.0\ m^{-1}$)

6.3.2 Time Step

The time step appears explicitly in the expression for the change in potential energy, Equation (6-5). In order to remove the diurnal effects of the meteorological conditions and to investigate only the effects of the time step, it is necessary to use the daily average meteorological conditions with sub-day time intervals. It should be emphasized that using daily average meteorological conditions with sub-day time steps is not representative of the conditions over a day. This case is included solely as a check on the dependence of the mixing scheme on the time step. Figure 6-7 shows that the predicted profile using a 1 day time step and the profile predicted for the end of the same time period using a time interval of three hours are in general within $0.3^{o}C$ of each other and that the difference in depth of the mixed layer is less than 1.5 meters. Hence the mixing scheme is not strongly dependent on the time step.

Diurnal effects are felt to the depth of the mixed layer, which varies over time. The primary diurnal fluctuation, however, occurs in the top 2-3 meters. The diurnal fluctuation is 1.5 - $3.0^{o}C$, similar to the range obtained when wind mixing is not considered.

6.3.3 Onset of stratification

The action of the wind may destroy weak stratification and cause circulation throughout the lake. Based on a comparison with case C in Chapter III, the inclusion of wind mixing shortened the predicted period of stratification in the hypothetical lake used in the sensi-

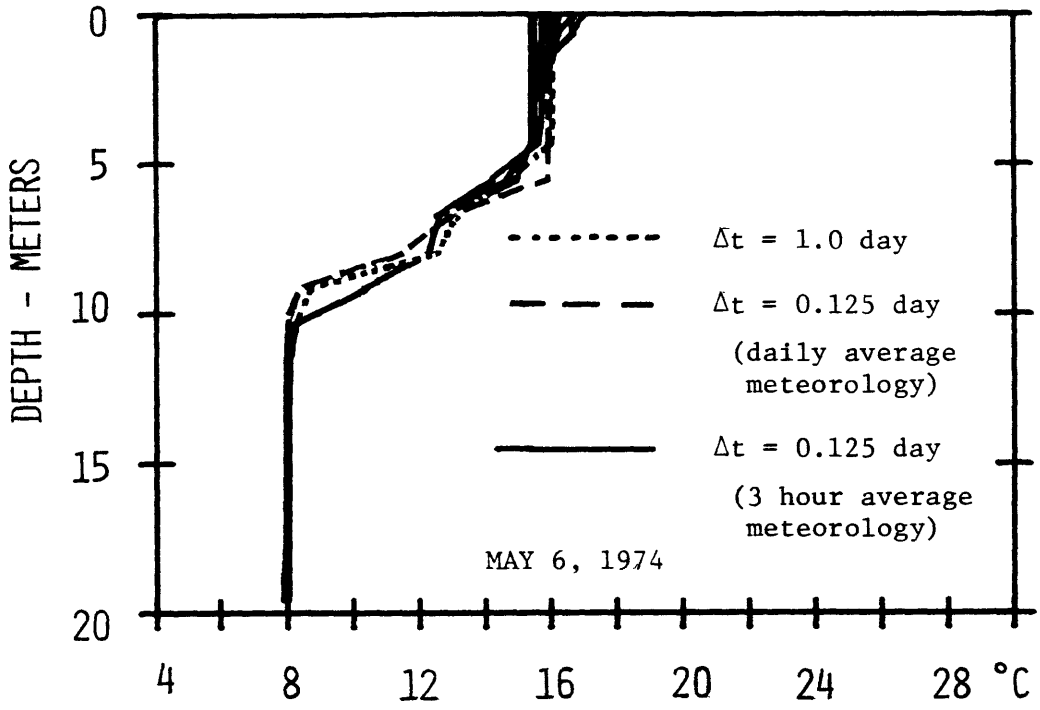

Figure 6-7 Comparison of Predicted Temperature Profiles with Wind Mixing with Different Tim Steps (molecular diffusion, $\eta = 1.0\ m^{-1}$)

tivity studies by 29 days. The criteria for defining the presence of stratification was the existence of at least a $2^{o}C$ temperature difference between the top and bottom elements in the lake. The yearly average surface temperature was reduced by only $0.03^{o}C$ by the inclusion of wind mixing, while the maximum surface temperature for the year was decreased by $0.7^{o}C$. The most dramatic change occured for the minimum surface temperature. The inclusion of wind mixing eliminated the large oscillations in the surface temperature predicted during January through March (see Figure 6-8). Eliminating the winter oscillations caused the predicted minimum temperature to increase from $-2.0^{o}C$ to $4.2^{o}C$. The M.I.T. Reservoir Model does not consider the latent heat of fusion, so predicted temperatures below $0^{o}C$ have no physical significance. The density dependence on temperature is correctly modelled below $4^{o}C$, so predictions in the range $0 - 4^{o}C$ are realistic. From May through September the inclusion of wind mixing had little effect on the predicted surface temperature. The largest influence on the surface temperature was found during those parts of the year when the stratification is weak.

6.3.4 Summary

Unless diurnal effects are of specific interest, a time step of 1 day gives satisfactory results. When meteorological data averaged over time intervals of less than 1 day are used in conjunction with sub-day time interval, the shear stress coefficient should be different than the shear stress coefficient used with daily averaged wind speeds

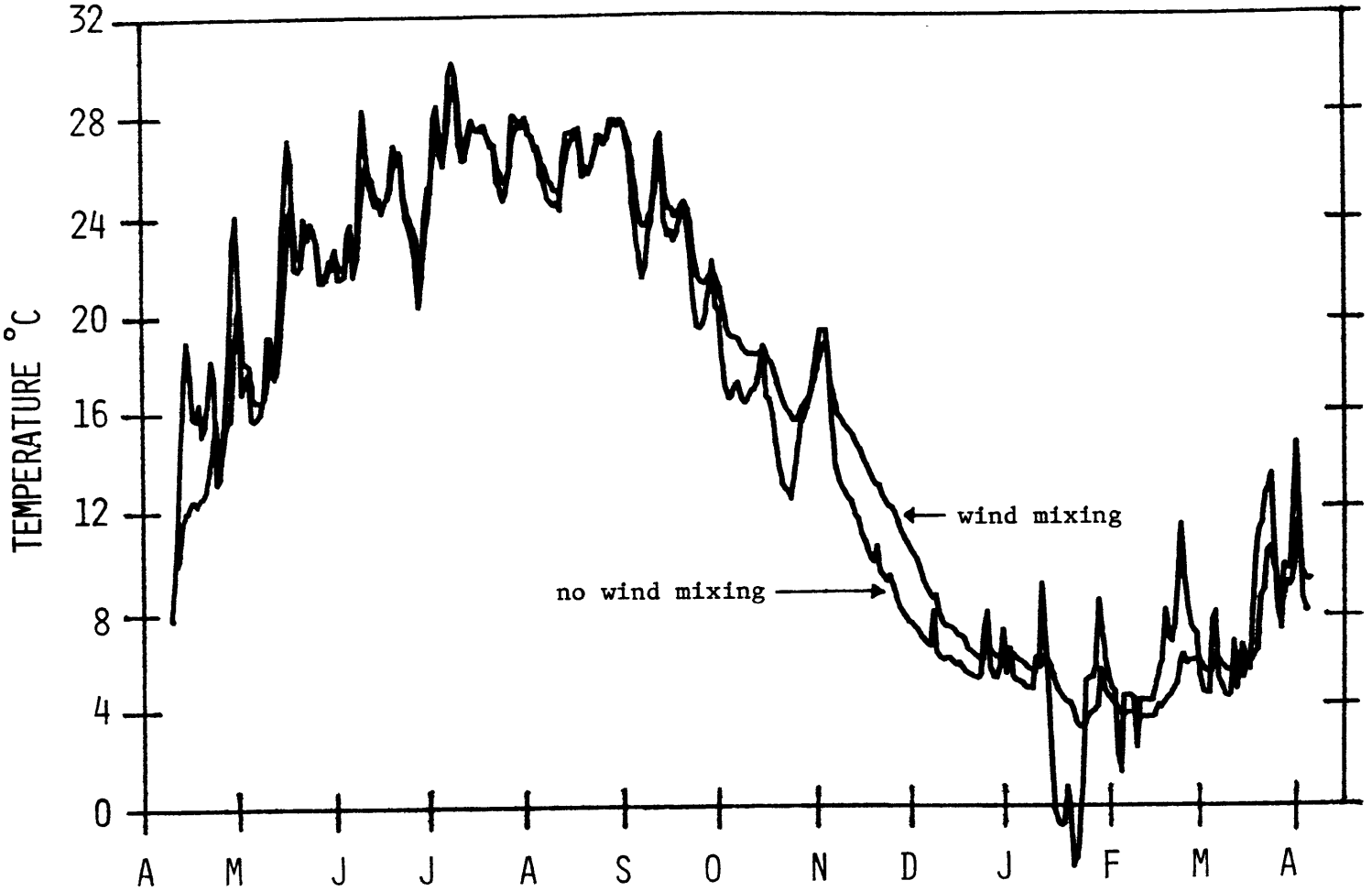

Figure 6-8 Comparison of Predicted Surface Temperatures with and without the Inclusion of Wind Mixing (molecular diffusion, $\eta = 1.0\ m^{-1}$)

in order that the same amount of kinetic energy is input for both cases in a given day. Decreasing the time step while using daily averaged meteorological conditions is not physically reasonable and does not significantly alter the predicted profiles.

When there is little or no through-flow, the element thickness should be of the order of 1 meter.

The inclusion of wind mixing substantially shortens the period of stratification predicted for a water body.

CHAPTER VII

APPLICATION OF THE MATHEMATICAL MODEL TO LAKE ANNA

7.1 Description of the Lake

Lake Anna, shown in Figure 7-1, is formed by a dam on the North Anna River. The lake is located in central Virginia, 41 miles northwest of Richmond and 40 miles east of Charlottesville. At a design elevation of 250 ft. above sea level, Lake Anna has a surface area of 9,600 acres, a volume of 10.6×10^9 ft^3, and an average depth of 25 ft. The maximum depth at the dam is 70 ft. The lake receives an average annual inflow of about 270 cfs. The lake elevation is maintained by radial gates at the dam. The outflow rate equals the inflow minus the rate of evaporation from the lake surface (estimated at about 60 cfs average).

Continuous lake temperature measurements have been taken in the Lake Anna since August 1974. A continuous monitoring system measures lake temperatures at hourly intervals at six stations (surface, mid-depth and bottom) and three additional surface locations. In addition, intensive temperature surveys were conducted at about two month intervals (the intervals between intensive surveys varied between one and three months). These intensive surveys measured the detailed vertical temperature distribution at 17 stations in the lake at various times of the day.

Beginning in April 1974, a meteorological station at Lake Anna made hourly measurements at an elevation of 15 meters of air temperature, dew point temperature, wind speed and short wave solar radiation.

Water releases from surface and subsurface radial gates were

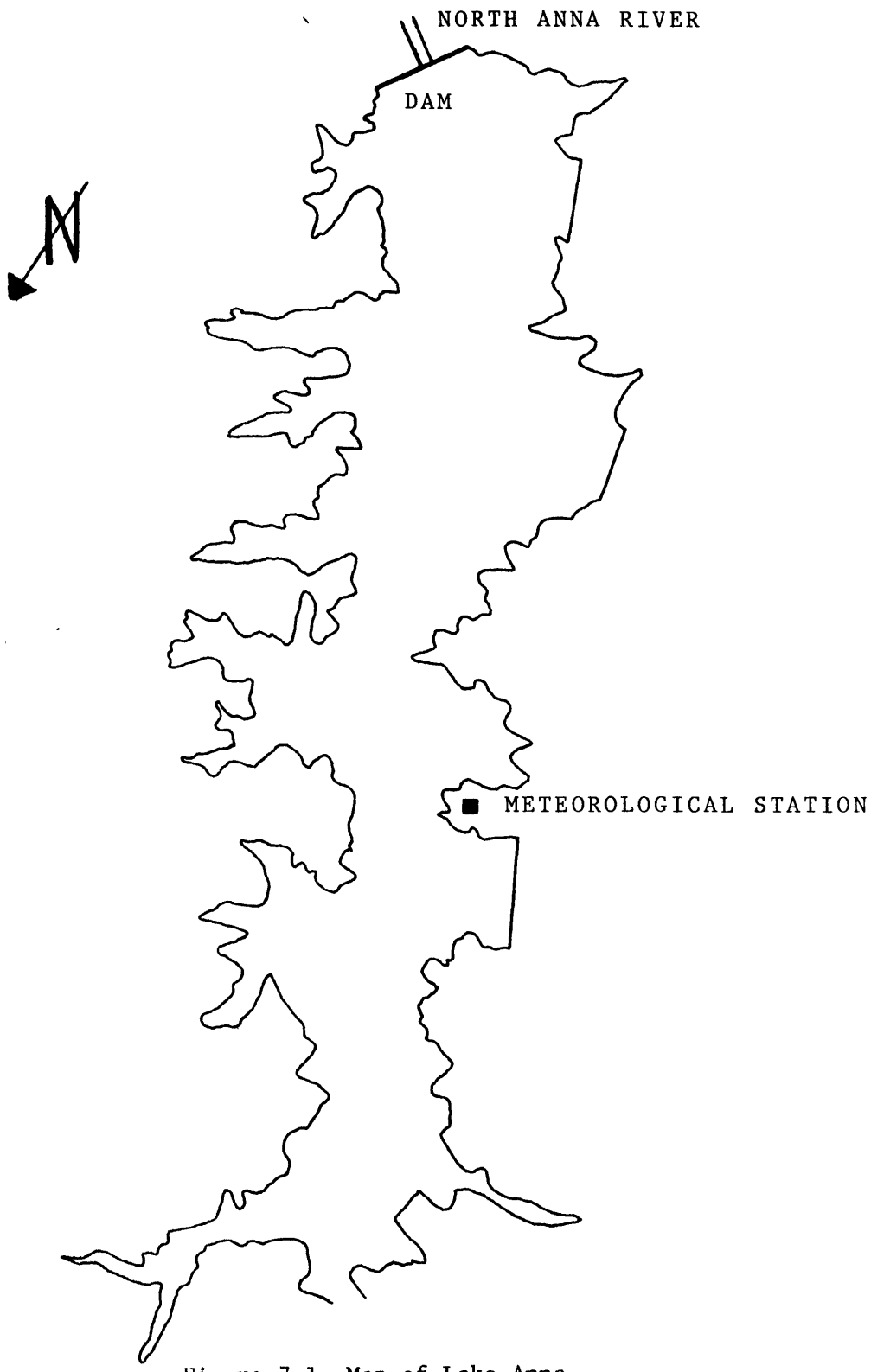

Figure 7-1 Map of Lake Anna

monitored, and daily release rates were available for a one year period. Inflow rates were not available.

This data base was considered ideal for a check of the accuracy of the M.I.T. Reservoir Model with wind mixing. For molecular diffusivity, the ratio of the rate of heat transport by diffusion to the rate of heat transport by advection, $\frac{AE}{QD}$, has a value of .15 so Lake Anna can be considered more a lake than a reservoir (see Section 3.2).

The objective of this chapter is to determine whether the mathematical model incorporating wind mixing will yield acceptable results for a field application.

7.2 Inputs to the Mathematical Model

7.2.1 Hydro-meteorological Data

Certain data were available on an hourly basis and other data on a daily basis. The program was run with a time step of one day and all hourly data were reduced to daily averages.

The input requirements of the model include daily averaged values of the air temperature, relative humidity at 2 meters, wind speed at 2 meters, cloud cover, and total daily short wave solar radiation. Air temperature and wind speed were averaged over the day to obtain daily values. Relative humidity was computed hourly and then averaged. Radiation was summed. Because cloud cover was not measured, it had to be calculated indirectly through a comparison of the measured daily short wave radiation and the values developed by Hamond, Weiss and Wilson (1954) for 100% of possible sunshine, using the empirical formula

$$\phi_s = \phi_{sc}(1.0-0.65C^2) \qquad (7\text{-}1)$$

where ϕ_s = incoming solar radiation (measured short wave)

ϕ_{sc} = clear sky incoming solar radiation

C = cloudiness ratio (fractions of unity)

The model uses cloud cover to compute daily values for long wave radiation from Wunderlich's (1972) modification of Swinbanks' (1963) clear sky formula

$$\phi_a = 0.937x10^{-5}\sigma T_a^{\,6}(1.0+0.17C^2) \qquad (7\text{-}2)$$

where ϕ_a = long wave radiation (atmospheric radiation)

σ = Stefan Boltzman constant

T_a = air temperature ^{o}K, 2 m above water surface

C = cloudiness ratio

Changes internal to the model were made to adjust vapor pressure and wind speed values from those measured at 15 meters to corresponding values at 2 meters, based on the assumption of logarithmic profiles. For wind speed, the conversion equation is

$$W_2 = W_{15}\frac{\ln(\frac{2}{z'})}{\ln(\frac{15}{z'})} \qquad (7\text{-}3)$$

where z', the roughness height for the wind speed profile is .001 meters.

For vapor pressure the conversion equation is

$$(e_{a_2} - e_s) = (e_{a_{15}} - e_s) \frac{\ln(\frac{2}{z'})}{\ln(\frac{15}{z'})} \qquad (7\text{-}4)$$

where z', the roughness height for the vapor pressure profile is .000067 meters.

The model also requires daily inflow and outflow rates as input data. Inflow rates were not available, but since the measured surface level of the lake remained approximately constant, the inflow was set equal to the sum of the outflows. The temperature of the inflow water was estimated by assuming it was at equilibrium temperature.

7.2.2 Geometric Data

Table 7-1 lists the areas and length of Lake Anna. Values at intermediate elevations are found by linear interpolation in the program. The average widths were computed by dividing the area by the length at each elevation. These values are also included in Table 7-1.

7.2.3 Other Program Parameters

The value of the surface absorption fraction, β, (see Equation (2-22)) was set equal to 0.5. The value of the absorption coefficient, η, was computed from Sechi disk depths using Equation (2-23). The Sechi disk depths were 2 to 3 meters, so η was taken as 0.75 m^{-1}. A vertical grid spacing of 1.22 m was used.

Table 7-1: Lake Anna Areas and Widths

Elevation Above Sea Level (ft.)	(m)	Area (m^2)	Width (m)
180	54.9	2977,000	343
190	57.9	2977,000	343
200	61.0	5310,000	613
210	64.0	7477,000	864
220	67.1	9361,000	1080
230	70.1	1168,000	1350
240	73.2	14360,000	1660
250	76.2	17388,000	2010

Length = 8650 m

7.3 Comparison of the Predictions with Measured Field Temperatures

In this section, the predicted lake surface temperatures and the vertical temperature distribution with and without wind mixing are compared with measured values. For the predictions without wind mixing, the eddy diffusivity is set equal to 50 times molecular diffusivity. This value was selected to give a best fit to the measured profiles. The initial isothermal temperature was taken as $8^{o}C$, the isothermal temperature to which the predictions return, approximately, at the beginning of every April in a ten year simulation with regional meteorological data with no wind mixing. For the predictions with wind mixing, the diffusivity is set equal to molecular diffusivity. The initial temperature is taken as $10^{o}C$, the isothermal temperature to which the predictions return after a year when wind mixing is considered. In the following figures, predicted values are indicated by solid lines and measurements by points. Measurements from three of the continuous temperature monitoring stations located along the center line of the lake are included.

Figure 7-2 indicates that the agreement between measured and predicted surface temperature is generally good with respect to absolute value and the transient behavior, regardless of whether wind mixing is included. However, when wind mixing is not included, the surface temperature prediction is less satisfactory with respect to rapid transients during the winter months. This may be caused by predicted periodic weak stratification during the winter. The inclusion of wind mixing eliminates the weak winter stratification, removing the rapid transients.

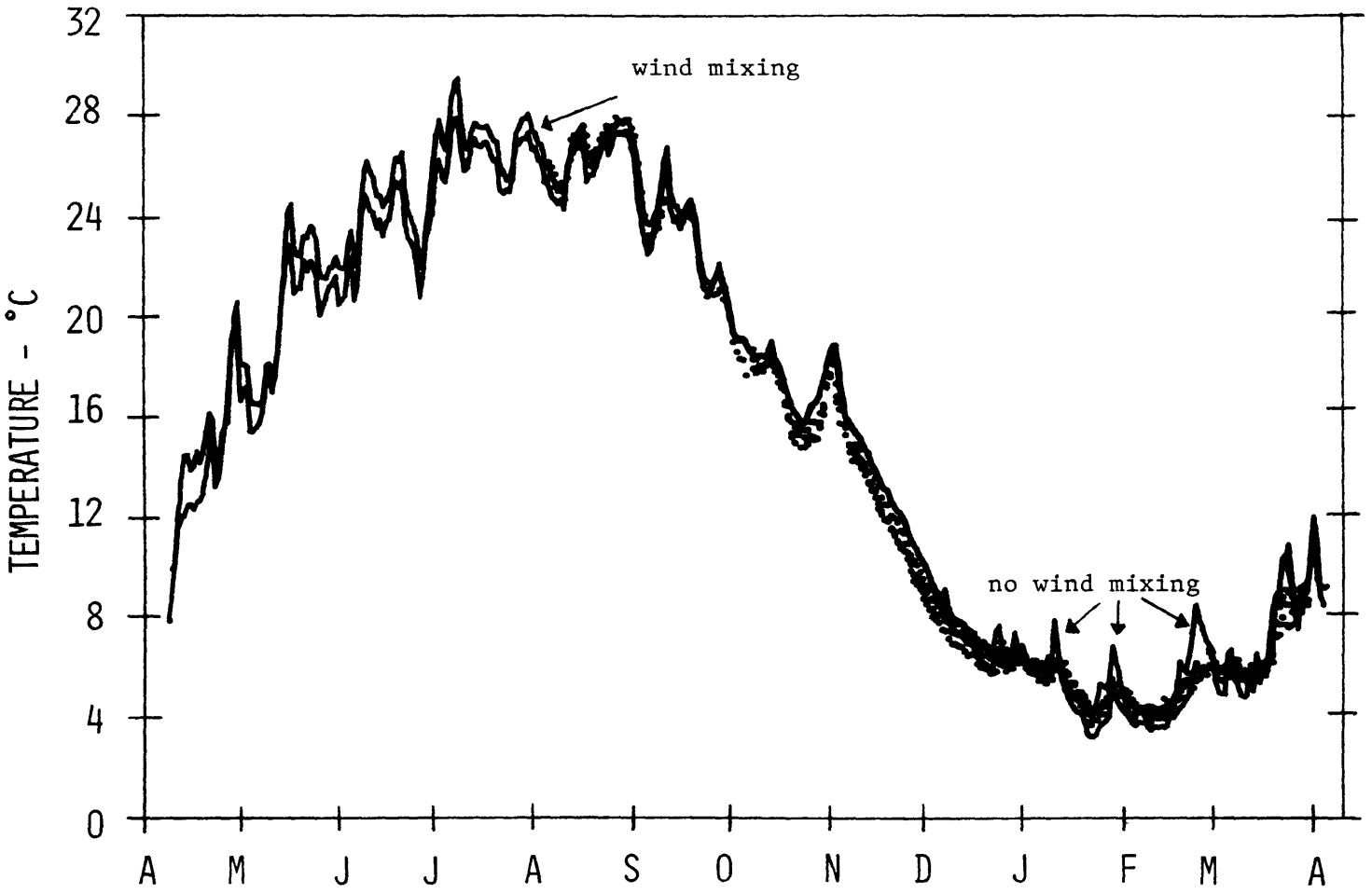

Figure 7-2 Comparison of Measured and Predicted Surface Temperatures with and without the Inclusion of Wind Mixing

Figures 7-3 through 7-6 indicate that agreement between measured temperature profiles and predicted temperature profiles with wind mixing is good. Without wind mixing, the agreement is poor. The profiles for May 7 and August 15 show the characteristic step in temperature at the bottom of the wind mixed layer. The predicted profile for July 10 exhibits two steps, reflecting the time history of the wind.

Most of the through-flow is released from a surface outlet. On rare occasions, when the surface outlet can not spill enough water to release all the inflow, flow is also released from a bottom outlet. Because of the outlet configuration, advection is expected to have a small role in transporting heat. This was checked by computing temperature profiles setting the inflow and outflow equal to zero. These profiles were essentially the same as the profiles predicted using flows.

Although the available weather data set extends for over two years, the predicted profiles during the second year could not be used to verify the model. Short wave solar radiation data for April of the second year was unavailable. This is the critical period for establishing the temperature of the hypolimnion for the rest of the year. Since the temperature is influenced by convective overturn on days with a negative net heat flux into the water body, the data gap could not be filled with a typical, constant value.

7.4 Summary of Field Results

It has been demonstrated that the mathematical model including wind mixing is capable of reproducing field measurements of the surface temperature of a lake with an accuracy of the order of $1^{o}C$ and is capable

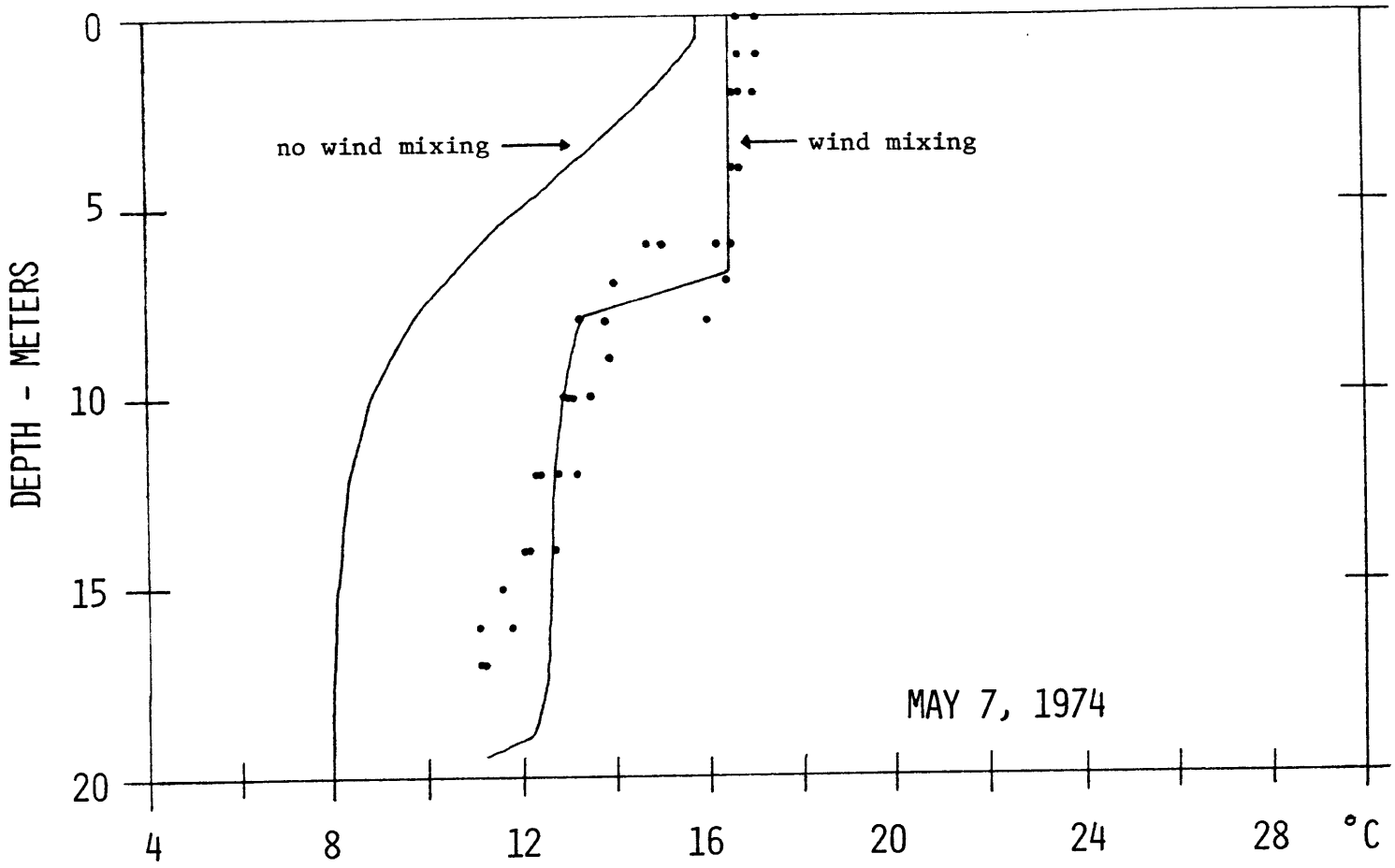

Figure 7-3 Comparison of Measured and Predicted Temperature Profiles with and without the Inclusion of Wind Mixing

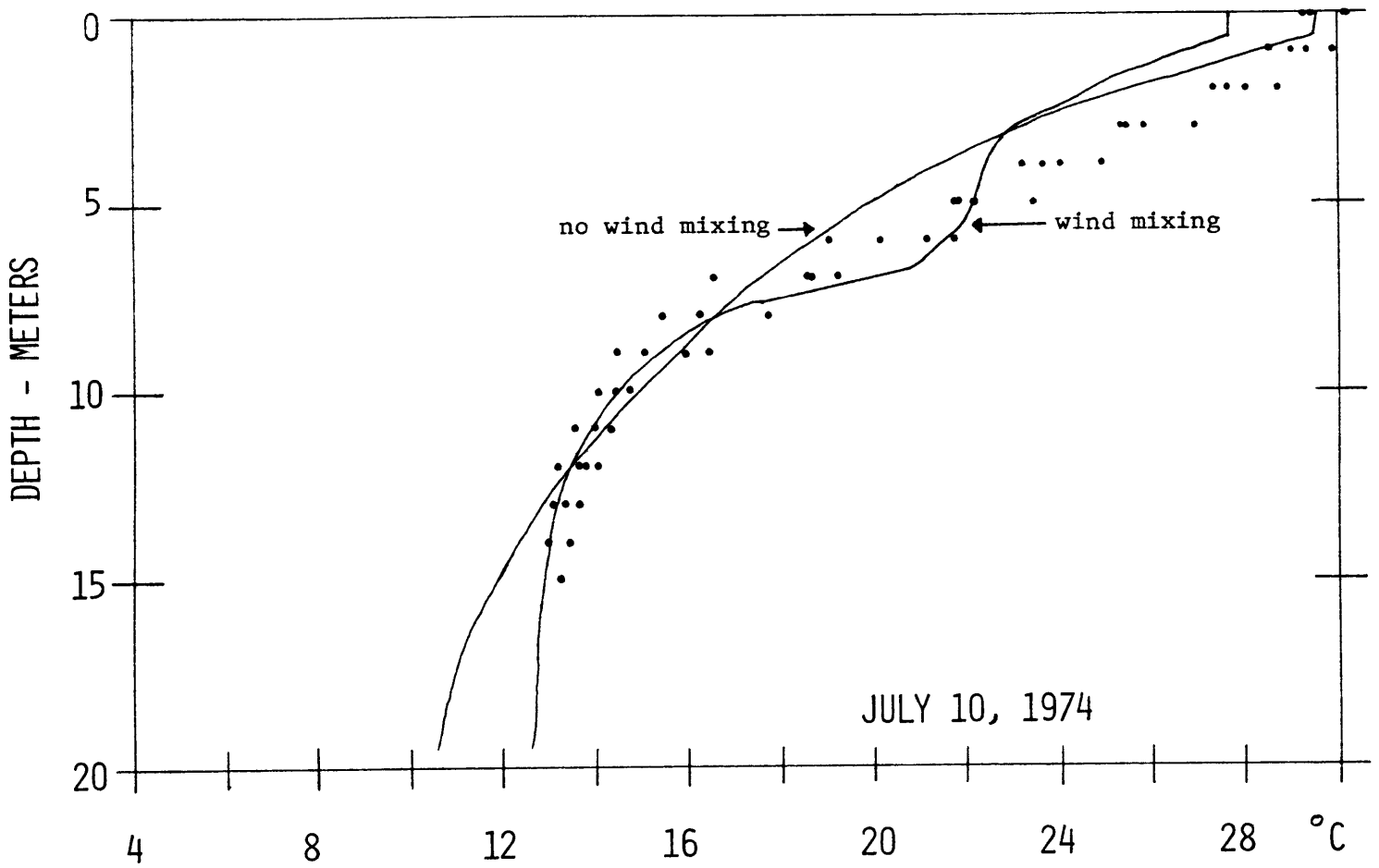

Figure 7-4 Comparison of Measured and Predicted Temperature Profiles with and without the Inclusion of Wind Mixing

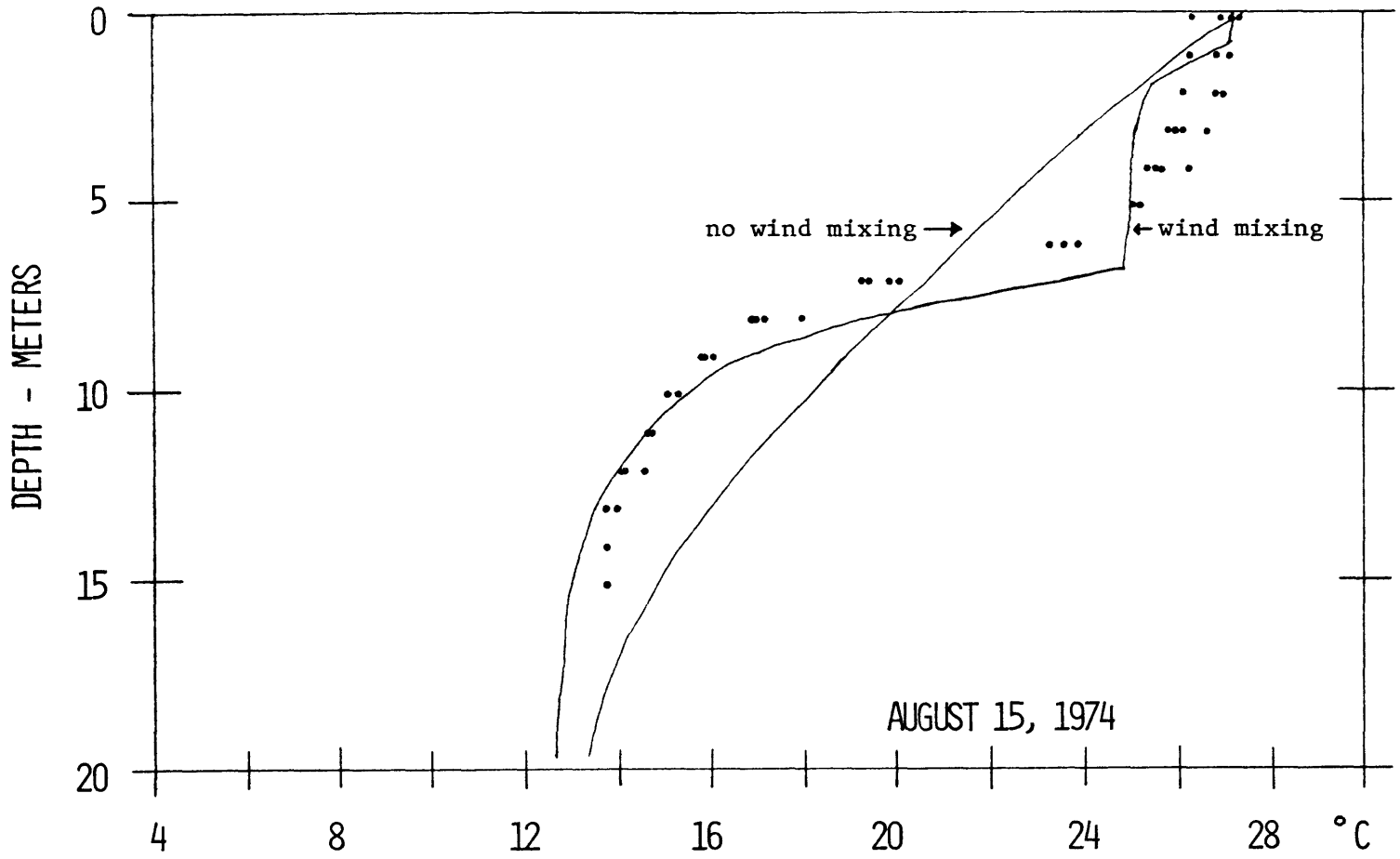

Figure 7-5 Comparison of Measured and Predicted Temperature Profiles with and without the Inclusion of Wind Mixing

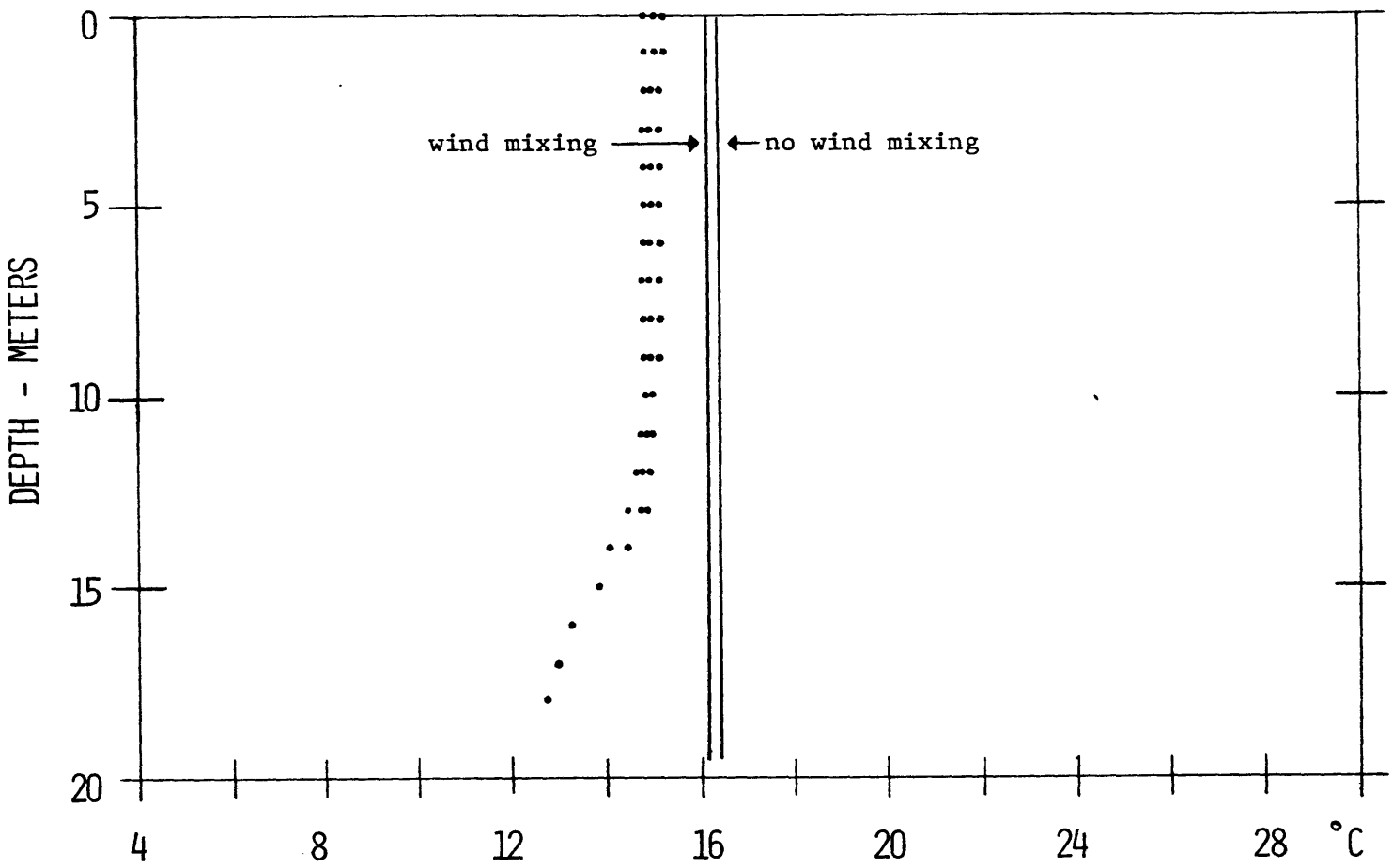

Figure 7-6 Comparison of Measured and Predicted Temperature Profiles with and without the Inclusion of Wind Mixing

of determining the depth of the thermocline with an accuracy of the order of 1 meter. The data input required by the model consists of data which would normally be available during the planning or design stage of a proposed impoundment.

REFERENCES

1. Beard, Leo R. and Willey, R.G., "An Approach to Reservoir Temperature Analysis", WRR, Vol. 6, No. 5, 1970

2. Bedford, K.W. and Babajimopoulis, C., "Vertical Diffusivities in Areally Averaged Models", ASCE, EE1, 1977

3. Bengtsson, L., "Wind Stress on Small Lakes", Tekniska Hogskolan, Lund, 1973

4. Blanton, J.O., "Rates of Vertical Entrainment in Stratified Lakes", Proceeding of the Symposium for the Hydrology of Lakes, Helsinki, 1973

5. Bowen, I.S., "The Ratio of Heat Losses by Conduction and by Evaporation from Air Water Surface", Physical Review, Vol. 27, 1926

6. Brunt, D., "Notes on Radiation in the Atmosphere", Quarterly Journal Royal Met. Soc., 58, 1932

7. Brutsaert, W., "On a Derivable Formula for Long-Wave Radiation from Clear Skies", WRR, Vol. 11, No. 5, 1975

8. Burt, W.V., "Verification of Water Temperature Forecasts for Deep, Stratified Reservoirs", WRR, Vol. 10, No. 1, 1974

9. Crapper, P.F. and Linden, P.F., "The Structure of Turbulent Density Interfaces", J. Fluid Mech., Vol. 65, 1974

10. Dake, J.M.K. and Harleman, D.R.F., "An Analytical and Experimental Investigation of Thermal Stratification in Lakes and Ponds", M.I.T., Department of Civil Engineering, Hydrodynamics Laboratory Technical Report No. 99, 1966

11. Debler, W.R., "Stratified Flow into a Line Sink", ASCE, EM3, 85, July 1959

12. Denman, K.L., "A Time Dependent Model of the Upper Ocean", J. of Phys. Oceanog., Vol. 3, 1973

13. Edinger, J.R. and Geyer, J.C., "Cooling Water Studies for Edison Electric Institute, Project No. RP-49-- Heat Exchange in the Environment", The Johns Hopkins University, June 1, 1965

14. Elder, R.A. and Wunderlich, W.O., "Evaluation of Fontana Reservoir Field Measurements", ASCE Specialty Conf. on Current Research into the Effects of Reservoirs on Water Quality, Portland, Oregon, January 1968

15. Goodling, J.S. and Arnold, T.G., "Deep Reservoir Thermal Stratification Model", WRR, Vol. 8, No. 4, 1972

16. Hamon, R.W., Weiss, L.L. and Wilson, W.T., "Insolation as an Emperical Function of Daily Sunshine Duration", Monthly Weather Review, Vol. 82, No. 6, 1954

17. Haney, R.L. and Davies, R.W., "The Role of Surface Mixing in the Seasonal Variation of the Ocean Thermal Structure", J. of Phys., Oceanog., Vol. 6, 1976

18. Hansen, N.B.O., "Effect of Wind Stress on Stratified Deep Lake", ASCE, HY , Vol. 101, 1975

19. Henderson-Sellers, B., "Role of Eddy Diffusivity in Thermocline Formation", ASCE, EE3, 1976

20. Huber, W.C. and Harleman, D.R.F., "Laboratory and Analytical Studies of Thermal Stratification in Reservoirs", M.I.T. Department of Civil Engineering, Hydrodynamics Laboratory Technical Report No. 112, 1968

21. Hutchinson, G.E.A., "Treatise on Limnology, Wiley, 1957

22. Idso, S.B. and Jackson, R.D., "Thermal Radiation from the Atmosphere", J. Geo. Res., Vol. 74, No. 23, 1969

23. Imberger, J., Patterson, J., Hebbert, B. and Loh, I., "Simulation of the Salinity Distribution in a Reservoir of Medium Size", J. Fluid Mech., 1977

24. Imberger, J., Thompson, R.T. and Fandry, C., "Selective Withdrawal from a Finite Rectangular Tank", J. Fluid Mech., 1976

25. Jassby, A. and Powell, T., "Vertical Patterns of Eddy Diffusion During Stratification in Castle Lake, California, " L. & O., Vol. 20, No. 4, 1975

26. Kao, T. W., "The Phenomenon of Block in Stratified Flow," J. Geo. Res., Vol. 70, No. 4, 1965

27. Kato, H. and Phillips, O. M., "On the penetration of a turbulent layer into stratified fluid," J. Fluid Mech., Vol. 37, No. 4, 1969

28. Kim, J.-W., "A Generalized Bulk Model of the Oceanic Mixed Layer," J. of Phys. Oceanog., Vol. 6, 1976

29. Koh, R. C. Y., "Viscous Stratified Flow Towards a Line Sink," W. M. Keck Laboratory Report KH-R-6, Calif. Inst. of Tech., 1964

30. Kraus, E. B. and Turner, J. S., "A One-Dimensional Model of the Seasonal Thermocline," Tellus XIX, 1967

31. Linden, P. F., "The interaction of a vortex ring with a sharp density interface: a model for turbulent entrainment," J. Fluid Mech., Vol. 60, No. 3, 1973

32. Linden, P. F., "The Deepening of a Mixed Layer in a Stratified Fluid," J. Fluid Mech., Vol. 71, 1975

33. Long, R. R., "The Influence of Shear on Mixing across Density Interfaces," J. Fluid Mech., Vol. 70, 1975

34. Mermier, M. and Seguin, B., "Comment on, 'On a Derivable Formula for Long-Wave Radiation from Clear Skies', by W. Brutsaert," WRR, Vol. 12, No. 6, 1976

35. Moore, M. J. and Long, R. R., "An experimental investigation of turbulent stratified shearing flow," J. Fluid Mech., Vol. 49, No. 4, 1971

36. Newbold, J. D. and Liggett, J. A., "Oxygen Depletion Model for Cayuga Lake," ASCE. EE1, Vol. 100, 1974

37. Niiler, P. P., "Deepening of the wind-mixed layer," J. of Marine Research, Vol. 33, 1975

38. Orlob, G. T., "Mathematical Models for Prediction of Thermal Energy Changes in Impoundments," Final Report to FWQA by Water Resources Engineers, Inc., 1969

39. Orlob, G. T. and Selna, L. G., "Temperature Variations in Deep Reservoirs," A.S.C.E., HY2, 1970

40. Parker, F. L., Benedict, B. A. and Tsai, C., "Evaluation of Mathematical Models for Temperature Prediction in Deep Reservoirs," EPA Report, EPA-660 3-75-038, June 1975

41. Phillips, O. M., Dynamics of the Upper Ocean, Cambridge University Press, 1969

42. Rahman, M. and Marcotte, N., "On Thermal Stratification in Large Bodies of Water," WRR, Vol. 10, No. 6, 1974

43. Roberts, B. R. and Street, R. L., "Two-Dimensional Hydrostatic Simulation of Thermally-Influenced Hydrodynamic Flows," T.R. 194, Dept. of Civil Engineering, Stanford University, 1975

44. Rohwer, E., "Evaporation from Free Water Surfaces," U.S. Dept. of Agriculture, Tech. Bulletin No. 271, 1931

45. Ryan, P. J. and Harleman, D. R. F., "Prediction of the Annual Cycle of Temperature Changes in a Stratified Lake or Reservoir; Mathematical Model and User's Manual," M.I.T., Department of Civil Engineering, R. M. Parsons Laboratory for Water Resources and Hydrodynamics, Technical Report No. 137, 1971

46. Ryan, P. J. and Harleman, D. R. F., "An Analytical and Experimental Study of Transient Cooling Pond Behavior," M.I.T., Department of Civil Engineering, R. M. Parsons Laboratory for Water Resources and Hydrodynamics, Technical Report No. 161, 1973

47. Snider, D. M. and Viskanta, R., "Combined Conduction-Radiation Energy Transfer in Stagnant Water," WRR, Vol. 10, No. 5, Oct. 1974

48. Spalding, D. B. and Svensson, U., "The Development and Erosion of the Thermocline," Proceedings 1976 Seminar of the International Center for Heat and Mass Transfer

49. Spraggs, L. D. and Street, R. L., "Three-Dimensional Simulation of Thermally-Influenced Hydrodynamic Flows," T.R. 190, Dept. of Civil Engineering, Stanford University, 1975

50. Stefan, H. and Ford, D. E., "Temperature Dynamics in Dimictic Lakes," A.S.C.E. HY 1, Vol. 101, 1975

51. Sudaram, T. R. and Rehm, R. G., "The seasonal thermal structure of deep temperate lakes," Tellus, XXV, 2, 1973

52. Sverdrup, H. U., Oceanography for Meteorologists, George Allen and Unwin, Ltd., London, 1945

53. Sweers, H. E., "Vertical Diffusivity Coefficient in a Thermocline," L. & O., Vol. 15, No. 2, 1970

54. Swinbank, W. C., "Longwave Radiation from Clear Skies," Quarterly Journal of Royal Met. Society, Vol. 89, 1963

55. Turner, J. S., "The influence of molecular diffusivity on turbulent entrainment across a density interface," J. Fluid Mech., Vol. 33, No. 4, 1968

56. Turner, J. S., Buoyancy Effects in Fluids, Cambridge University Press, 1973

57. USGS "Water Loss Investigations: Lake Hefner Studies," USGS Prof Paper 269, 1954

58. Van Dorn, W., "Wind Stress on an Artificial Pond," Journal of Marine Research, Vol. 12, No. 3, 1953

59. Wiegel, R. L., Oceanographical Engineering, Prentice-Hall, Inc., 1964

60. Wu, Jin, "Wind Stress and Surface Roughness at Air-Sea Interface," Journal of Geophysical Research, Vol. 74, No. 2, 1969

61. Wu, Jin, "Anemometer Height in Froude Scaling of Wind Stress," A.S.C.E., WW1, 1971

62. Wu, Jin, "Wind-induced turbulent entrainment across a stable density interface," J. Fluid Mech., Vol. 61, No. 2, 1973

63. Wu, Jin, "Effects of Pulsating Wind on Velocity Profiles and Microstructures," J. of Phys., Oceanog., Vol. 5, 1975

64. Wunderlich, W. O., "Heat and Mass transfer between a Water Surface and the Atmosphere," T.V.A. Engineering Laboratory, Report No. 14, Norris, Tennessee, 1972